



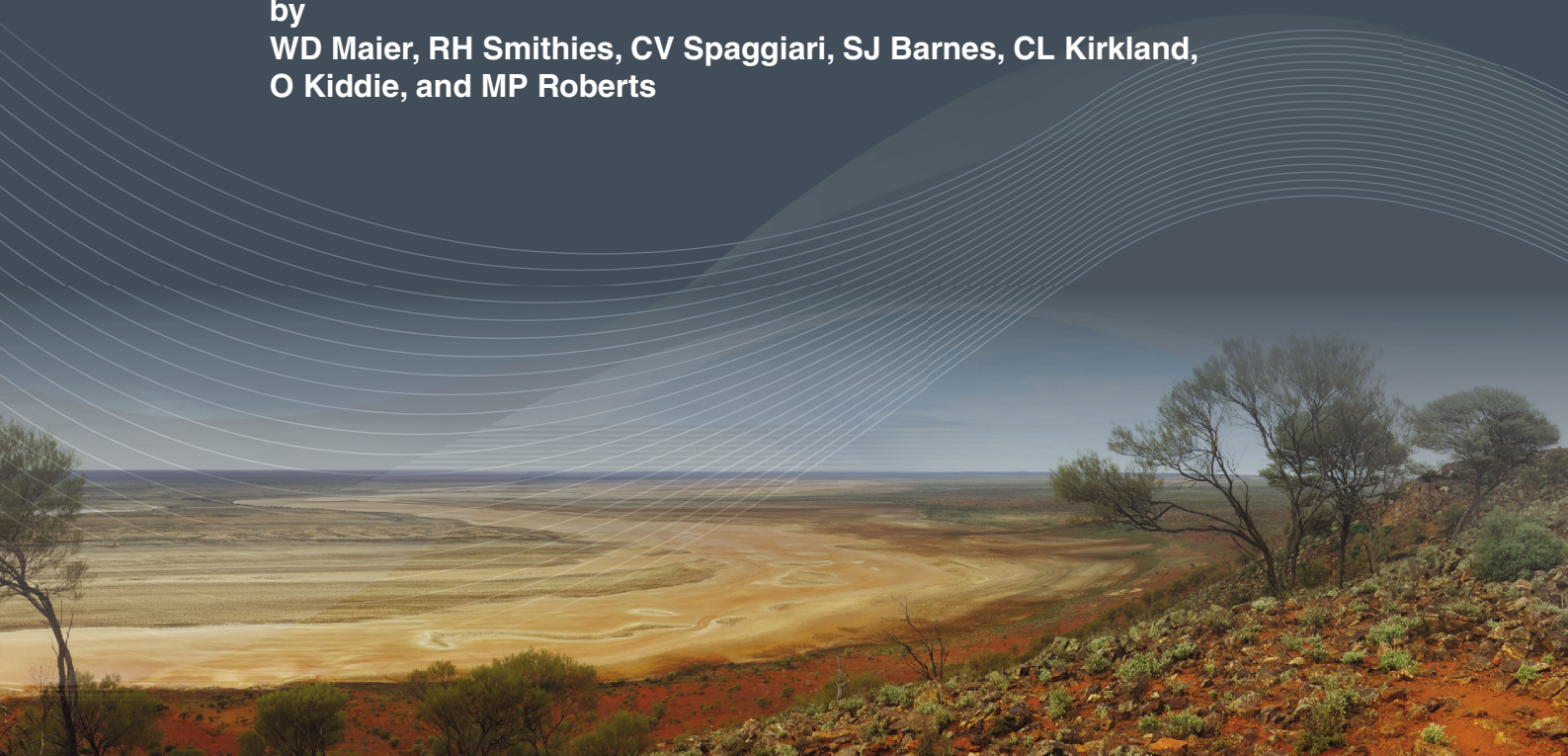
Government of **Western Australia**
Department of **Mines and Petroleum**

RECORD 2016/8

THE EVOLUTION OF MAFIC AND ULTRAMAFIC ROCKS OF THE MESOPROTEROZOIC FRASER ZONE, ALBANY–FRASER OROGEN, AND IMPLICATIONS FOR NI–CU SULFIDE POTENTIAL OF THE REGION

by

WD Maier, RH Smithies, CV Spaggiari, SJ Barnes, CL Kirkland,
O Kiddie, and MP Roberts



**Geological Survey of
Western Australia**



Curtin University



**THE UNIVERSITY OF
WESTERN
AUSTRALIA**



Government of **Western Australia**
Department of **Mines and Petroleum**

Record 2016/8

THE EVOLUTION OF MAFIC AND ULTRAMAFIC ROCKS OF THE MESOPROTEROZOIC FRASER ZONE, ALBANY–FRASER OROGEN, AND IMPLICATIONS FOR NI–CU SULFIDE POTENTIAL OF THE REGION

by

**WD Maier¹, RH Smithies, CV Spaggiari, SJ Barnes², CL Kirkland³,
O Kiddie⁴, and MP Roberts⁵**

1 School of Earth and Ocean Sciences, Cardiff University, CF10 3AT, UK

2 CSIRO, Mineral Resources, Underwood Avenue, Floreat WA 6102

3 Centre for Exploration Targeting – Curtin Node, Department of Applied Geology, Western Australian School of Mines, Curtin University, Bentley WA 6102

4 Creasy Group, 8 Kings Park Road, West Perth WA 6005

5 Centre for Microscopy Characterisation and Analysis, The University of Western Australia, Stirling Highway, Nedlands WA 6009

Perth 2016



**Geological Survey of
Western Australia**

MINISTER FOR MINES AND PETROLEUM
Hon. Sean K L'Estrange MLA

DIRECTOR GENERAL, DEPARTMENT OF MINES AND PETROLEUM
Richard Sellers

EXECUTIVE DIRECTOR, GEOLOGICAL SURVEY OF WESTERN AUSTRALIA
Rick Rogerson

REFERENCE

The recommended reference for this publication is:

Maier, WD, Smithies, RH, Spaggiari, CV, Barnes, SJ, Kirkland, CL, Kiddie, O and Roberts, MP 2016, The evolution of mafic and ultramafic rocks of the Mesoproterozoic Fraser Zone, Albany–Fraser Orogen, and implications for Ni–Cu sulfide potential of the region: Geological Survey of Western Australia, Record 2016/8, 49p.

National Library of Australia Card Number and ISBN PDF 978-1-74168-693-7

Grid references in this publication refer to the Geocentric Datum of Australia 1994 (GDA94). Locations mentioned in the text are referenced using Map Grid Australia (MGA) coordinates, Zone 51. All locations are quoted to at least the nearest 100 m.



Curtin University



**THE UNIVERSITY OF
WESTERN AUSTRALIA**

Disclaimer

This product was produced using information from various sources. The Department of Mines and Petroleum (DMP) and the State cannot guarantee the accuracy, currency or completeness of the information. DMP and the State accept no responsibility and disclaim all liability for any loss, damage or costs incurred as a result of any use of or reliance whether wholly or in part upon the information provided in this publication or incorporated into it by reference.

Published 2016 by Geological Survey of Western Australia

This Record is published in digital format (PDF) and is available online at <www.dmp.wa.gov.au/GSWApublications>.

Further details of geological products and maps produced by the Geological Survey of Western Australia are available from:

Information Centre
Department of Mines and Petroleum
100 Plain Street
EAST PERTH WESTERN AUSTRALIA 6004
Telephone: +61 8 9222 3459 Facsimile: +61 8 9222 3444
www.dmp.wa.gov.au/GSWApublications

Cover image: Elongate salt lake on the Yilgarn Craton — part of the Moore–Monger paleovalley — here viewed from the top of Wownaminy Hill, 20 km southeast of Yalgoo, Murchison Goldfields. Photograph taken by I Zibra for the Geological Survey of Western Australia

Contents

Abstract	1
Introduction	2
Regional synthesis	2
The Fraser Zone	5
Magmatic rocks formed during Stage I of the Albany–Fraser Orogeny	6
Sample material	6
Outcrop descriptions and petrography	6
Main gabbro	6
Hybrid gabbros	7
Rocks from the Nova–Bollinger drillcore SRFR0017	9
Rocks from the Plato Prospect	10
Mineral compositions	12
Whole-rock geochemistry	12
Chalcophile element geochemistry	17
Strontium, Nd and S isotope geochemistry	19
Discussion	19
Petrogenesis	19
Source of the main gabbros, and Plato cumulate and noncumulate rocks	20
Petrogenesis of the hybrid gabbros	21
Petrogenesis of the Nova–Bollinger intrusion	21
Emplacement of the Nova–Bollinger intrusion	23
Tectonic setting of the Fraser Zone	24
Spatial and compositional trends of the Recherche Supersuite through time	24
Insight into the geodynamic evolution of the Fraser Zone	25
Summary and conclusions	27
References	28

Appendices

1. Analytical methods	30
2. Whole-rock major and trace-element geochemical data	31
3. Platinum group elements data (ppb)	39
4. S and Sr isotope data	39
5. Nd isotope data	40
6. Mineral compositions	41

Figures

1. Simplified bedrock geology of the east Albany–Fraser Orogen	3
2. Gravity image of the Fraser Zone and sample localities	4
3. Field photos of the Fraser Range Metamorphics	7
4. Photomicrographs of Fraser Zone rocks	8
5. Plot of Th vs La, K ₂ O and Pb	9
6. Aeromagnetic images showing the drillhole sites at the Plato Prospect	11
7. Photos of core from the Plato Prospect	12
8. Photomicrographs of rocks from the Plato Prospect	13
9. Plot of Ni vs Fo in olivine from Nova–Bollinger and from Plato cumulate rocks	13
10. Plot of MgO vs major elements and Mg [#]	14
11. Plot of MgO vs Ba, Sr, Pb, Th, Zr, Ni, Cr, La/Th, Th/Nb and Cr/V	15
12. N-MORB normalized multi-element plots of Fraser Zone rocks	16
13. N-MORB normalized multi-element plot ignoring trace elements strongly partitioned into observed cumulate minerals	18
14. Plot of chalcophile elements vs MgO	18
15. Plot of height vs sulfur and selected chalcophile elements in drillcore SFRD0017	20
16. Nd isotope data for rocks of the Albany–Fraser Orogen	20
17. Plot of MgO vs Zr	22
18. Plot of Th vs La, Pb vs Zr, and Pb vs La	23
19. Plot of selected major- and trace-element concentrations with depth in drillcore SFRD0017	24
20. Plot of Ce/Sm ratio vs Ce and LOI for rocks from Nova–Bollinger	25
21. Geographical variation in age, composition and Nd isotopic composition for granites of the Gora Hill Suite	26
22. Compositional variation and tectonic discrimination for granitic rocks of the Recherche Supersuite	26
23. Schematic tectonic diagram for the Albany–Fraser Orogeny Stage I	27

The evolution of mafic and ultramafic rocks of the Mesoproterozoic Fraser Zone, Albany–Fraser Orogen, and implications for Ni–Cu sulfide potential of the region

by

WD Maier¹, RH Smithies, CV Spaggiari, SJ Barnes², CL Kirkland³,
O Kiddie⁴, and MP Roberts⁵

Abstract

The Albany–Fraser Orogen is located along the southern and southeastern margins of the Archean Yilgarn Craton and formed from at least c. 1810 to 1140 Ma during reworking of the craton, accompanied by variable additions of juvenile mantle material. The Fraser Zone is an approximately 425 km long and 50 km wide, geophysically and structurally distinct zone within the orogen, hosting abundant intrusions of predominantly c. 1305 to 1290 Ma metagabbroic rocks emplaced into sedimentary rocks belonging to the Snowys Dam Formation of the Arid Basin. Magma emplacement was most likely in a dominantly extensional setting and possibly related to orogenic collapse. The primary mafic magma had ~8.8% MgO and was derived from a depleted mantle source. This magma was contaminated with small (<<10%) amounts of crust before and during ascent and emplacement. The Fraser Zone has been the focus of considerable exploration for Ni–Cu sulfides following the discovery of the Nova–Bollinger deposit in 2012–13 in an intrusion consisting of interlayered olivine gabbro-noritic, noritic, and peridotitic cumulates. Disseminated sulfides in drillcore intersecting the structurally upper portion of the intrusion, above the main ore zone, have tenors of approximately 4–5% Ni, 1–4% Cu and very low PGE concentrations (<100 ppb), consistent with derivation from magma with broadly the same composition as the regional Fraser Zone metagabbros. However, mineral chemistry suggests that the Nova–Bollinger rocks crystallized from slightly more primitive parental melts, with higher ϵ_{Sr} (38–52) and more variable $\delta^{34}\text{S}$ (–2 to +4) than the regional metagabbros (ϵ_{Sr} 17–32, $\delta^{34}\text{S}$ around 0), which is consistent with the geochemical evidence for enhanced crustal assimilation of the metasedimentary country rock in a relatively large magma staging chamber.

Our data identify several factors potentially critical in determining whether or not Fraser Zone mafic magmas are mineralized. These data relate to intrusion history and local geodynamic conditions. Favourable sets of factors include initial emplacement of large magma chambers within the Arid Basin, assimilation of sulfur-rich metasedimentary rock, convective compositional homogenization and sulfur-saturation prior to olivine fractionation, and tectonically induced final transport and emplacement processes which modified or sorted both silicate and sulfide minerals and drained them of liquid. Unfavourable factors include initial emplacement beneath the base of the Arid Basin, early olivine fractionation, later emplacement within the Fraser Zone as small chambers that were unable to assimilate significant volumes of country rock or to convectively homogenize subsequent hybridized magma, and final emplacement during relative tectonic quiescence. Early olivine fractionation is monitored by whole-rock and mineral $\text{Mg}^\#$, effective contamination by Arid Basin metasedimentary rocks is monitored by sulfur and Sr isotopic composition, the stage of sulfur-saturation is monitored by Ni concentration of olivine, and the intensity of tectonic activity is monitored by textural features of the cumulate rocks including the ratio of cumulate minerals to liquid. Cumulate rocks with high whole-rock and olivine $\text{Mg}^\#$, Ni-depleted olivine, crustal sulfur and Sr isotopic compositions, and extremely low concentrations of strongly incompatible trace elements reflecting cumulates with very little interstitial liquid, would all be considered indicative of high Ni–Cu sulfide prospectivity within the Fraser Zone.

KEYWORDS: geochemistry, Ni–Cu sulfides, tectonics

1 School of Earth and Ocean Sciences, Cardiff University, CF10 3AT, UK

2 CSIRO, Mineral Resources, Underwood Avenue, Floreat WA 6102

3 Centre for Exploration Targeting – Curtin Node, Department of Applied Geology, Western Australian School of Mines, Curtin University, Bentley WA 6102

4 Creasy Group, 8 Kings Park Road, West Perth WA 6005

5 Centre for Microscopy Characterisation and Analysis, The University of Western Australia, Stirling Highway, Nedlands WA 6009

Introduction

The Neoproterozoic to Mesoproterozoic Albany–Fraser Orogen is located along the southern and southeastern margins of the Archean Yilgarn Craton (Fig. 1), and remains one of the major greenfields exploration regions of Western Australia. The region has seen relatively little mineral exploration in the past due to the perception that a prevailing geological history of high metamorphic grades and timing of tectonic activity renders the region unprospective. This view changed with the discovery of the 7.89 Moz Tropicana gold deposit in 2005 in the Tropicana Zone in the northwest of the orogen (Fig. 1; Doyle et al., 2015). The discovery in 2012–13 of the Nova–Bollinger Ni–Cu sulfide deposit (Fig. 1) within the Fraser Zone further fuelled exploration activity, in part based on the premise that Ni–Cu ore deposits tend to occur in clusters. The Nova–Bollinger Ni–Cu sulfide deposit is placed at 14.6 million metric tons grading 2.2% Ni and 0.9% Cu (Bennett et al., 2014).

Major factors contributing to the discovery of the Nova–Bollinger deposit were a soil geochemical anomaly highlighted by a regional Geological Survey of Western Australia (GSWA) regolith geochemical survey (Morris et al., 2000), and regional aeromagnetic data. Early drilling included diamond hole SFRD0017, co-funded by the Exploration Incentive Scheme (EIS). This penetrated 280 m into mafic–ultramafic rocks carrying disseminated Ni–Cu sulfides. Subsequent drilling to greater depth identified the Nova massive and net-textured sulfide mineralization (Gollam, 2012; Bennett et al., 2014). The deposit has since been extensively explored, identifying the host rocks as a sequence of gabbroic and ultramafic rocks at least 400 m thick and 900 m long, interlayered with semipelitic to pelitic, metasedimentary rocks. These rocks have undergone significant deformation and granulite-facies metamorphism, typical of other igneous–sedimentary sequences within the Fraser Zone. In February 2013, Sirius Resources announced the Bollinger discovery, a dominantly flat-lying body located to the east of the Nova deposit and interpreted to be connected to the Nova deposit by a feeder zone (Bennett et al., 2014).

Exploration for Ni–Cu sulfides within the Fraser Zone is still in its infancy. However, a critical aspect of the Nova–Bollinger discovery is that it highlighted the prospectivity of granulite-facies, c. 1300 Ma, mafic–ultramafic intrusive rocks within a poorly exposed but regionally extensive zone (the Fraser Zone). Based on geophysical properties (Fig. 2), the Fraser Zone is both well defined and dominated by mafic–ultramafic intrusive rocks. These intrusions were potentially cogenetic, or even comagmatic, with the intrusions at Nova–Bollinger. To assess the level of regional prospectivity of the Fraser Zone, three questions need to be addressed:

1. What was the primary magma composition, the mechanism of sulfur-saturation, and the source of sulfur?
2. What were the structural conditions and crustal levels that controlled intrusion?

3. Were all or any of these conditions/requirements replicated elsewhere in the Fraser Zone?

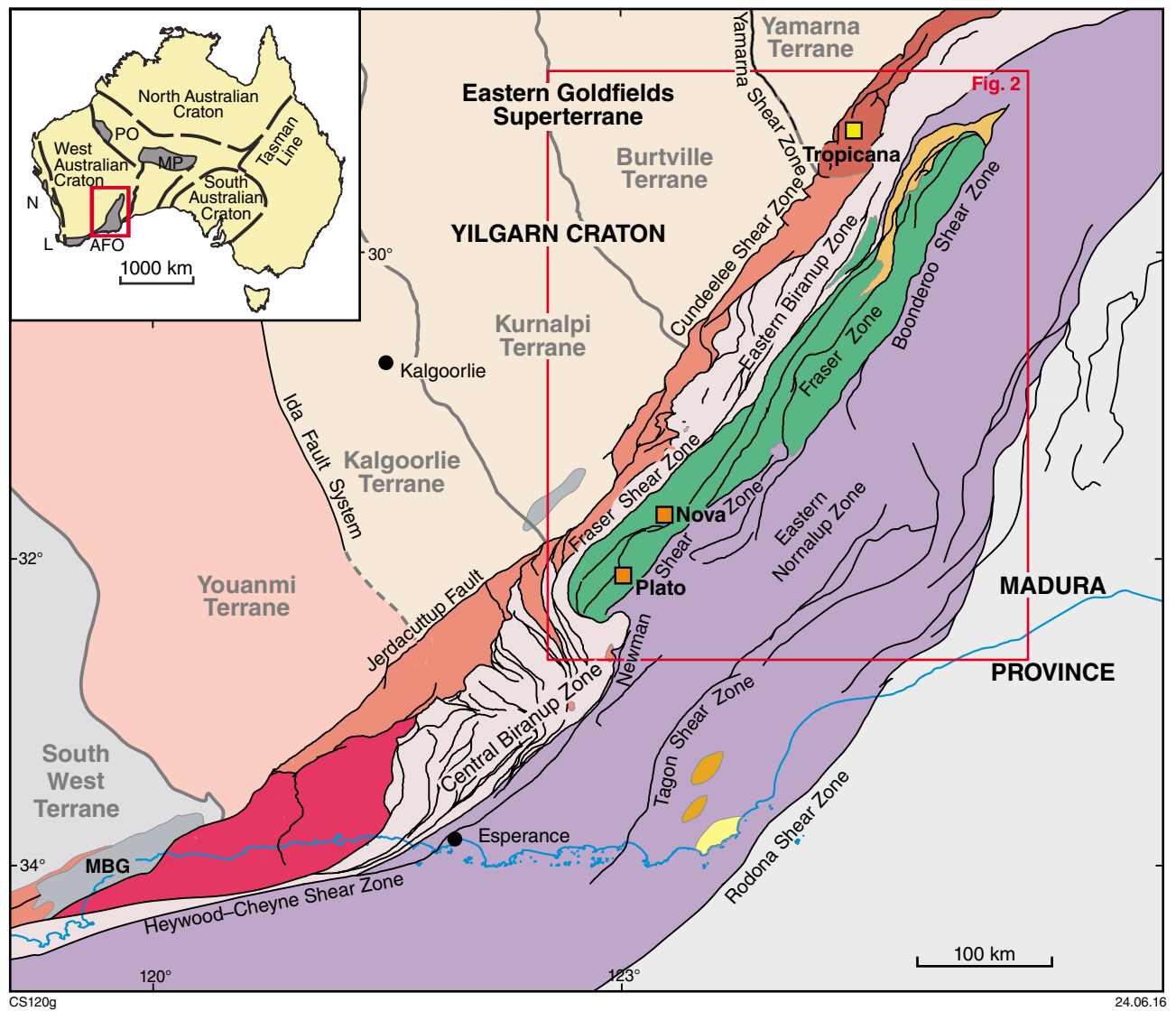
The discovery, in 2014, of disseminated Ni–Cu sulfide (up to 0.47% Ni and 0.15% Cu) in ultramafic cumulate rocks 54 km to the southwest of Nova–Bollinger at the Plato Prospect (Enterprise Metals Ltd., WAMEX report A103177; Venables, 2014) (Figs 1,2), and of traces of orthomagmatic Ni-sulfides in early exploration programs in that region (see Bennett et al., 2014), suggests that the answer to the third question might be yes, even though exploration around the Plato Prospect has so far failed to identify economic mineralization.

The methodology adopted in GSWA's Albany–Fraser Orogen regional geoscientific mapping program is to integrate geophysical interpretations with lithological relationships and structural, geochronological, and geochemical analysis of available outcrop and subsurface sampling. A critical aspect of our geochemical sampling has been access to both EIS co-funded and donated company diamond drillcore. Also important has been access to bottom-of-hole rock chip samples from regional RAB drilling programs conducted by the Creasy Group of Companies, 130–150 km northwest of Nova–Bollinger (Fig. 2).

This Record updates and adds to findings presented in GSWA Record 2013/5 (Smithies et al., 2013). We examine the composition of the mafic–ultramafic rocks of the Fraser Zone, including those from EIS co-funded drillcore obtained from the Nova–Bollinger deposit and from the Plato Prospect. We use these data and the resulting constraints on magmatic petrogenesis to evaluate potential petrogenetic relationships between these rocks, and attempt to identify potential constraints on the formation of orthomagmatic sulfide deposits within this region of the Albany–Fraser Orogen.

Regional synthesis

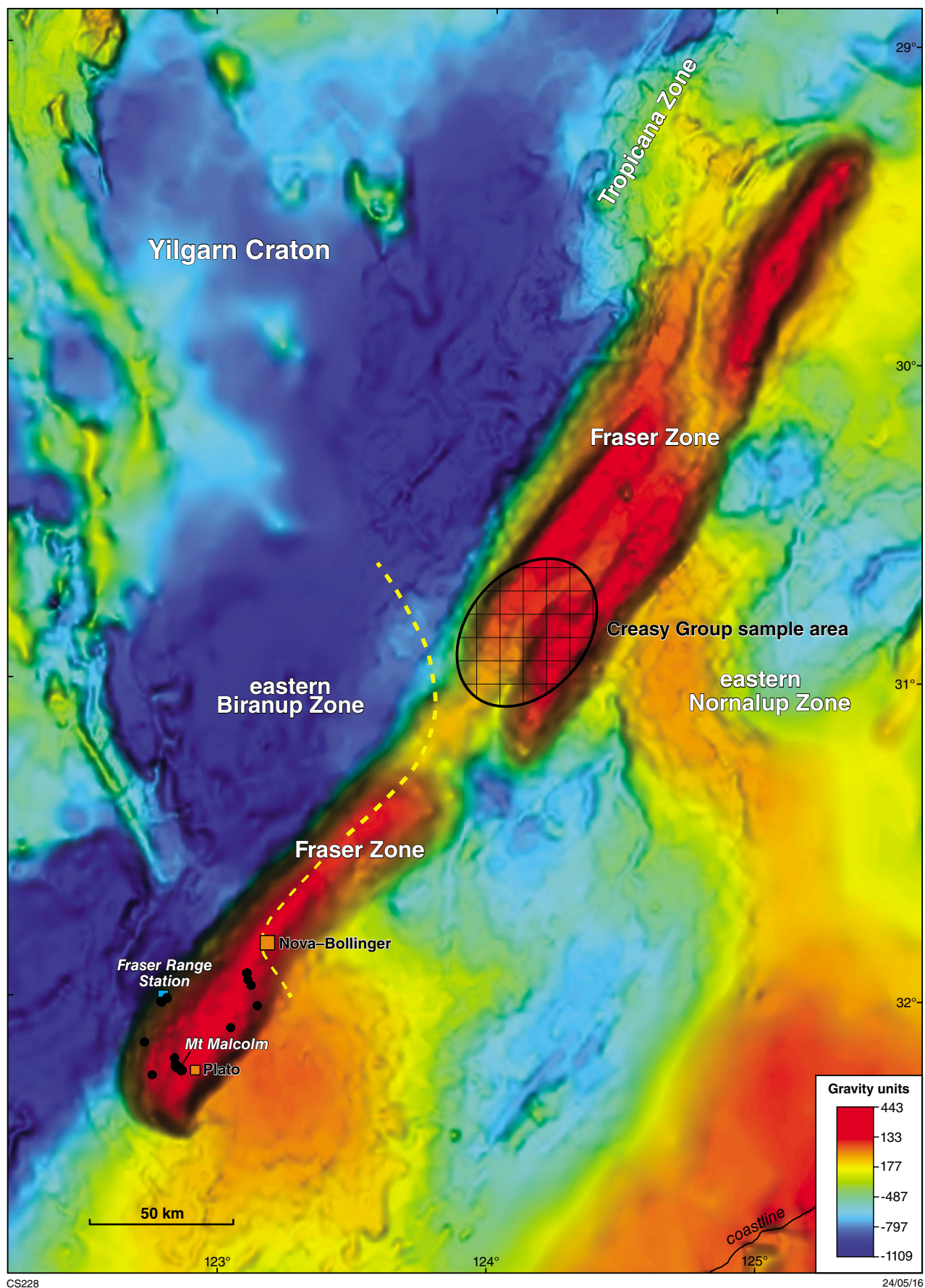
The Albany–Fraser Orogen is part of the West Australian Craton and formed through Neoproterozoic to Mesoproterozoic events that reworked the southern and southeastern margin of the Archean Yilgarn Craton (Kirkland et al., 2011; Spaggiari et al., 2014a, 2015a). This reworked Archean crust extends as far east as the Rodona Shear Zone, which separates the orogen from the Madura Province (Fig. 1; Spaggiari et al., 2012, 2014b, 2015a; Smithies et al., 2015). The Albany–Fraser Orogen comprises two main tectonic units that differ in their structural position and degree of craton modification — the Northern Foreland and the Kepa Kurl Booya Province. The Northern Foreland is the thrust-dominated transition zone between nonreworked rocks of the Yilgarn Craton and the Kepa Kurl Booya Province. It comprises minor remnant greenstones within Neoproterozoic metagranite and granite gneiss of the Yilgarn Craton which were deformed and metamorphosed during the Mesoproterozoic Albany–Fraser Orogeny (Spaggiari et al., 2011).



CS120g

24.06.16

Figure 1. Simplified, pre-Mesozoic interpreted bedrock geology of the east Albany–Fraser Orogen and tectonic subdivisions of the Yilgarn Craton (modified from Spaggiari et al., 2014a)



CS228

24/05/16

Figure 2. Gravity image showing the full extent of the Fraser Zone (strong gravity response), approximate limit of outcrop (south and west of yellow dashed line), and sample localities. Black dots are the locations of the outcrop samples listed in Record 2013/5. Hatched ellipse is the area where samples from the Creasy Group of Companies were obtained.

The Kupa Kurl Booya Province is divided into the Tropicana, Biranup, Fraser and Nornalup Zones (Spaggiari et al., 2009, 2014a; Occhipinti et al., 2014). The Tropicana Zone is dominated by Neoproterozoic rocks interpreted to have an affinity with the Yilgarn Craton, but with a different history and structural position to those of the Northern Foreland (Occhipinti et al., 2014; Kirkland et al., 2014; Tyler et al., 2014). The Biranup Zone is dominated by midcrustal orthogneiss and metagabbro with ages of 1810–1625 Ma, and contains isolated remnants of Yilgarn Craton granite (Spaggiari et al., 2011; Kirkland et al., 2011). The eastern Nornalup Zone contains Paleoproterozoic basement rocks of similar age and isotopic character to the Biranup Zone, but is more extensively intruded by Mesoproterozoic granitic rocks of the 1330–1280 Ma Recherche Supersuite and the 1200–1140 Ma Esperance Supersuite (Kirkland et al., 2014; Smithies et al., 2015).

A dominantly extensional geodynamic regime is interpreted to have persisted throughout much of the Albany–Fraser Orogen's history, exemplified by its two extensive basin systems — the 1815–1600 Ma Barren Basin and the 1600–1305 Ma Arid Basin (Spaggiari et al., 2014c, 2015a). Formation of the Barren Basin was accompanied by voluminous magmatism during the 1815–1800 Ma Salmon Gums Event, the 1780–1760 Ma Ngadju Event, and the 1710–1650 Ma Biranup Orogeny (Spaggiari et al., 2014a,c; Smithies et al., 2015). This magmatism records progressive recycling of Yilgarn crust as it extended, together with episodic addition of juvenile mafic material (Spaggiari et al., 2014c, 2015a; Kirkland et al., 2014; Smithies et al., 2015). Hyperextension of the craton margin resulted in the formation of an ocean–continent transition flanked by a passive margin, and deposition of the Arid Basin (Spaggiari et al., 2014c, 2015a). By c. 1450 Ma the tectonic setting had changed to convergence, leading to accretion of the juvenile, oceanic and oceanic-arc crust of the Madura Province (Loongana Arc), and triggering Stage I (1330–1260 Ma) of the Albany–Fraser Orogeny (Spaggiari et al., 2015a; Smithies et al., 2015). Craton-vergent thrusting during accretion was accompanied by foreland basin development, allowing sediments derived from the accreted portion of the Madura Province to be deposited inboard (Snowys Dam Formation of the upper part of the Arid Basin; Spaggiari et al., 2014c, 2015a). Stage II (1225–1140 Ma) of the Albany–Fraser Orogeny was a response to widespread melting and magmatism (Esperance and Moodini Supersuites) that engulfed the southeastern part of the orogen and the Madura Province, accompanied by reactivation of major structures (Spaggiari et al., 2011; Kirkland et al., 2014; Smithies et al., 2015; Spaggiari and Smithies, 2015).

The Fraser Zone

The extent of the Fraser Zone is defined by a strong, northeasterly trending gravity anomaly that is approximately 425 km long and 50 km wide (Fig. 2). The strong gravity signal is interpreted to be due to significant accumulations of mafic to ultramafic rocks. These rocks

are bound to the northwest by the Fraser Shear Zone, and to the southeast by the Newman and Boonderoo Shear Zones (Spaggiari et al., 2011). Interpretations of deep crustal seismic reflection data suggest that these shear zones form a V-shape to approximately 13 km depth (Spaggiari et al., 2014b). Only the southern portion of the Fraser Zone is exposed, whereas the northern portion is covered by thick sandy regolith and limestones of the Eucla Basin.

The Fraser Zone is dominated by voluminous sheets of metagabbro (Fraser gabbro) and less-abundant metagranitic rocks, both of which have intruded sedimentary rocks of the Snowys Dam Formation of the Arid Basin (Spaggiari et al., 2014c, 2015a). These rocks have been deformed and metamorphosed to granulite facies, forming complex layering from primary and secondary processes (the Fraser Range Metamorphics; Spaggiari et al., 2009, 2011; Clark et al., 2014). Ultramafic rocks appear to be less common than gabbroic rocks. They typically occur in the central portions of some of the gabbroic sills (e.g. at Mount Malcolm), but also form an important component within larger cumulate bodies, including the host rocks to the Nova–Bollinger Ni–Cu sulfide deposit, discussed in more detail below.

The Snowys Dam Formation is a succession of upper amphibolite to granulite facies, pelitic, semipelitic to calcic, locally iron- and/or sulfide-rich metasedimentary rocks with abundant layers and sills of Fraser gabbro. These rocks have a maximum depositional age of 1332 ± 21 Ma, and their detrital zircon provenance indicates derivation from the accreted Loongana Arc and oceanic crust of the Madura Province (Spaggiari et al., 2014c, 2015b). The maximum depositional age indicates deposition shortly before intrusion into the Fraser Zone of contemporaneous gabbroic and felsic rocks between 1305 and 1280 Ma (De Waele and Pisarevsky, 2008; Spaggiari et al., 2014c, 2015a; Kirkland et al., 2014). The intrusion age-range overlaps available metamorphic dates indicating a strong connection between these processes (Clark et al., 2014). Pelitic rocks of the Snowys Dam Formation record peak granulite facies metamorphism of c. 850 °C at 7–9 kbar at c. 1290 Ma (Clark et al., 2014). The P–T conditions were determined from metamorphic assemblages with a gneissic fabric (Oorschot, 2011) and probably relate to folding and, potentially, crustal thickening (Smithies et al., 2013). An Rb–Sr whole-rock biotite age from a thick gabbroic sill suggests that at least the internal parts of the Fraser Zone, from where the sample was collected, cooled below the biotite closure temperature at c. 1268 Ma (Fletcher et al., 1991). This indicates that the Fraser Zone had been exhumed and cooled prior to Stage II (1225–1140 Ma) of the Albany–Fraser Orogeny. However, significant movement on the major bounding shear zones, and potentially localized internal shear zones, must have taken place during Stage II when the Fraser Zone was juxtaposed against the adjacent Biranup and eastern Nornalup Zones, which record upper amphibolite to granulite facies metamorphism at this time (Kirkland et al., 2011, 2014).

Magmatic rocks formed during Stage I of the Albany–Fraser Orogeny

The 1330–1280 Ma Recherche Supersuite (Nelson et al., 1995; Clark et al., 2000; Smithies et al., 2015) is the magmatic expression of Stage I of the Albany–Fraser Orogeny. Magmatic rocks of the Fraser Zone form components of this supersuite, and the granitic rocks are broadly subdivided into two groups, or suites. Local anatectic melts of Arid Basin metasedimentary rocks are typically peraluminous syenogranites, referred to as the Southern Hills Suite (Smithies et al., 2014, 2015). Typically metaluminous granites form part of the Gora Hill Suite and are relatively rare within the Fraser Zone, but are more regionally distributed throughout the southeastern part of the Biranup Zone and the eastern Nornalup Zone (Smithies et al., 2015). Within the Fraser Zone, the Gora Hill Suite is restricted to rocks of granodioritic composition. Geochemical and isotopic data suggest that compositional variation within the Gora Hill Suite can be largely attributed to variable mixing between mantle-derived melts equivalent to the parental melts of the Fraser gabbro and felsic partial melts of crust formed during the Paleoproterozoic events (Kirkland et al., 2014; Smithies et al., 2014, 2015).

Condie and Myers (1999) argued that the Fraser gabbro has trace-element characteristics typical of subduction-related magmatism, and proposed that the Fraser Zone represented the remnants of oceanic arcs accreted at c. 1300 Ma. This model had a strong influence on subsequent interpretations of the Mesoproterozoic tectonic evolution of southwestern and central Australia (Clark et al., 2000; Bodorkos and Clark, 2004). However, recent Hf isotope data and the analysis of inherited zircons in granites (Kirkland et al., 2011) have shown that the Fraser gabbro represents juvenile magma additions to extended crust of the Yilgarn Craton margin. The geochemical signature of the gabbros can be modelled as having assimilated small amounts (<<10%) of known basement material, rather than requiring a significantly subduction-modified source (Smithies et al., 2013).

Sample material

More than 150 samples of mafic–ultramafic intrusive rocks from the Fraser Zone have been sampled for major- and trace-element geochemistry. Samples collected by GSWA, including those from EIS cores, were for the purpose of characterizing primary magma compositions, magma evolution trends, and investigating potential petrogenetic relationships.

The whole-rock dataset includes all samples discussed by Smithies et al. (2013). Added to these samples are 26 samples from the SFRD 0017 drillcore that was located just above the main ore zone of the Nova–Bollinger deposit, and 27 samples from EIS co-funded drillcore from the Plato Prospect of Enterprise Metals (Ltd) (Venables, 2014). To help better constrain petrogenetic processes throughout the Fraser Zone, the Creasy Group of

Companies has donated fresh (bottom of drillhole [BOH]) bedrock rock chips from a representative range of mafic and ultramafic rocks. These are sourced from exploration tenements within unexposed portions of the Fraser Zone, approximately 130–150 km to the northeast of Nova–Bollinger (Fig. 2). The Creasy Group of Companies also provided access to diamond core comprising sulfide-bearing metasedimentary rocks of the Snowys Dam Formation, from their Sunline Prospect within these tenements.

Selected sample suites have also been analysed for their Nd isotopic composition, whole-rock and mineral (sulfide) sulfur isotopic compositions, mineral (plagioclase) Sr isotopic composition, whole-rock platinum group element (PGE) concentrations and mineral (olivine, pyroxene, plagioclase) major element compositions. Analytical procedures are discussed in Appendix 1. New whole-rock major- and trace-element data from Nova–Bollinger and from the Plato Prospect that were not presented in Smithies et al. (2013) are presented in Appendix 2. PGE data are presented in Appendix 3. Isotopic data are presented in Appendices 4 (S and Sr) and 5 (Nd).

Outcrop descriptions and petrography

Metagabbros of the Fraser Zone form sheets up to hundreds of metres wide within metasedimentary rocks of the Snowys Dam Formation. These sheets appear to thicken to the southeast where, for example, in the vicinity of the Plato Prospect (Figs 1 and 2), metagabbroic rocks become much more abundant than the metasedimentary host rocks. At many localities, the common occurrence within the metagabbros of metasedimentary inclusions, stringers, and schlieren, and of mingling textures, provides clear evidence for the incorporation of metasedimentary country rock. Local melts of country rock, or contemporaneous granodiorite intrusions, are also preserved (Fig. 3). Thus the metagabbros can be broadly divided into hybrid rocks (further subdivided into two groups below) and rocks that show no field or geochemical evidence for contamination — referred to as the ‘main gabbros’. All rocks studied here have been subjected to granulite facies conditions. Fine-grained rocks are typically strongly recrystallized, but many medium- to coarse-grained mafic and ultramafic rocks retain their igneous textures, including subophitic textures in gabbroic rocks and ortho- to adcumulate textures.

Main gabbro

Samples of the main gabbro (Fig. 4a) show a range of textures, from near pristine igneous intergranular or subophitic to granoblastic (metamorphic). The full range of textures can be observed at single localities, indicating that magmatism was prolonged, or occurred in several stages, and outlasted local metamorphic events. Zones of relatively high strain show pronounced foliation, but in many cases this is overprinted by a granoblastic texture. Crosscutting contact relationships between individual

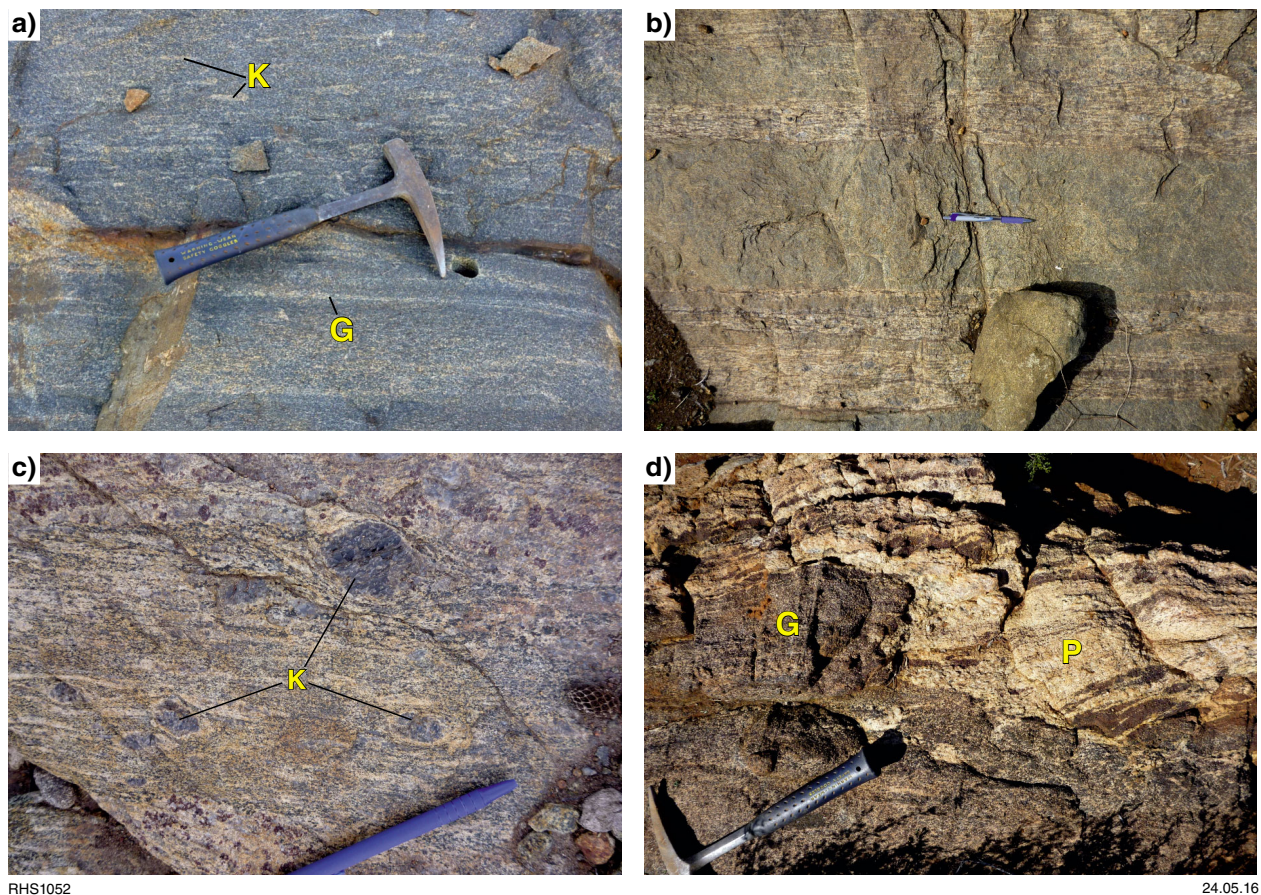


Figure 3. Field photos of the Fraser Range Metamorphics, southern Fraser Zone: a) metagabbro with wispy and thin layers of granitic material, and sparse K-feldspar phenocrysts (K), Phil's Quarry; b) metagabbro (dark) interlayered with granite (pale), gully exposure at Wyranilu Hill; c) K-feldspar porphyroclasts (K) in hybrid metagabbroic to metagranitic rocks, Wyranilu Hill; d) gabbro (G) intruded into psammitic gneiss (P) of the Snowys Dam Formation, near the Yardilla prospect

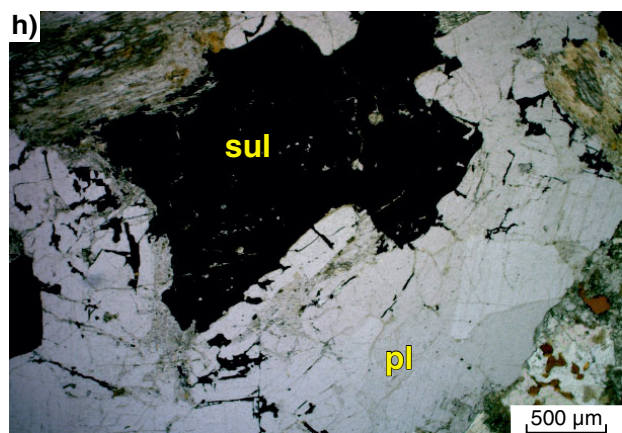
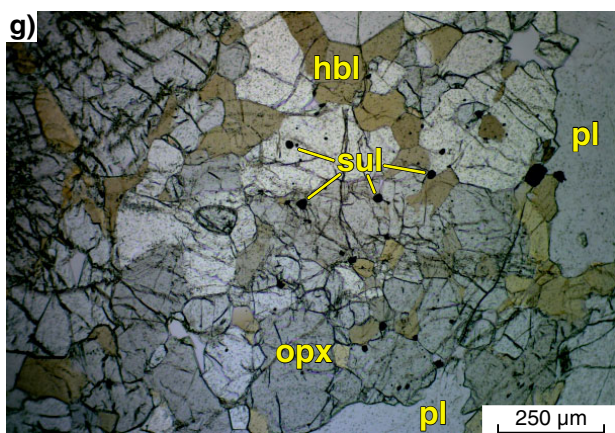
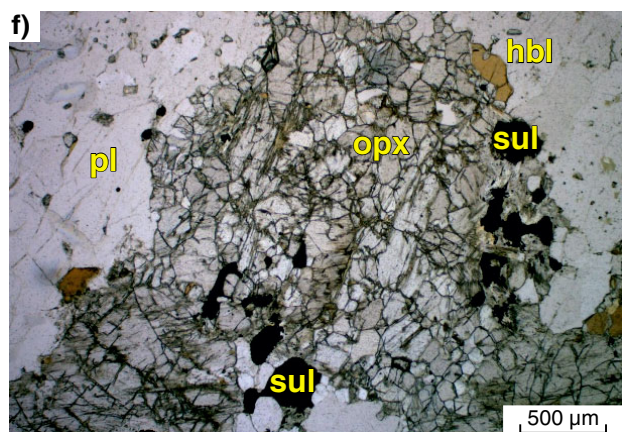
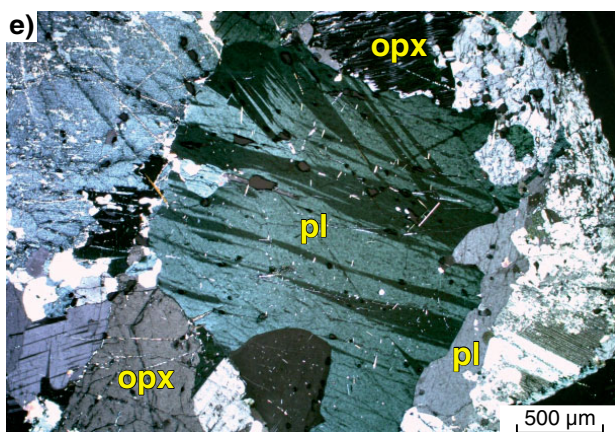
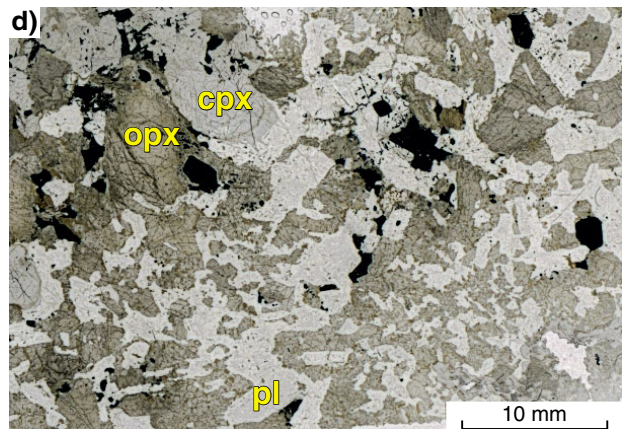
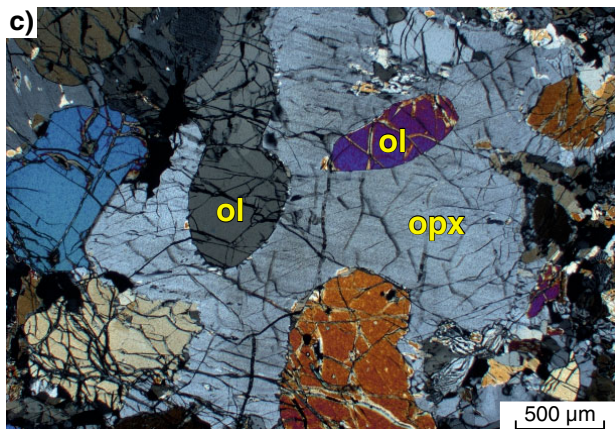
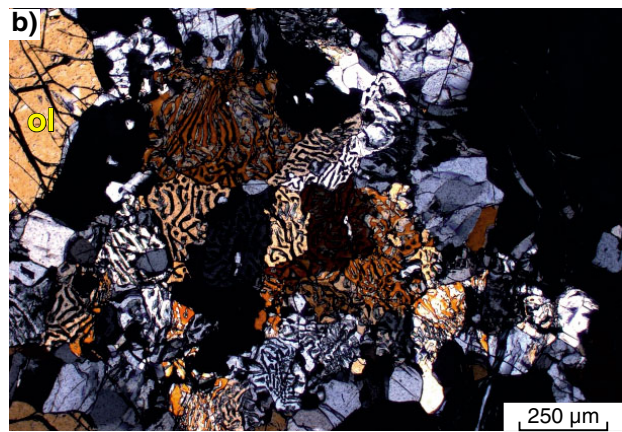
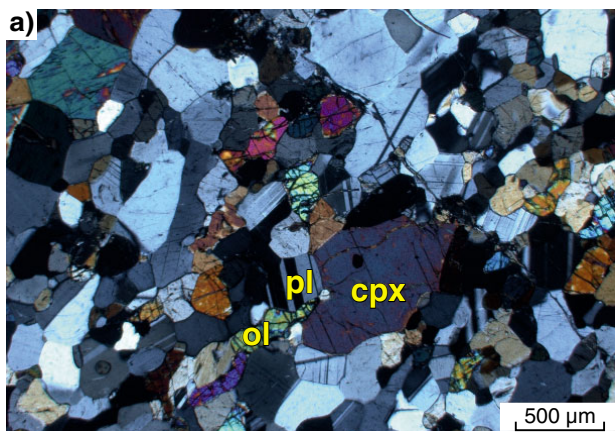
sheets, and the presence of gabbro inclusions in texturally distinct gabbro host rocks, clearly indicate a complex intrusion history. The main gabbros comprise fine- to medium-grained, mesocratic olivine gabbro and olivine gabbro-norite, containing 35–60% plagioclase (An_{55-70}), up to 15% anhedral to subhedral olivine that is partially enclosed within orthopyroxene, up to 50% intergranular, poikilitic or granoblastic pyroxene, with clinopyroxene being more abundant than orthopyroxene, up to 5% magnetite, as well as up to 10% brown biotite. Rare, fine- to medium-grained samples from Mount Malcolm contain up to 25% olivine and have weakly developed cumulate textures.

In granoblastic rocks, biotite is either absent or forms flakes which may be strongly aligned with the gneissic foliation. Brown hornblende is a notable component of most of the rocks, forming up to 20% of the mode. It rims biotite and pyroxene, commonly as granoblastic aggregates. Sulfides are rare and are mainly confined to the Mount Malcolm locality where they form blebs consisting of pyrrhotite, flame and granular pentlandite and chalcopyrite.

Hybrid gabbros

The hybrid gabbros have been subdivided into 'Group 1' and 'Group 2'. These groups are readily distinguished geochemically, for example, in terms of their Th vs La, K, Pb trends (Fig. 5; Smithies et al., 2013). Field observations indicate that whereas the Group 2 hybrid gabbros have physically incorporated (e.g. mingled with) felsic material at the level of intrusion, such evidence is rare in the case of Group 1 hybrids.

Both groups are fine- to medium-grained, mesocratic rocks, commonly showing well-developed granoblastic textures. In some cases, they preserve an igneous intergranular to subophitic texture. In contrast to the main gabbros, they typically contain little or no olivine and some samples contain rare interstitial quartz. Some samples, for example from the Wyralinu Hill locality, contain garnet poikiloblasts up to 6 mm in size. Where present, hornblende is typically brown but locally ranges to brown-green to green. Some Group 2 hybrid gabbros are texturally heterogeneous and complex, comprising fine-grained granoblastic domains enclosing felsic



RHS1056

25.05.16

Figure 4. (opposite) Photomicrographs of Fraser Zone rocks: a) gabbronorite from the Mount Malcolm area, sample GSWA 183654; b) lherzolite from Nova-Bollinger EIS core SFRD0017, sample GSWA 201236, 96 m depth — note symplectitic intergrowth of pyroxene and plagioclase with secondary green spinel; c) harzburgite from Nova-Bollinger EIS core SRFR0017, sample GSWA 201236, 96 m depth; d–h) gabbronorite from Nova-Bollinger EIS core SRFR0017, sample GSWA 201255, 56.85 m — note the heterogeneous texture in d), with domains of relatively fine-grained norite interpreted as fragments; e) deformation of plagioclase expressed by bent and spindle-like twin lamellae; f–g) fragments of fine-grained sulfide-rich orthopyroxenite; h) remobilized vein-style sulfides in the periphery of intercumulus sulfide

domains forming layers, elongate blebs or wisps up to 3 cm long, and consisting of plagioclase (commonly antiperthitic), lesser amounts of quartz and rare perthite.

Rocks from the Nova-Bollinger drillcore SRFR0017

Samples taken from the Nova-Bollinger drillcore SRFR0017 include lherzolite, wehrlite, websterite, gabbronorite and anorthosite. The rocks are mostly medium grained (Figs 4b–h), but some of the gabbronoritic and noritic rocks are fine-grained. Contacts between these two grain-size variants tend to be gradational on the scale of millimetre to centimetre. In the lower portion of the drillcore, the metagabbro is interlayered with metasedimentary rocks, and there are several decimetre-scale dolerite veins. Most samples are relatively unaltered, or are weakly to moderately altered in the form of sericitization of plagioclase, locally abundant brown hornblende, and serpentine veins in olivine. The textures are typically granular, but harzburgites consisting of orthopyroxene oikocrysts and olivine chadacrysts also occur (Fig. 4c). Gabbronoritic sample GSWA 201255 contains fine-grained domains of granular norite embedded in a matrix of medium- to coarse-grained gabbronorite (Figs 4g–h). The fine-grained domains contain elevated contents of finely disseminated sulfides (pyrrhotite, pentlandite and chalcopyrite) and are interpreted to represent autoliths of a mineralized intrusive within a less-mineralized matrix.

Ultramafic cumulates show a range of lithologies, the most common being pokilitic lherzolite with clinopyroxene and subordinate orthopyroxene oikocrysts up to 1 cm in diameter. These are interlayered with granular lherzolite containing subequant olivine and orthopyroxene, typically 1–2 mm in diameter, and orthopyroxenite and websterite with minor olivine and patches of interstitial plagioclase. Clinopyroxene is typically rimmed with brown hornblende. The interstitial space in the pyroxene-rich lithologies is typically occupied by a distinctive symplectitic intergrowth of pyroxene (probably inverted pigeonite) and plagioclase. Orthopyroxene and

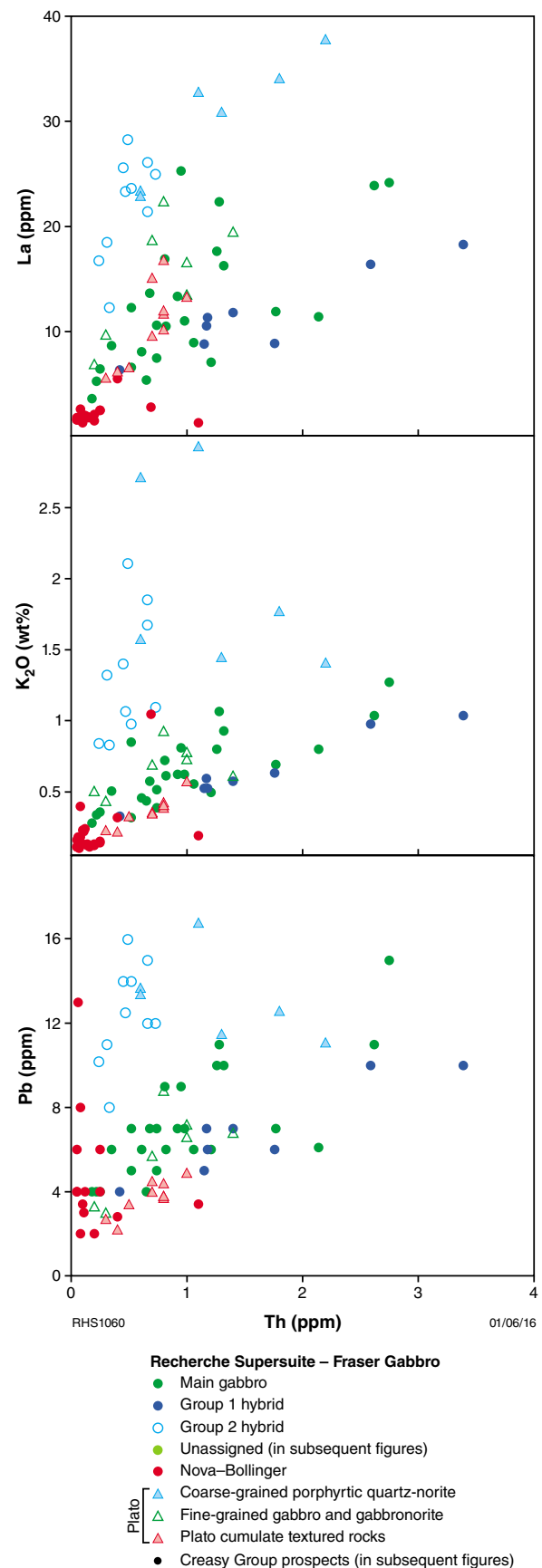


Figure 5. Compositional variation diagrams (Th vs La, K₂O and Pb) discriminating between main gabbros and Group 1 and Group 2 hybrid gabbros

clinopyroxene typically constitute 10–20% of the rock, except in websterite. A metamorphic overprint exists in the form of subgrain coronas of pyroxene around olivine, abundant small grains of green and brown spinel, and symplectic intergrowths of pyroxene and plagioclase with secondary green spinel (Fig. 4b). These textures resemble those displayed by ultramafic rocks of the Giles intrusions in central Australia (Glickson et al., 1996; Maier et al., 2015) where they were interpreted to reflect Al-transfer from plagioclase to spinel during high-pressure cooling. Plagioclase is mostly intercumulus, but subhedral cumulus grains also occur. Brown mica and apatite are accessory phases and chromite is a ubiquitous trace phase in the olivine cumulates. Veins contain calcite and epidote, and have locally vuggy or colloidal forms. There are also fibrous zones associated with brittle deformation and veining, and brecciated zones. Sulfides constitute up to approximately 10% of the rock, either in the form of intercumulus or droplet-like grains, mostly smaller than 0.5 mm. As discussed above, in some of the rocks there appear to be two distinct modes of occurrence: i) within fine- to medium-grained, granular textured domains of the rocks (see above) with a typically magmatic assemblage of pyrrhotite, granular pentlandite and chalcopyrite, and ii) as interstitial and vein-style sulfides in the coarser grained portions of gabbro and anorthosite, and as fracture fillings dominated by chalcopyrite (Fig. 4h).

Rocks from the Plato Prospect

Drilling at the Plato Prospect was designed to investigate a broadly southeast-trending, remnant magnetized, magnetic anomaly (Fig. 6), coincident with an electromagnetic (EM) anomaly and a Ni–Cu–Co soil anomaly (Venables, 2014). Our investigation of the EIS drillcores from this prospect identifies three main rock types. These include: i) coarse-grained, plagioclase-porphyrific quartz-norite or diorite (Fig. 7a); ii) fine-grained gabbro to gabbro-norite (Fig. 7b), and; iii) medium- to coarse-grained, cumulate-textured, gabbro-norite, norite and olivine-norite (Fig. 7c). All rocks have been subjected to granulite facies recrystallization, producing local to near pervasive granoblastic textures, and minor brown hornblende at the expense of pyroxene.

Coarse-grained plagioclase-porphyrific quartz-norite and diorite define the margins of, or are peripheral to, the geophysical anomaly (PLDT 005 and 006; Fig. 6). The quartz-norite or diorite typically comprises subhedral plagioclase crystals up to 1.5 cm in size, or plagioclase aggregates forming up to 80% of the mode. Quartz forms <5% of the mode and, although occurring as anhedral phenocrysts (possibly xenocrysts) up to 3 mm in size, it is primarily restricted to interstitial spaces between plagioclase crystals. Orthopyroxene is the main mafic mineral (~15%), present mostly as a fine-grained aggregate between feldspar phenocrysts. Blebbly opaque minerals form ~5% of the mode and brown biotite is a late phase forming flakes and rims associated with orthopyroxene and opaque minerals.

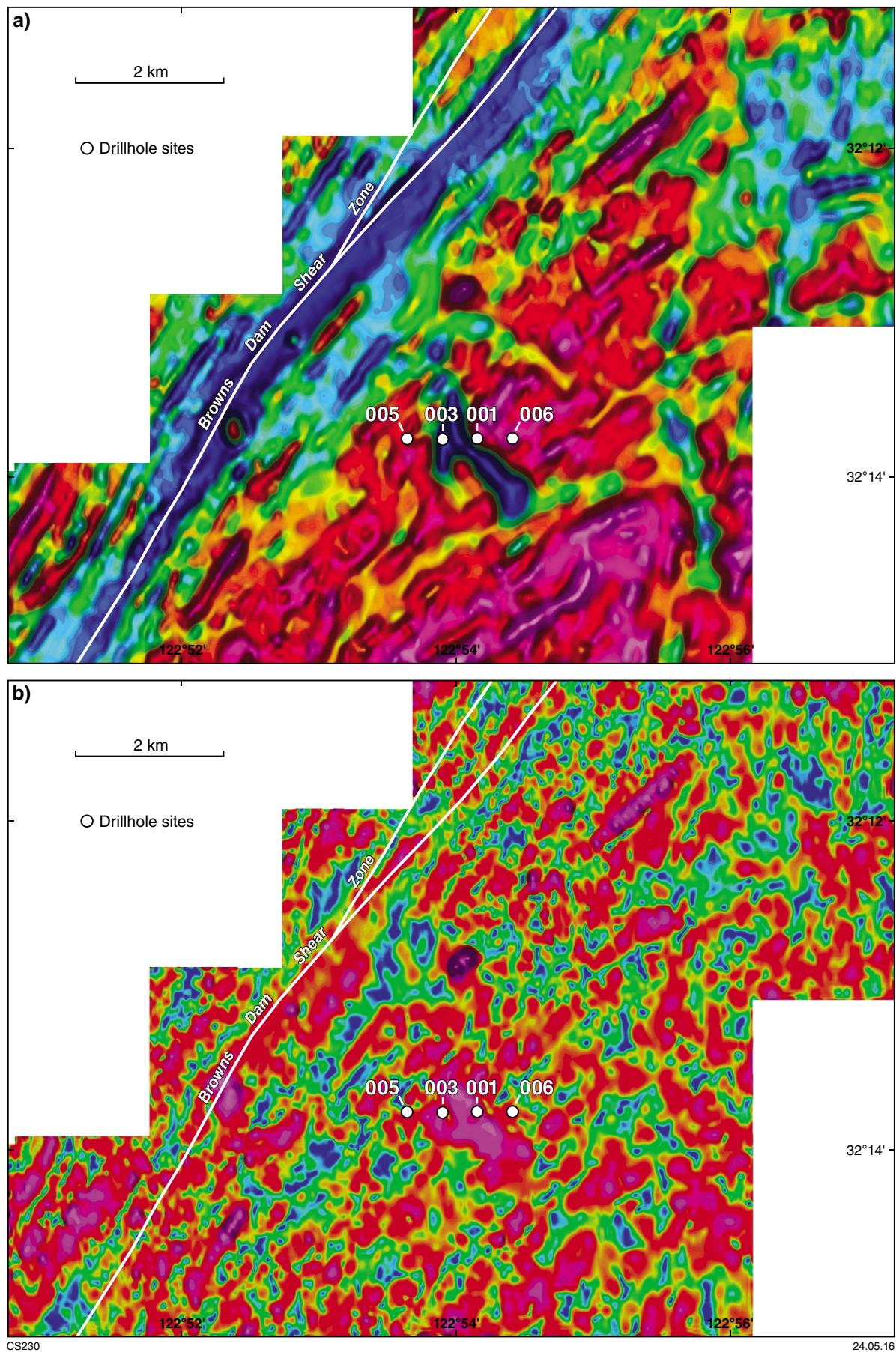
Fine-grained gabbro to gabbro-norite intrudes the quartz-norite or diorite but also forms a significant component within the geophysical anomaly shown in Figure 6 (PLDT 001 and 003). The fine-grained gabbro to gabbro-norite typically has a granoblastic texture, at least locally superimposed on a subophitic primary texture, and reflecting medium- to high-grade metamorphic recrystallization. These rocks contain between 30 and 50% pyroxene (orthopyroxene > clinopyroxene) and up to 5% each of opaque minerals and late brown biotite.

Although the nature of contacts are never unequivocal, the fine-grained gabbro to gabbro-norite at least locally appears to be gradational to medium- to coarse-grained, ortho- to mesocumulate-textured, gabbro-norite, norite and olivine-norite, which is the dominant host to the magmatic sulfides. The gabbro-norite and norite comprise up to 60% mafic minerals. The mafic assemblage is dominated by a loose to near interlocking network of subhedral to euhedral orthopyroxene crystals (Fig. 8a,b), in some cases with olivine cores and locally partially enclosed by, or included within, clinopyroxene crystals and oikocrysts. Recrystallization of orthopyroxene has resulted in blebs of clinopyroxene and conspicuous zones containing abundant elongate exsolution lamellae of rutile alternating with lamellae-free zones and reflecting originally zoned crystals. Intercumulus plagioclase forms up to 50% of the mode while opaque minerals, brown biotite, brown hornblende and green spinel are accessory phases. The olivine-melanorite contains up to 70% rounded (resorbed) olivine (Fig. 8c,d), locally rimmed or included by orthopyroxene and both partially enclosed within rare clinopyroxene. Pyroxene typically constitutes 15–25% of the mode, intercumulus plagioclase forms 15–20% of the mode, while opaque minerals, brown biotite, brown hornblende and green spinel are accessory phases.

A notable contrast between the drillcores from Nova-Bollinger and the Plato Prospect is the local abundance of metasedimentary lithologies in the former. At Plato, metasedimentary xenoliths are inferred on the basis of garnet-bearing felsic rock, but these are extremely rare and small.

Previous petrographic descriptions of samples from Plato (in Venables, 2014) note the presence of primary sulfides in all rocks — mainly pyrrhotite with subordinate chalcopyrite and pentlandite — but typically in amounts less than 2–3%.

Figure 6. (opposite) Aeromagnetic images showing the drillhole sites at the Plato Prospect, from west to east: PLDT005 (dominantly gabbro-noritic 'main gabbro'), PLDT003 (mix of gabbro-noritic main gabbro and cumulate rocks), PLDT001 (mostly cumulate rocks), and PLDT006 (dominantly gabbro-noritic main gabbro): a) reduced to pole magnetic image; b) analytic signal magnetic image. Note the crosscutting, remnant magnetized intrusion that correlates with the cumulate rocks. Open file, 100 m line-spacing magnetic dataset 70470, Enterprise Metals Ltd., Fraser Range Area 2.



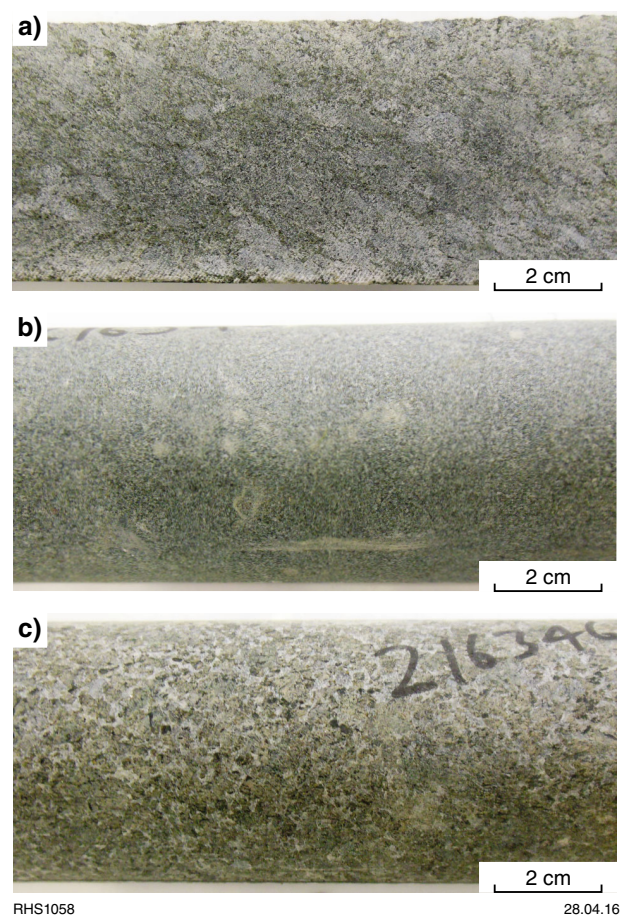


Figure 7. Photos of core from the Plato Prospect; a) coarse-grained, plagioclase-porphyritic quartz-norite (PLDT005, 358.9 m, sample 216377); b) fine-grained gabbro (PLDT005, 359.2 m, sample 216340); c) medium-grained cumulate-textured olivine norite (PLDT001, 392.7 m, sample 216346). Width of core is 5 cm.

Mineral compositions

The compositions of olivine, orthopyroxene, clinopyroxene, and plagioclase were determined by Electron Probe Micro-Analysis (EPMA) (Appendix 6) from norites, gabbro-norites, and harzburgites sourced from the Nova-Bollinger intrusion, and norite and olivine-gabbro-norite from the Plato Prospect.

The forsterite content of olivine from the Nova-Bollinger intrusion varies from $\sim\text{Fo}_{80}$ to Fo_{83} , with olivine in the harzburgites having slightly higher forsterite content than in the norites and gabbro-norites. Olivine in olivine-norite from Plato is considerably more Fe rich than olivine in the Nova-Bollinger core, ranging from Fo_{75} to Fo_{77} . The Ni content of olivine in the Nova-Bollinger harzburgite and gabbroic samples broadly overlap within range of ~ 900 – 1700 ppm (Fig. 9) and there is little systematic variation with sample depth for individual rock types.

In general, most Nova-Bollinger olivines are relatively depleted in Ni compared to olivines from most layered intrusions and basic-ultrabasic lavas globally (Fig. 9). In contrast, olivine in the Plato olivine-norite is Ni-undepleted, ranging to higher Ni concentrations (1560–2200 ppm) at much lower forsterite content (Fig. 9).

The $\text{Mg}^\#$ of orthopyroxene in Nova-Bollinger samples is between 71 and 84. Concentrations of Cr_2O_3 in orthopyroxene are up to 0.62 wt% in harzburgite but <0.1 wt% in orthopyroxene from norite and olivine gabbro. Al_2O_3 contents of orthopyroxene vary from 1.5 wt% in norite to 4 wt% in gabbro-norite and harzburgite. In the Plato samples, the $\text{Mg}^\#$ of orthopyroxene in norite is between 70 and 72 and in the olivine-norite is between 78 and 79. Concentrations of Cr_2O_3 in orthopyroxene are both within the range of 0.15 and 0.34 wt% and Al_2O_3 contents range from ~ 2.8 wt% in the norite to ~ 1.8 wt% in the olivine-norite.

Clinopyroxene in the Nova-Bollinger samples has $\text{Mg}^\#$ between 79 and 89, with up to 1.27 wt% Cr_2O_3 in harzburgite. In the norite from Plato, the $\text{Mg}^\#$ of clinopyroxene is between 71 and 79 and Cr_2O_3 contents of clinopyroxene range between 0.2 and 0.51 wt%.

Plagioclase in Nova-Bollinger samples is a cumulus phase and ranges in composition from An_{62} to An_{89} . Plagioclase in the Plato samples is mainly an intercumulus phase and shows a much narrower and evolved compositional range from An_{48} to An_{63} .

Whole-rock geochemistry

Selected major- and trace-element variations in the mafic and ultramafic rocks are plotted against MgO in Figure 10. The compositions of some key minerals are also plotted in some of the individual diagrams based on microprobe data from Nova-Bollinger and Plato samples.

Apart from a few samples from Mount Malcolm, samples of the main gabbro do not show cumulate textures. With decreasing MgO, these main gabbros and Group 1 hybrid gabbros show mainly continuous trends to higher SiO_2 , TiO_2 , FeO, K_2O , Na_2O and P_2O_5 and decreasing Al_2O_3 and CaO (Fig. 10) consistent with a typical tholeiitic liquid line of descent. At lower MgO values (<6 wt%), the Group 2 hybrids extend these major element trends, except for FeO and TiO_2 , both of which decrease sharply, as is typical of evolved tholeiitic magmas that crystallize abundant magnetite. These trends, as well as ranges to higher concentrations of SiO_2 (to 59.01 wt%), K_2O (2.53 wt%), Ba, Pb, Zr, and higher La/Th ratios than most main gabbros, distinguish the Group 2 hybrids (Fig. 11). For most major- and trace-element compositions, Group 1 hybrids typically lie within the range of the main gabbros, but to the higher end of that range for elements such as Th and Pb and for ratios such as Th/Nb, which are sensitive to crustal contamination.

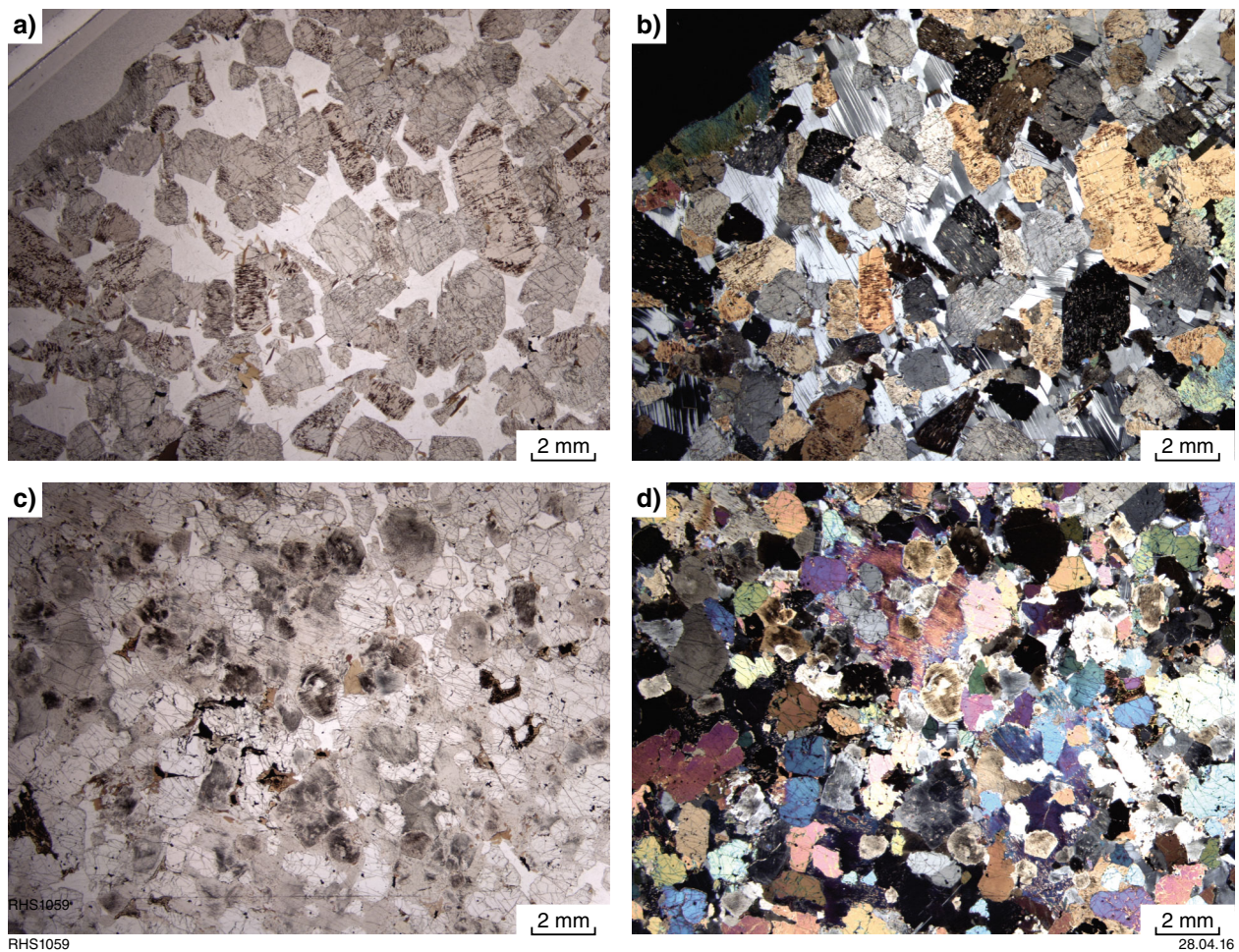


Figure 8. Photomicrographs of rocks from the Plato prospect: a) norite (PLDT001, 392.7 m, sample 216346) in plane-polarized light; b) norite under cross-polarized light; c) olivine-norite (PLDT003, 271.6 m, sample 216351) in plane-polarized light; d) olivine-norite under cross-polarized light

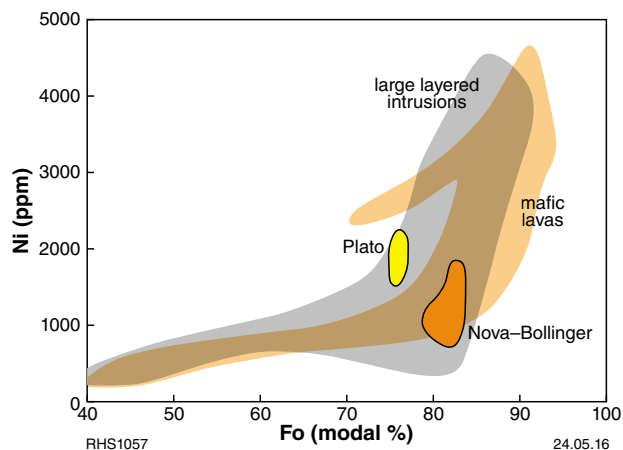


Figure 9. Plot of Ni vs Fo in olivine from Nova-Bollinger and from Plato cumulate rocks, compared to layered intrusions globally (layered intrusion and mafic lava data compiled from Teigler and Eales, 1996; Maier and Eales, 1997; Raedeke, 1982 and Sobolev et al., 2011)

Excluding the cumulate Mount Malcolm samples, the main gabbros have on average 185 ppm Ni and 240 ppm Cr, consistent with basaltic compositions. The bulk of the main gabbros show limited variation in terms of differentiation indexes such as Cr/V (1–3) and $Mg^\#$ (0.55 – 0.65) (Figs 10 and 11), likely suggesting that relatively fast cooling, typically in sills and sheets, prevented significant cumulate formation. The hybrid gabbros extend to lower Cr/V and $Mg^\#$. Compared to mid-ocean ridge basalt (MORB), the main gabbros are strongly enriched in large-ion lithophile elements (LILE) and light rare earth elements (LREE), but have MORB-like concentrations of Nb (and Ta), Zr, Hf and heavy rare earth elements (HREE) (Fig. 12). On an N-MORB-normalized trace-element spidergram, three samples of main gabbro (GSWA 183624, 183654, 183665 — red lines on Figure 12) show less enriched (to depleted) trace-element patterns; in one case (GSWA 183624) with normalized high field strength element (HFSE) abundances clearly reflect derivation from a mantle source more depleted than an N-MORB source (Smithies et al., 2013).

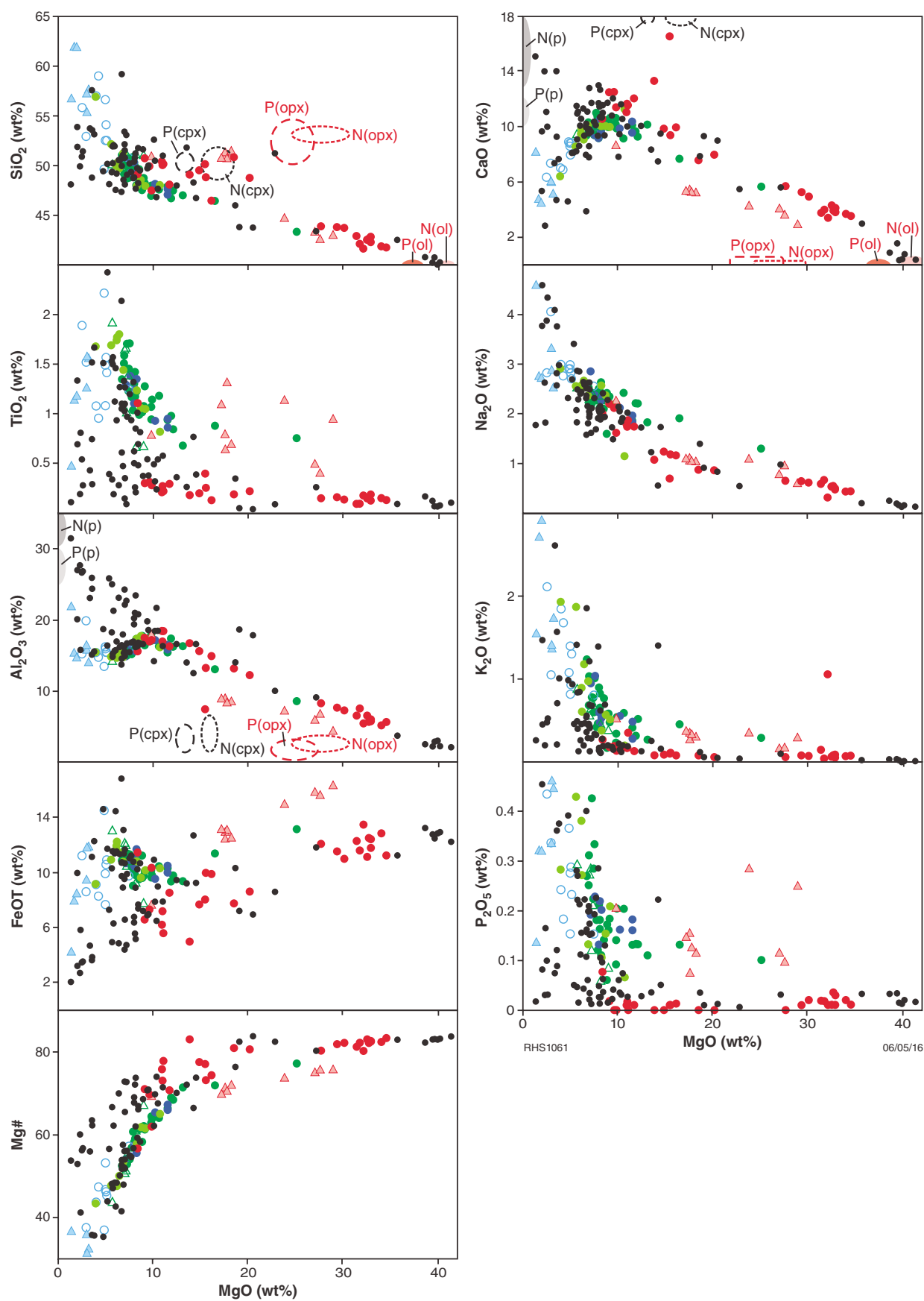


Figure 10. Compositional variation diagrams showing MgO vs major elements and Mg#. Composition of main minerals (see Appendix 6) is indicated in some diagrams. Symbols as for Figure 5. Mineral fields: Plato [P(p) = plagioclase, P(cpx) = clinopyroxene, P(opx) = orthopyroxene, P(ol) = olivine]; Nova-Bollinger [N(p) = plagioclase, N(cpx) = clinopyroxene, N(opx) = orthopyroxene, N(ol) = olivine].

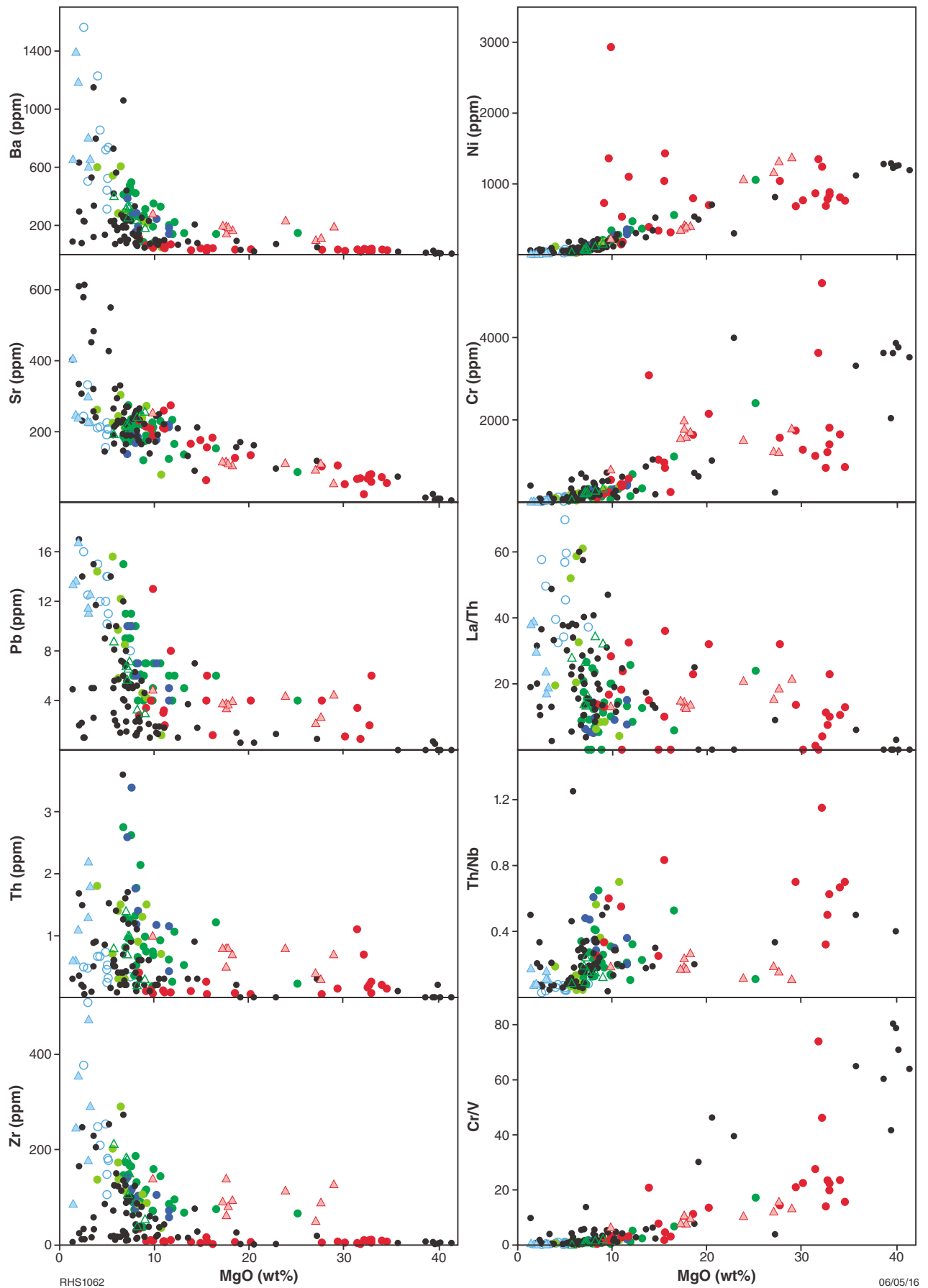


Figure 11. Compositional variation diagrams showing MgO vs Ba, Sr, Pb, Th, Zr, Ni, Cr, La/Th, Th/Nb and Cr/V. Symbols as for Figure 5.

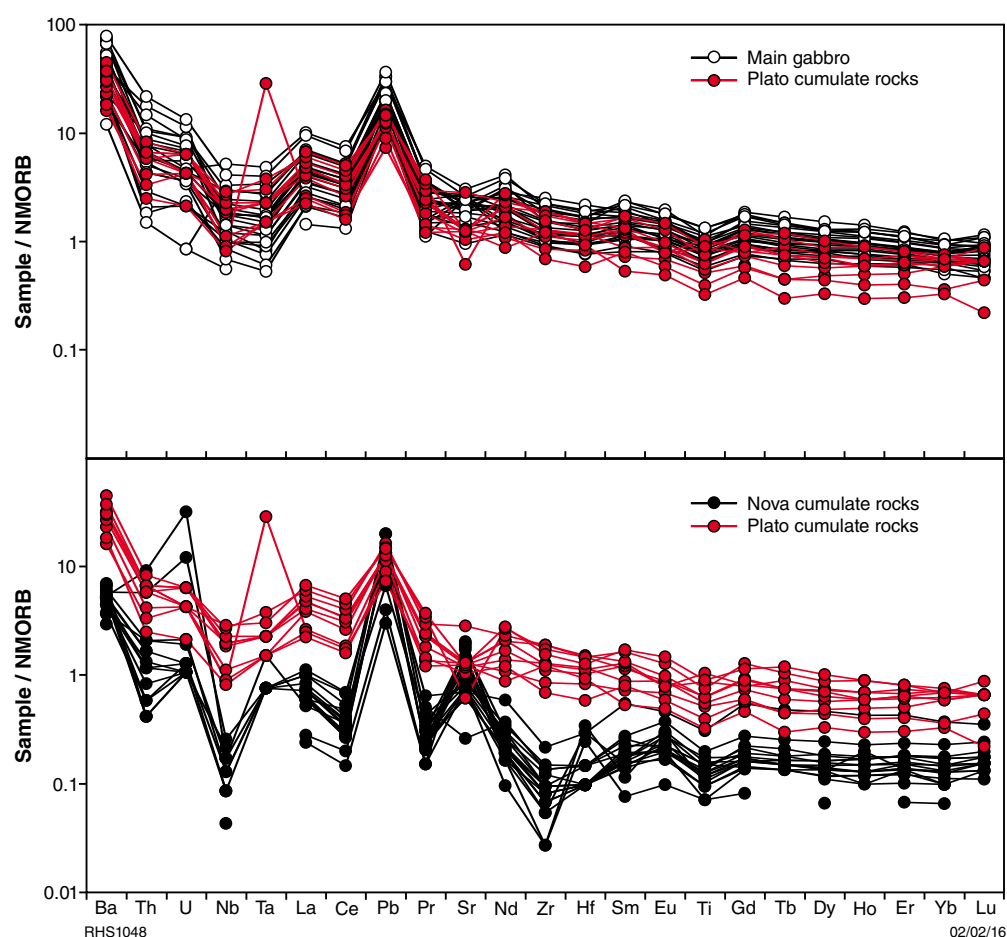


Figure 12. N-MORB normalized multi-element plots of Fraser Zone mafic and ultramafic rocks (normalization factors from Sun and McDonough, 1989)

Samples from Plato include both cumulate- and noncumulate-textured rocks. The noncumulate-textured rocks include the coarse-grained, plagioclase-porphyritic quartz-norite or diorite and the fine-grained gabbro to gabbro-norite. Fine-grained gabbro to gabbro-norite has a major- and trace-element compositional range very similar to that of the main gabbro. These rocks can most likely be regarded as part of the main gabbro group. The major- and trace-element compositional range for the coarse-grained, plagioclase-porphyritic quartz-norite and diorite rocks overlaps the compositional range for the Group 2 hybrid gabbros and appears to extend that range to even more evolved compositions. The similarities between the noncumulate rocks from Plato and the main gabbro and Group 2 hybrids are particularly obvious in terms of the respective normalized trace-element patterns.

Immediately obvious from the compositional variation diagrams are the contrasting compositions and compositional trends displayed between most of the noncumulate rocks (main gabbros and the hybrid gabbros) and the cumulate-textured rocks. These differences are most notable in plots of MgO vs either Al_2O_3 or CaO (Fig. 10), with the cumulate rocks showing strong negative correlations in contrast to the positive correlations shown by most of the noncumulate rocks, which are controlled

by liquid evolution trends. However, in plots of MgO vs either Al_2O_3 or CaO there is an inflection in the trend for the main gabbros at approximately 8.5 wt% MgO, with a small number of the most MgO-rich samples following the cumulate, rather than the liquid, trend presumably reflecting a significant cargo of cumulate olivine \pm pyroxene. A significant cumulate cargo in these rocks is not obvious petrographically, although this might be a result of later metamorphic recrystallization. Nevertheless, it appears that cumulate processes may have influenced the compositions of a slightly greater proportion of main gabbros than originally thought, and such cumulate processes are not simply confined to samples from Mount Malcolm.

The major- and trace-element compositions of the cumulate-textured gabbro-norites, norites and olivine-norites from Plato are distinct from those of Nova-Bollinger. The latter group have higher Al_2O_3 and CaO, and lower FeO and TiO_2 at a given MgO content, and show significantly lower concentrations of incompatible trace elements (e.g. TiO_2 , P_2O_5 , K_2O , Ba, Zr, and LREE) than samples from Plato (Figs 10 and 11). Two samples of the main gabbro with partial cumulate chemistry (including one from Mount Malcolm) have MgO contents >15wt%, $\text{Mg}^\# > 70$ and high concentrations of

Ni (559 and 1055 ppm) and Cr (1115 and 2405 ppm). On compositional variation diagrams these rocks lie between the distinctive trends defined by Nova–Bollinger and Plato cumulate rocks, although typically they are much closer in composition to the Plato rocks (Figs 10 and 11).

Additional significant differences exist between the Nova–Bollinger cumulate rocks and the cumulate rocks of the Plato Prospect in terms of their N-MORB normalized incompatible trace-element patterns (Fig. 12). The Nova–Bollinger cumulates show ‘spiky’ normalized patterns typical of cumulate rocks, mainly controlled by positive anomalies for Pb, Sr and Eu and negative anomalies for Zr and Nb. Patterns for Plato (and cumulates from Mount Malcolm — not shown) are identical to those for the noncumulate main gabbros, which are generally more fractionated than those for Nova–Bollinger and show significant anomalies only for Nb and Pb. We suggest that these Plato and Mount Malcolm cumulates are almost certainly derived from magmas very similar in composition to those forming the main gabbros — and most likely are simply cumulate-crystal rich equivalents of the noncumulate main gabbros. Clearly, the proportion of cumulate minerals (mainly orthopyroxene and olivine) in the Plato and Mount Malcolm cumulate rocks has no significant effect on incompatible trace-element ratios, although the abundance of these trace elements is controlled by the ratio of liquid to cumulate minerals. The enrichments in all incompatible elements at Plato and Mount Malcolm, compared to samples from Nova–Bollinger, mainly reflect a greater interstitial liquid component in the former.

Most samples from Nova–Bollinger have $Mg^\# > 70$ and $Cr/V > 10$ reflecting relatively unevolved compositions. These cumulates have up to 35% MgO and their compositional evolution is mainly controlled by modal variations in plagioclase and olivine (\pm clinopyroxene and orthopyroxene), as reflected by the well-defined negative correlations in plots of MgO vs Al_2O_3 , CaO and Sr (Figs 10 and 11). The lever rule also indicates that olivine and plagioclase are the main cumulate components, each reaching modal proportions of approximately 75% in the ultramafic and mafic rocks, respectively. A best-fit tie line through the Nova–Bollinger cumulates intersects the MgO axis at approximately 45% MgO, and the MgO vs FeO ratio suggests that olivine has a composition of approximately $Fe_{0.80-0.85}$, consistent with the microprobe data for olivine in Nova–Bollinger samples. Very low concentrations of incompatible elements (including TiO_2 , P_2O_5 , K_2O , Ba, Zr, and LREE) show that these rocks incorporated only very minor intercumulus liquid. The ‘spiky’ normalized trace-element pattern for these rocks (Fig. 12) is controlled mainly by the cumulate mineralogy. Removing those trace elements that preferentially partition into the observed cumulate phases (mainly Sr and Eu in plagioclase) and the siderophile element Pb, gives a clearer idea of intercumulus liquid compositions and, again, reveals an enriched composition very similar to that of the main gabbro liquid line of descent (Fig. 13). These patterns indicate Nb/Yb ratios (0.66) lower than the N-MORB values (0.76 — Sun and McDonough,

1989) which, like the patterns for the least-enriched main gabbros, reflect a source more depleted than an N-MORB source. It is unclear why the patterns include a significant negative Zr anomaly, although this too might reflect a distinct cumulate mineral control (e.g. Woodhead et al., 2011).

Many of the samples from the Creasy Group of Companies are cumulates, including peridotites with >40 wt% MgO, although there are also several typically gabbroic samples that have compositions similar to those of the main gabbros (Figs 10 and 11). Like the cumulates from Nova–Bollinger, most Creasy Group cumulates are characterized by low concentrations of TiO_2 , P_2O_5 , K_2O , Ba, Zr, and LREE (Figs 10 and 11). However, the data for these rocks typically shows considerable scatter, likely because these data were obtained from drill chips rather than from diamond drillcore or fresh outcrop.

Chalcophile element geochemistry

The presence of sulfide in the Nova–Bollinger samples results in the scatter in plots of Ni and Cu vs MgO (Fig. 11). Sulfide-poor Nova–Bollinger samples have <1000 ppm Ni, consistent with the relatively Ni-depleted compositions of olivine. In contrast, samples from Plato define reasonably well-constrained positive trends in plots of Ni vs MgO suggesting that Ni is contained in olivine rather than in sulfide minerals. This again is consistent with olivine chemistry, which shows Ni-undepleted compositions for Plato.

Cu contents in the main gabbros and hybrid gabbros, as well as rocks from Plato, are mostly 30–70 ppm, with an average of 50 ppm (Fig. 14), which is lower than typical N-MORB values (average 73 ppm, Gale et al., 2013). Only a few samples (two from Plato, one from Verde Austral Quarry) have >100 ppm Cu. The scarcity of samples with elevated Cu contents in these lithologies suggests that the parental magmas were sulfur undersaturated during crystallization. A similar conclusion is reached based on the Ni-undepleted compositions of olivine in the Plato rocks. Group 2 hybrid gabbros have relatively low Cu/Zr, as a result of slightly higher Zr and lower Cu (Fig. 14). Sulfur contents of the main gabbros, Group 1 hybrids and nonmineralized samples from Plato define a group clustering around 1000 ppm, but with several samples trending towards lower values (50–200 ppm). The sulfur content of the main sample group (~ 1000 ppm) is likely representative of the liquid, based on similarities with MORB data (Wallace and Carmichael, 1992), whereas the sulfur depleted samples may have undergone metamorphic sulfur loss. Group 2 hybrid gabbros tend to have lower sulfur than the main gabbros, which combined with the slightly higher Zr and lower Cu concentrations, reflects dilution with a Zr-rich and sulfur- and Cu-poor contaminant (see discussion below). Notably, this hybridization process does not appear to have triggered sulfide saturation in the mafic magma.

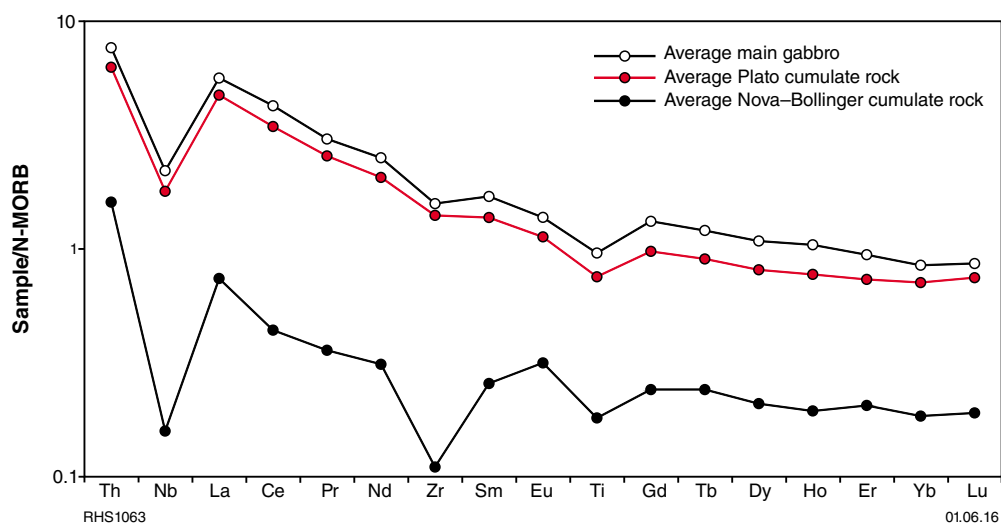


Figure 13. N-MORB normalized multi-element plot ignoring trace elements strongly partitioned into observed cumulate minerals and comparing resulting patterns for cumulate rocks from Nova-Bollinger with Fraser Zone main gabbros and cumulate rocks from Plato (normalization factors from Sun and McDonough, 1989)

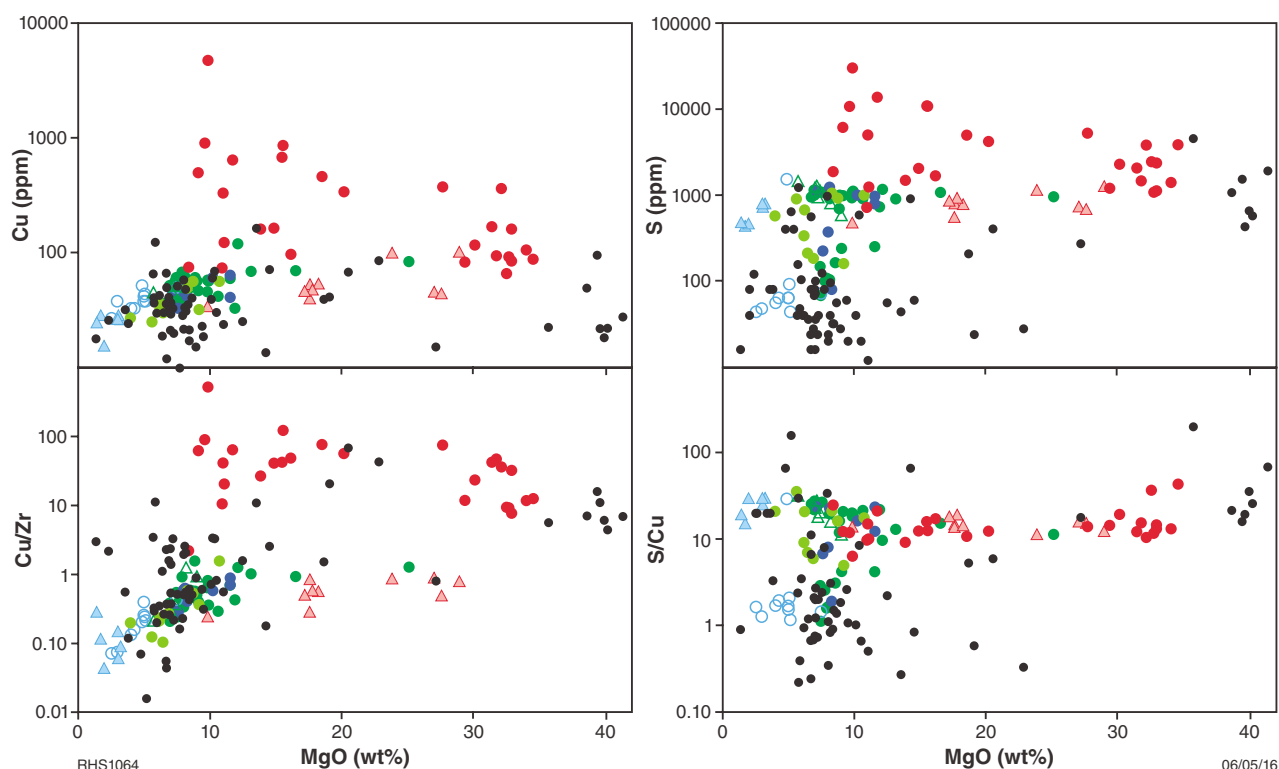


Figure 14. Compositional variation diagrams of chalcophile elements vs MgO for Fraser Zone mafic and ultramafic rocks. Symbols as for Figure 5.

Cu and sulfur contents in the Nova–Bollinger samples are as high as 5000 and 4000 ppm, respectively (Fig. 14). Moreover, the average Cu and sulfur contents are significantly higher than in the Fraser Zone main and hybrid gabbros, and there is very little overlap between the populations. Cu/Zr at Nova–Bollinger is >10 , indicating that all samples, including gabbro-norites and peridotites, contain cumulus sulfide.

Selected elements and element ratios from the Nova–Bollinger drillcore SFRD0017 are plotted against depth in Figure 15. The data illustrate that sulfur contents vary based on rock type rather than stratigraphic level; i.e. sulfur contents $>10\,000$ ppm are confined to the gabbro-norites, irrespective of stratigraphic position. Ni/Cu ratios in the gabbros are $0.5 - 2$. In view of the low modal proportion of olivine and pyroxene, this largely reflects the metal ratio in the sulfide. The ultramafic rocks have higher Ni/Cu. This is only partly due to higher olivine contents of the rocks since the available data indicate that olivine has <2000 ppm Ni. The higher Ni/Cu in the peridotites also reflects the presence of a more primitive (higher Ni/Cu) sulfide component.

The sample suite collected by the Creasy Group tends to have lower Cu contents, in the range of the Fraser Zone main gabbros, with the exception of one gabbroic rock containing ~ 200 ppm Cu. However, most of the samples have elevated Cu/Zr indicating the presence of a small amount of cumulus sulfide.

All rocks of the Fraser Zone are highly depleted in PGE relative to Ni and Cu. The highest value measured is 20 ppb Pt+Pd, and the most sulfide-rich sample (with 8% sulfide) has only ~ 10 ppb Pt+Pd.

Strontium, Nd and S isotope geochemistry

Five samples of main gabbro show a range in ϵ_{Nd} from 0.04 to -3.65 , which encompasses the range for the Group 1 hybrids ($\epsilon_{\text{Nd}} = -0.90$ to -2.09 ; four analyses), Group 2 hybrids (single sample with ϵ_{Nd} of -2.95) and samples from the Nova–Bollinger SFRD0017 drillcore ($\epsilon_{\text{Nd}} = 0.43$ to -1.29 ; three samples) (Fig. 16). Together, these data form an array consistent with mixing between a mantle-derived magma and available crustal components such as the Gora Hill Suite (granites contemporaneous with the mafic–ultramafic rocks) or felsic rocks formed during the earlier Biranup Orogeny. These trends show that all mafic and ultramafic rocks of the Fraser Zone probably formed from mantle-derived parental magmas that incorporated a minor crustal component. However, samples from Nova–Bollinger lie at the more radiogenic end of the mixing array (Fig. 16) suggesting mantle-dominated compositions, while the hybrid samples cluster at the less radiogenic end of the array, reflecting a larger crustal contribution consistent with their major- and trace-element compositions and with field and textural observations.

In situ S isotope analysis of sulfides from four samples of the main gabbro from Mount Malcolm gave $\delta^{34}\text{S}$ values around 0 and overlap with the range for mantle sulfur

(-2 to $+2$, Ripley, 1999). In contrast, sulfides in samples from Nova–Bollinger have $\delta^{34}\text{S}$ values of 0 to $+4$, indicating a significant sulfur contribution from a crustal source. Similarly, in situ Sr isotope data from the same samples all show enriched signatures, but samples from Nova–Bollinger ($\epsilon_{\text{Sr}} = 38$ – 52) are more enriched than samples from Mount Malcolm ($\epsilon_{\text{Sr}} = 17$ – 32). These preliminary sulfur and Sr isotopic data appear to indicate an *additional* crustal component within the Nova–Bollinger cumulates.

Discussion

Petrogenesis

The age of intrusion of all granitic, mafic and ultramafic rocks of the Fraser Zone that have been subjected to high-grade metamorphism is constrained to an age bracket between c. 1310 and 1283 Ma (Kirkland et al., 2014; Clark et al., 2014). Ages from felsic and mafic intrusive rocks overlap, which indicates they were contemporaneous. The maximum depositional age of the Snowys Dam Formation is 1332 ± 21 Ma (youngest single analysis), and its minimum age is defined by a metamorphic date of 1304 ± 7 Ma (Spaggiari et al., 2014c). Peak metamorphic conditions of ~ 850 °C at pressures of 7–9 kbar were reached at c. 1290 Ma, coincident with mafic intrusions at that time (Clark et al., 2014). Locally, the folded succession of interleaved metagabbro and metasedimentary rocks appears to be cut by younger intrusions, as shown in the aeromagnetic data over the Plato Prospect (Fig. 6). In the case of the Plato Prospect, the younger intrusion is also metamorphosed and the data presented shows that it likely crystallized from magmas geochemically identical to the main gabbro. These relationships are consistent with the geochronology and P-T analysis of Clark et al. (2014), and the observation that the manifestation of granulite-facies metamorphism and deformation on the igneous rocks is variable, even within a local area. It also clearly shows that the magmatic, structural and metamorphic histories of the Fraser Zone are intimately related.

Assuming that the mafic and ultramafic rocks of the Fraser Zone are contemporaneous, we use the geochemical and isotopic data to assess whether the Nova–Bollinger and Plato cumulate rocks and the main gabbros could have crystallized from a common parental magma composition. We further investigate the petrogenetic processes that may have led to compositional diversity among the various rock types (e.g. main gabbro, hybrid gabbros, Plato cumulates and Nova–Bollinger cumulates). We make the assumption that the most primitive noncumulate main gabbros provide the best estimate of primitive liquid compositions from the Fraser Zone. Based on Nd isotopic compositional arrays (Fig. 16), we also suggest that all mafic–ultramafic magmas of the Fraser Zone represent mantle-derived melt already blended with a minor crustal component isotopically and geochemically compatible with available crustal components, such as the Gora Hill Suite, or felsic rocks formed during Paleoproterozoic events (Salmon Gums and Ngadju Events, Biranup Orogeny; Smithies et al., 2015).

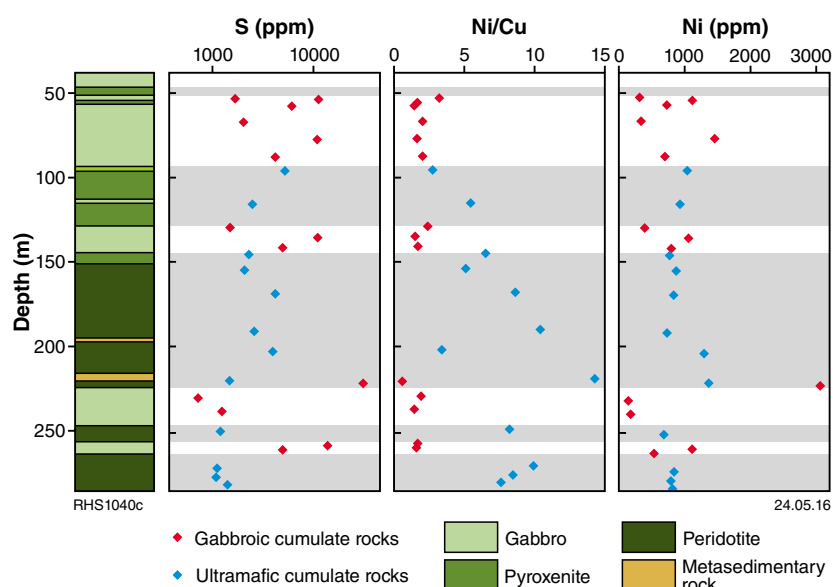


Figure 15. Depth vs compositional variation in sulfur, Ni/Cu and Ni in drillcore SFRD0017

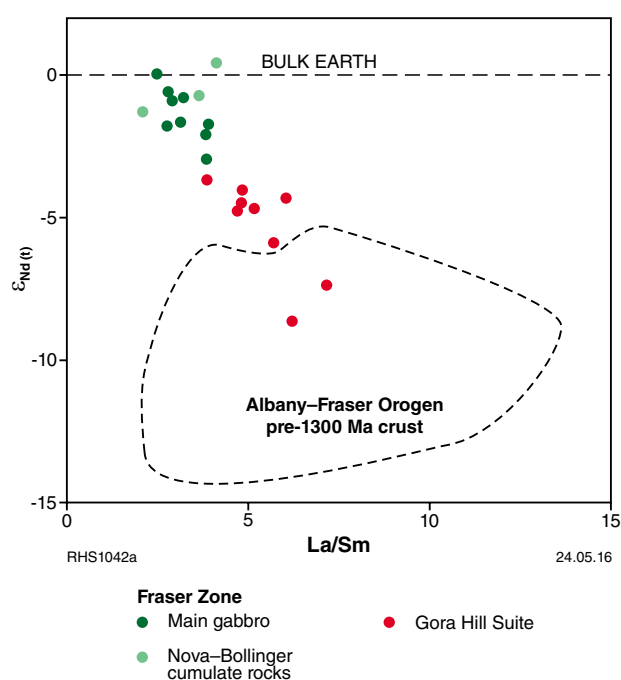


Figure 16. Nd isotope data for rocks of the Albany–Fraser Orogen. Data for main gabbros and for cumulate rocks at Nova are compositionally indistinguishable. They have ϵ_{Nd} values lying on or slightly below Bulk Earth, reflecting minor, early contamination of mantle-derived melts by crust. These data points plot along the same array as data for the granites of the contemporaneous Gora Hill Suite (Recherche Supersuite). This array defines an Assimilation-Fractional Crystallization (AFC) relationship between primary mantle-derived magmas and assimilated components of the pre-c. 1300 Ma Albany–Fraser crust (Biranup Zone basement to the Fraser Zone).

Source of the main gabbros, and Plato cumulate and noncumulate rocks

Our geochemical data show that the noncumulate fine-grained gabbro to gabbro-norite unit at Plato belongs to the main gabbro suite. Our data also show that all cumulate rocks from Plato are simply main gabbro liquids with a significant cumulate mineral cargo (i.e. are orthocumulate equivalents of the main gabbro). Hence, the petrogenesis of all these rocks can be considered together.

The combined whole-rock and mineral compositional data suggest that the main gabbros crystallized from basaltic magmas having approximately 8.8 wt% MgO. Thermodynamic modelling using PELE (Boudreau, 1988) suggests that the order of mineral crystallization from this primitive main gabbro magma (at QFM) would be olivine–orthopyroxene–clinopyroxene at 5 kbar, consistent with petrographic observations, although predicted mineral compositions are slightly more Mg rich (e.g. predicted olivine Fo_{84} vs Plato olivine Fo_{76}). Modelling at higher pressures (e.g. 8 kbar) predicts the crystallization order orthopyroxene–clinopyroxene–plagioclase, which is not observed in any mafic rocks of the Fraser Zone. On this basis, we suggest that the main gabbro was emplaced from magma chambers that last equilibrated at depths shallower than 20 km.

All main gabbros are low-K tholeiitic rocks (Smithies et al., 2013) with Th, U, and REE concentrations greater than N-MORB values, but with mantle-normalized depletions in HFSE (Nb, Ta, Zr, Hf) (Fig. 12). In the case of the most Nb-depleted samples (GSWA 183624, 183654, 183665), Nb concentrations are lower than N-MORB values and correspondingly low Nb/Zr ratios (0.011 – 0.019 c.f. N-MORB value ~ 0.03 ; Sun and McDonough, 1989) cannot be accounted for through

cumulate process. These compositions require a mantle source that was more depleted than the source for N-MORB. This depleted source is potentially the mantle source component to all main gabbros. Jolly et al. (2001) used concentrations of Nb and Yb in basalt, normalized to 9.0 wt% MgO, to estimate the degree of mantle partial melting. A similar treatment of the data for the main gabbros suggests that the parent melts could have formed through <10% partial melting of a spinel lherzolite mantle. Similarly, the relatively low concentrations of Cr in the least-evolved noncumulate gabbros (<700 ppm) suggest that some clinopyroxene remained in the mantle source after melting. This would also limit the degree of melting to well below 20% (e.g. Sinton et al., 2003). These relatively low degrees of partial mantle melting would explain the very low PGE contents in the Fraser Zone magmas and cumulates, as the complete dissolution of mantle sulfide is thought to require more than approximately 20% partial melting (Mungall and Brenan, 2014).

The enrichments in (for example) Th and LREE relative to HFSE and HREE in many of the main gabbros (Fig. 12) are characteristic of subduction-related magmas. Such patterns formed the basis of the model of Condie and Myers (1999) who interpreted the gabbros of the Fraser Zone to have formed in an oceanic-arc setting. However, an oceanic-arc setting can be discounted since geochronological, isotopic and geochemical data show that the same felsic crustal material lies on both sides of the Fraser Zone and includes Paleoproterozoic granites derived through recycling of Archean crust prior to and during the Biranup Orogeny (Kirkland et al. 2011; Spaggiari et al., 2014b, 2015a; Smithies et al., 2015). In addition, the Fraser gabbros themselves intrude a clastic sedimentary succession (Snowys Dam Formation) interpreted as initially deposited within a foreland basin no more than 20 million years prior to gabbro intrusion (Spaggiari et al., 2015a).

Subduction-like trace-element patterns can also result through assimilation of crust by mantle-derived magmas. In the case of the Fraser Zone main gabbros, this process would be more consistent with the observed geological, geochemical and isotopic data. Indeed, earlier modelling has shown that the average trace-element characteristics of main gabbro can be reproduced if a magma derived from a depleted mantle source is contaminated by <<10% locally available Biranup basement (Smithies et al., 2013).

Hence, magmas that crystallized the main gabbro (including most rocks at Plato) formed through relatively low degree (<10%) partial melting of spinel-lherzolite asthenosphere that was slightly more depleted than an N-MORB source. They all underwent minor (<<10%) contamination from felsic Biranup basement prior to emplacement in staging chambers within the upper 20 km of Fraser Zone crust, before final emplacement.

Petrogenesis of the hybrid gabbros

The hybrid gabbros associated with the main gabbros and locally forming cumulate rocks at Plato (i.e. the

coarse-grained, plagioclase-porphyritic quartz-norites and diorites), can be subdivided into two groups that form distinct high- and low-La/Th trends broadly enveloping the field for the main gabbros (Fig. 5). This suggests that the hybrid gabbros formed through two distinct and unrelated processes. It is also apparent, from field observations and from the typically higher $Mg^\#$ of the main gabbros, that the main gabbro is not simply a mix between the two groups of hybrid gabbro. Importantly, examples of each hybrid group occur at many sampling sites and thus the petrogenetic processes involved are not isolated phenomena.

Group 2 hybrids (including the hybrids at Plato) are typically significantly enriched in SiO_2 and have much lower $Mg^\#$, consistent with the field evidence for mingling. Group 1 hybrids cover the same range of SiO_2 concentrations and $Mg^\#$ values as the main gabbros, although they range to higher concentrations of incompatible trace elements. A range of incompatible trace-element variation diagrams (in particular, Th vs K or LREE, Fig. 5) shows that the Group 1 hybrids consistently plot to the more 'crustal' side (i.e. high Th) of the main gabbros and the simplest explanation for these hybrids is that they define the upper limit of early contamination of primitive main gabbro magmas by partial melts of felsic Biranup basement, prior to emplacement within the Fraser Zone.

In contrast, Group 2 hybrids are defined by distinctly lower Th/K, Th/Pb, and Th/LREE ratios than both Group 1 hybrids and the main gabbros (Fig. 5). Only the most primitive granodioritic end members of the Gora Hill Suite consistently lie on the Group 2 hybrid trend. This granodioritic component of the Gora Hill Suite is restricted to the Fraser Zone. Thus it seems likely that Group 2 hybrids are local physical mixes (i.e. at or near the sampled level of emplacement) of comagmatic main gabbro and Gora Hill granodiorite. Such a process also explains the low sulfur and Cu, and high Zr concentrations in the Group 2 hybrids — these being characteristics of the Gora Hills granodiorite. Such interaction is clearly rare and produces only minor magma volumes.

Petrogenesis of the Nova-Bollinger intrusion

Apart from being host to the only economic accumulation of orthomagmatic Ni-Cu sulfides so far recognized in the Fraser Zone, the Nova-Bollinger cumulate rocks appear to be distinct from most other mafic and ultramafic rocks of the Fraser Zone in terms of their more primitive whole-rock and mineral compositions and their sulfur and Sr isotopic compositions; the latter suggests a crustal contaminant was present in addition to the assimilated Biranup basement component detected in all mafic magmas of the Fraser Zone. Important questions here include: a) do these distinctions necessarily negate any suggestion of a petrogenetic link with the main gabbros; and b) are the processes causing these compositional distinctions also related to the enhanced Ni-Cu sulfide concentrations?

On plots of MgO vs incompatible trace elements (Fig. 11), well-defined trends shown by the Nova–Bollinger rocks contrast with scattered, poorly defined trends shown by the Plato data. The scattering in the Plato data reflects large variations in cumulate/liquid ratios, but all of the variation can be accounted for by varying degrees of mixing of a hypothetical liquid having the compositional range of the main gabbro, with a Nova–Bollinger cumulate assemblage of variable olivine/plagioclase ratio (Fig. 17). However, our data also demonstrate that primary mineral compositions from Plato are typically significantly more evolved than those from Nova–Bollinger (Fig. 10). This is further indicated in whole-rock compositional trends that show that all Nova–Bollinger samples, and several Creasy Group samples, have lower FeO contents at any given MgO content than the main gabbros and samples from Plato (Fig. 10).

The differences in mineral compositions between Plato and Nova–Bollinger may simply reflect the degree to which cumulate olivine and pyroxene has re-equilibrated with evolved (trapped) liquid. In this case, the Plato cumulate assemblages may have extensively equilibrated with trapped liquids, but at Nova–Bollinger, re-equilibration might have been minimized because most of the evolved liquid was expelled. Such crystal–liquid exchange can have a significant effect on the Mg[#] of olivine and pyroxenes (Barnes, 1986), but often has significantly less effect on (for example) the anorthite content of plagioclase. This can be indicated, for example, by a typically more pronounced compositional zonation of plagioclase relative to pyroxene in igneous rocks. For all Plato cumulates, plagioclase shows very little compositional variation and is typically significantly more evolved (An_{48–63}) than in the Nova–Bollinger cumulates (An_{62–89}), with no An-rich cores that could suggest an originally more primitive mineral assemblage. These data suggest that the Plato cumulate assemblage crystallized from a more fractionated magma than the Nova–Bollinger cumulate assemblage.

Even if the cumulate rocks at Nova–Bollinger crystallized from a more primitive magma than those at Plato, the trapped intercumulus liquid, or noncumulate component of Plato and Nova–Bollinger has very similar trace-element ratios and matches the composition of the noncumulate main gabbro. This strongly suggests that all of these rocks share a common bulk source. If all of these rocks are indeed petrogenetically related, then major element and mineral geochemical data suggest that either the Nova–Bollinger parental magmas represent higher degree partial melting of the same mantle source component and/or, the typical intrusion history of the main gabbro involved a stage of early olivine (and/or orthopyroxene) fractionation that did not occur in the Nova–Bollinger parental magmas (i.e. a slightly different intrusion history).

The combined isotope data indicate that all Fraser Zone mafic magmas share a common source for Nd but the Nova–Bollinger rocks show more crustal sulfur and Sr isotopic signatures. Hence, in addition to the more primitive magma compositions outlined above, these isotopic data identify an additional crustal component contributing S and Sr to the Nova–Bollinger rocks.

Metasedimentary rocks of the Snowys Dam Formation (Arid Basin) — the sedimentary host to the Nova–Bollinger deposit — are locally sulfide rich. These rocks have been sampled in drillcore from the Sunline Prospect approximately 130 km northeast of Nova–Bollinger. Two sulfur isotope analyses of this core give $\delta^{34}\text{S}$ values of +3.6 and +5.2, identical to values from sulfides at Nova–Bollinger. A dominant detrital source component of the Snowys Dam Formation is from erosion of c. 1400 Ma rocks of the Haig Cave Supersuite (Loongana oceanic arc, Madura Province), deposited as an oceanic arc was accreted to the southeastern edge of the Albany–Fraser Orogen, triggering Stage I of the Albany–Fraser Orogeny (Spaggiari et al., 2014c, 2015a). The Nd isotopic composition of this sedimentary material is more radiogenic ($\epsilon_{\text{Nd}} = 3.33$ to -0.30) than any rocks of the Fraser Zone at c. 1300 Ma. This detrital material may also have undergone surficial processes (e.g. weathering, erosion, sea-floor alteration) capable of changing primary S and Sr isotopic compositions to more crustal values, but not altering the isotopic composition of Nd, a less fluid-mobile trace element. Additional indications that this material may be a contaminant within the Nova–Bollinger rocks can be seen in plots of Th vs La, and Pb vs Zr and La (Fig. 18), with the Nova–Bollinger cumulates forming a distinct trend consistent with the addition of a paragneiss component. However, these trends are not compelling, particularly because of the very low concentrations of many of these trace elements in these cumulate rocks.

Thus, the combined data are consistent with the suggestion that whereas all primitive, mantle-derived, magmas intruding the Fraser Zone first assimilated minor felsic Biranup basement, parental magmas to the Nova–Bollinger rocks additionally incorporated Snowys Dam Formation after they intruded the Fraser Zone. Given the Ni-depleted compositions of olivine in the Nova–Bollinger rocks (Fig. 9), we suggest that this additional assimilation occurred within a chamber large enough to allow

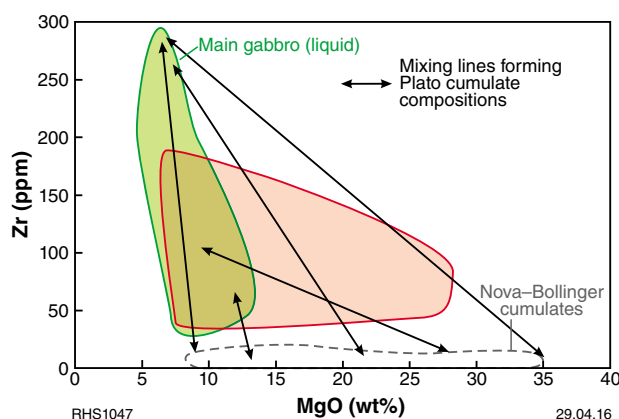


Figure 17. Plot of MgO vs Zr. The field for the main gabbros represents liquid compositions whereas the field for Nova cumulates represents cumulate rocks essentially purged of intercumulus liquid. Mixing lines between these two fields account for the full compositional range of the Plato cumulate rocks — consistent with petrographic and geochemical data that these rocks are liquid-rich cumulate suspensions.

convective homogenization and resulted in widespread sulfur-saturation of the magma, and early sulfide removal, at an early stage of (or before) olivine crystallization. This was likely well below the level of final emplacement.

Hence, although the Nova–Bollinger rocks appear to be distinct from the other mafic and ultramafic rocks of the Fraser Zone in terms of their more primitive whole-rock and mineral compositions and their sulfur and Sr isotopic compositions, the combined data clearly suggest that a petrogenetic link remains plausible. These differences can be accounted for through a slightly different intrusion history that allowed for an early, additional, olivine/orthopyroxene fractionation stage in the main gabbros (but not for the Nova–Bollinger magmas) and also allowed for effective interaction of Snowys Dam Formation metasedimentary rocks with Nova–Bollinger magmas, but not with main gabbro magmas. Both of these distinctions are potentially important in terms of the enhanced Ni–Cu sulfide concentrations of Nova–Bollinger-type magmas. A simple explanation for these differences is that the ascent of most of the Biranup-contaminated mantle-derived melts stalled at the base of the Fraser Zone, where they underwent early olivine/orthopyroxene fractionation before emplacement as small (nonconvecting) staging chambers within the sub-basin hosting Snowys Dam Formation, and final emplacement as main gabbro magmas. Some magmas — perhaps more voluminous batches — did not stall, but were directly emplaced as large, convecting, staging chambers of unfractionated magma that effectively assimilated significant amounts of their Snowys Dam Formation host rock.

Emplacement of the Nova–Bollinger intrusion

Compositional data from Nova–Bollinger drillcore SFRD0017 identifies alternations of two distinct compositions: gabbro (9–16% MgO; Ce/Sm 3–5) and peridotite (30–35% MgO; Ce/Sm 5–8) (Fig. 19). Only in the upper portion of the section, between units 5–6 and 7–8, is there some evidence for compositions intermediate between these end-members, with MgO in the gabbros reaching 20% and in the peridotite falling to 27%. This suggests possible fractionation or hybridization of the magmas from which these two groups crystallized.

It remains unclear how representative this *apparent* bimodal distribution of cumulate assemblages is of the host intrusion to the orthomagmatic Nova–Bollinger deposit. However, the persistently higher Ce/Sm ratio in the ultramafic cumulates is interesting because this ratio should increase with decreasing ratio of cumulate plagioclase to olivine+pyroxene from a common magma composition. A positive correlation between Ce/Sm ratios and Ce concentrations in the ultramafic cumulates, and lack of any correlation between Ce/Sm ratios and loss on ignition (LOI) (Fig. 20), makes alteration an unlikely explanation for the higher Ce/Sm ratios in these rocks. The different Ce/Sm ratios more likely reflect different liquid compositions relating to slightly different parental magma compositions. These data suggest that the intrusion sampled by drillcore SFRD0017 is a composite body accumulated through intrusion from deeper level chambers of at least two magma batches or crystal-laden

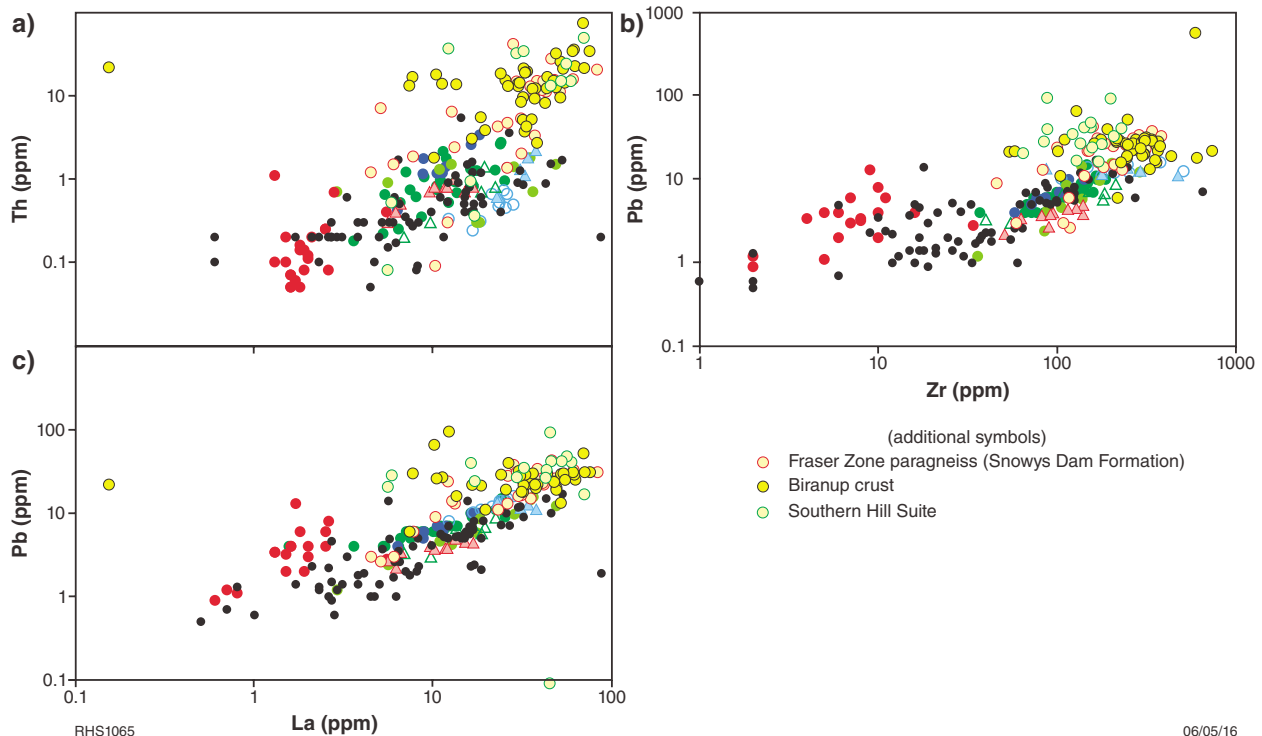


Figure 18. Binary variation diagrams of: a) Th vs La; b) Pb vs Zr; c) Pb vs La. Note contrasting compositional fields of main and hybrid gabbros in a). In b) and c), note that samples from Nova–Bollinger and ultramafic rocks from the Creasy Group of Companies define trends that are distinct from those of the main and hybrid gabbros. This is best explained by contamination either with granitic rocks of the Southern Hills Suite or sedimentary rocks of the Arid Basin. Symbols as for Figure 5.

slurries, with slightly differing incompatible trace-element ratios, perhaps related to variable and early assimilation of sulfidic metasedimentary rocks of the Snowys Dam Formation. These alternatively crystallized cumulate assemblages with relatively low MgO (9–16 wt%) and high MgO (30–35 wt%), and occasionally mixed to form hybrid assemblages.

A crystal- and sulfide-charged slurry model is consistent with the occurrence of variably sulfide mineralized pyroxenite fragments within coarse gabbroic rocks (sample GSWA 201255). Such textures suggest a relatively dynamic emplacement environment in which the migrating magma can entrain fragments of earlier crystallized magmatic assemblages forming the wall rocks to the conduits. Other examples for which emplacement of ultramafic slurries has been proposed include Kabanga (Maier and Barnes, 2010) and the recently discovered Xiarihamu Ni–Cu deposit in China (Li et al., 2015). This contrasts with processes that formed the cumulate assemblages at the Plato Prospect. The Plato cumulate rocks are orthocumulate rocks essentially characterized by often euhedral cumulate minerals suspended, or forming a loose framework, in a plagioclase-dominated assemblage crystallized from trapped or stagnant liquid, and likely formed in a more structurally shielded environment than Nova–Bollinger.

Hence, irrespective of intrusion history and attainment (or otherwise) of sulfur-saturation up to the point of final emplacement, the tectonic environment under which final emplacement occurs might be a critical factor determining if significant sulfide accumulations occur.

Tectonic setting of the Fraser Zone

The Albany–Fraser Orogen represents the reworked margin of the Yilgarn Craton and offers an opportunity to

examine the complexity of craton margin environments and the related potential for magmatic mineralization. Begg et al. (2010) emphasized that craton margins are particularly prospective for magmatic Ni–Cu–PGE deposits because they can divert fertile upwelling mantle into abundant large fractures and weak zones through which magmas can ascend.

The Fraser Zone developed during Stage I of the Albany–Fraser Orogeny. During this period, between c. 1330 and 1260 Ma, voluminous mafic and felsic magmatism (Recherche Supersuite), complex deformation, and typically high-grade metamorphism took place in response to the accretion of primitive and largely oceanic crust of the Madura Province along the Rodona Shear Zone (Fig. 1; Spaggiari et al., 2015a). The onset of accretion is constrained between c. 1390 Ma, the youngest age of magmatism relating to oceanic-arc construction in the Madura Province, and c. 1330 Ma, the oldest age of Recherche Supersuite granites that indicate the presence of Madura Province lithosphere (Smithies et al., 2015; Spaggiari and Smithies, 2015).

Spatial and compositional trends of the Recherche Supersuite through time

The main components of the Recherche Supersuite in the east Albany–Fraser Orogen are the mafic rocks exposed mainly within the Fraser Zone and granites of the Gora Hill Suite, which intruded the eastern Nornalup Zone between the Rodona Shear Zone and the northwest margin of the Fraser Zone.

Magmatism began at c. 1330 Ma with Gora Hill Suite syenogranites that intruded into the far southeast peripheries of the orogen in proximity to the Rodona Shear Zone, sourced mainly from crust of the Madura Province.

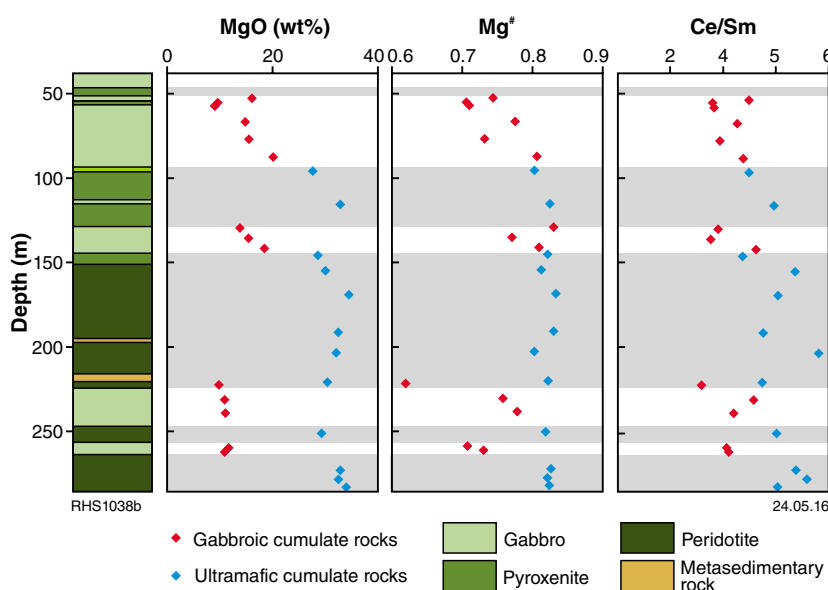


Figure 19. Depth vs compositional variation in MgO, Mg[#] and Ce/Sm ratio in Nova EIS drillcore SFRD0017

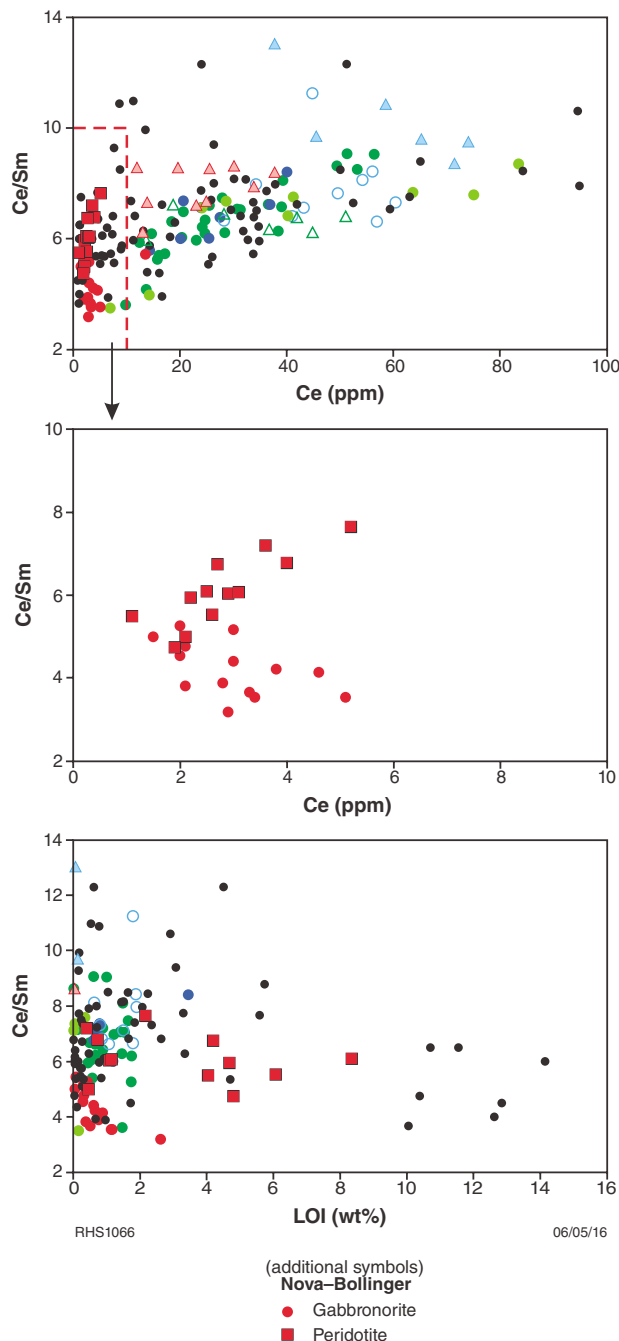


Figure 20. Compositional variation diagram showing Ce/Sm ratio vs Ce and loss on ignition (LOI) for rocks from Nova-Bollinger. Symbols as for Figure 5.

The nature of the source is best demonstrated in terms of Nd (or Hf) isotopic compositions (Fig. 21), showing the crust of the Madura Province at c. 1300 Ma being considerably more juvenile than the reworked Archean components that dominate the crust of the Albany–Fraser Orogen.

Immediately to the northwest, the Gora Hill Suite granitic rocks are slightly less compositionally evolved (in the monzogranite to syenogranite range), slightly younger (c. 1325 Ma) and sourced entirely from crust of the Albany–Fraser Orogen. From this point, there is a systematic trend to the northwest to compositionally less evolved granitic rocks (through monzogranite to granodiorite) derived from increasingly radiogenic (i.e. more mantle-like) bulk sources, at increasingly younger ages (down to c. 1285 Ma) (Fig. 21). The systematic trend reflects the increasing extent to which mantle-derived magmas mixed with crustal melts with decreasing age (Smithies et al., 2015). The trend terminates with the main gabbros and magmas parental to mafic and ultramafic cumulates at Nova-Bollinger and Plato, in the Fraser Zone itself.

Insight into the geodynamic evolution of the Fraser Zone

The systematic compositional trends in space and time implicate plate tectonic processes. Nevertheless, granite compositions are not typical of a syn-subduction setting, but are akin to the more Fe-rich (ferroan) and incompatible trace element-rich felsic magmas found in syn- to post-collisional settings (Smithies et al., 2015) (Fig. 22). We interpret the compositional evolution of the Recherche Supersuite to reflect progressive north-westward orogenic collapse, with associated lithospheric delamination, of Albany–Fraser Orogen crust that was previously thickened during overthrusting of the Madura Province and burial of the craton edge (Fig. 23; Spaggiari et al., 2015b). Given that no c. 1330–1260 Ma rocks have been found in the Madura Province, and that Stage I of the Albany–Fraser Orogeny appears to be restricted to the craton margin (Spaggiari and Smithies, 2015), this interpretation is now preferred to that of Spaggiari et al. (2014c, 2015a), which invoked west-dipping subduction at c. 1300 Ma to place the Fraser Zone in a back-arc setting.

Recherche Supersuite magmatism is unknown northwest of the Fraser Zone and the southeastern margin of the Biranup Zone, where it appears to terminate abruptly. This suggests that the faulted margin separating thick Yilgarn Craton lithosphere from reworked and extended Yilgarn crust (i.e. the Albany–Fraser Orogen) represented an effective buttress and a primary control in the evolution of the Fraser Zone (Fig. 23).

The lack of c. 1330 to 1280 Ma rocks in the Madura Province suggests that extensional relaxation, after accretion and possibly combined with delamination, is all that was required to produce the Recherche Supersuite. We find no evidence of continued subduction, or of continental collision, during Stage I of the Albany–Fraser Orogeny. Likewise, the spatial and temporal trends in magma compositions do not implicate mantle plume-like processes.

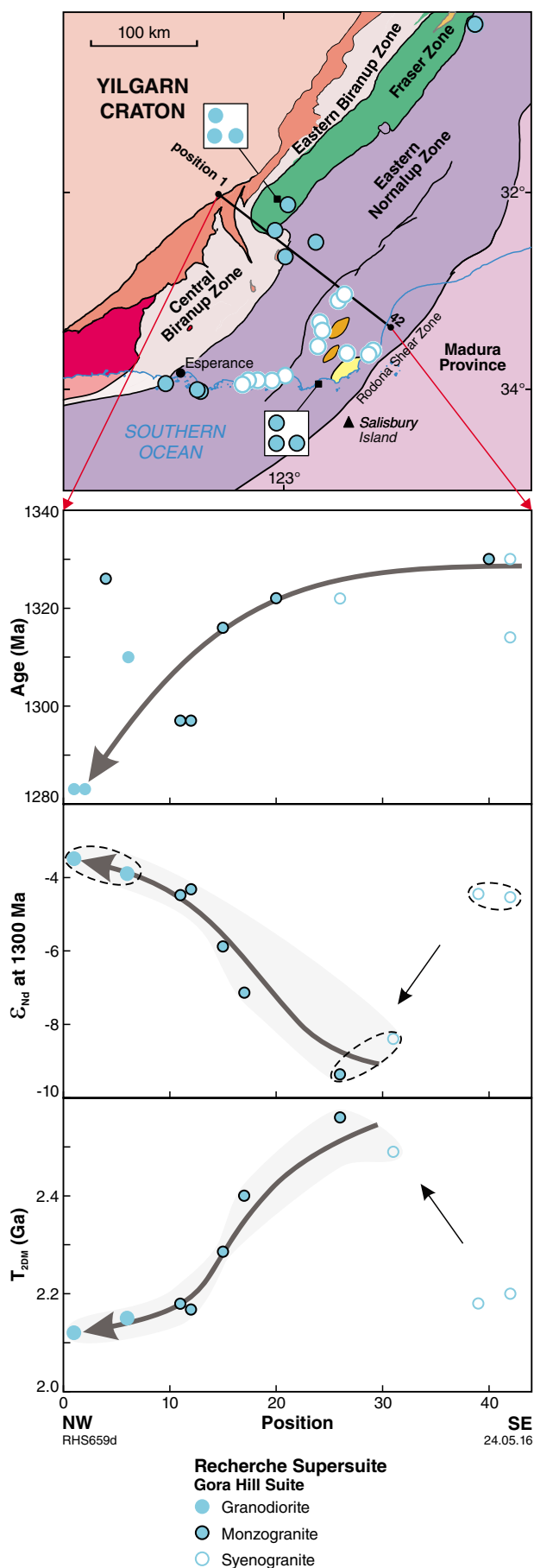


Figure 21. (left) Geographical variation in age, composition and Nd isotopic composition for granitic rocks of the Gora Hill Suite (Recherche Supersuite). 'Position' refers to the relative order of samples along the traverse line shown in Figure 21a.

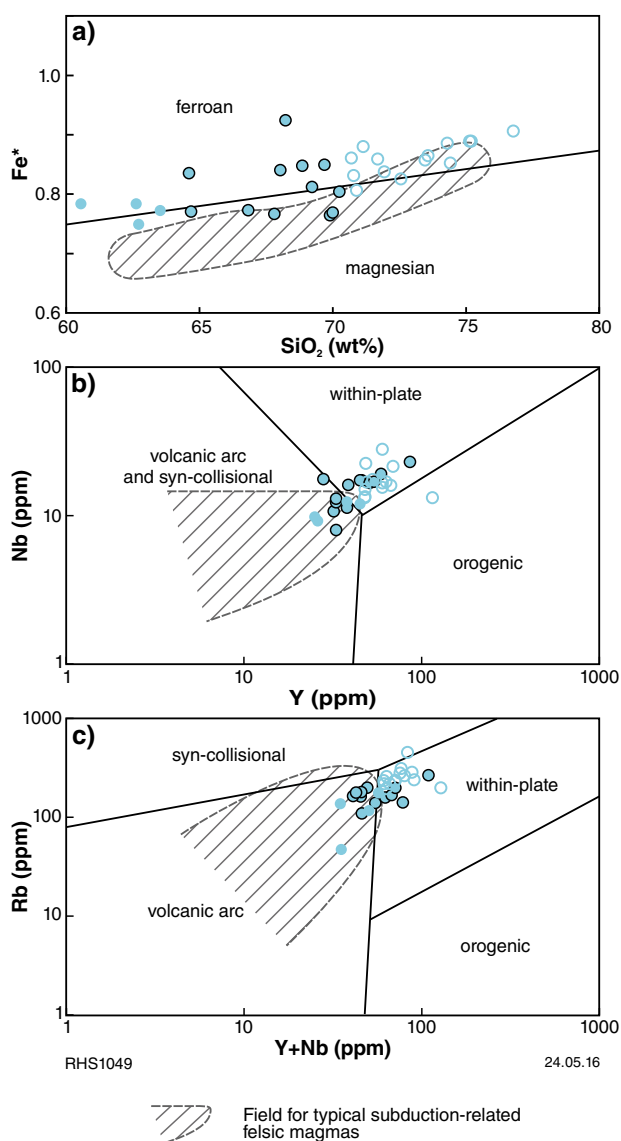


Figure 22. a) Compositional variation diagram showing SiO_2 vs Fe^* [= ratio of $\text{FeO}/(\text{FeO}+\text{MgO})$ — after Frost et al. 2001]; b) and c) tectonic discrimination diagram (after Pearce et al., 1984). Field outlines region where synsubduction felsic magmas typically plot. The tectonic discrimination diagrams are not used here to infer a 'within plate' affinity for the Recherche Supersuite, only that their composition is generally atypical of subduction-related suites — an observation consistent with several other independent lines of geological evidence (e.g. Spaggiari et al., 2014c). Nevertheless, their compositions diverge from subduction-related magmas in ways that implicate high-temperature interaction between dry and typically reduced melts of upwelled mantle and lower crustal melts.

c. 1300 Ma

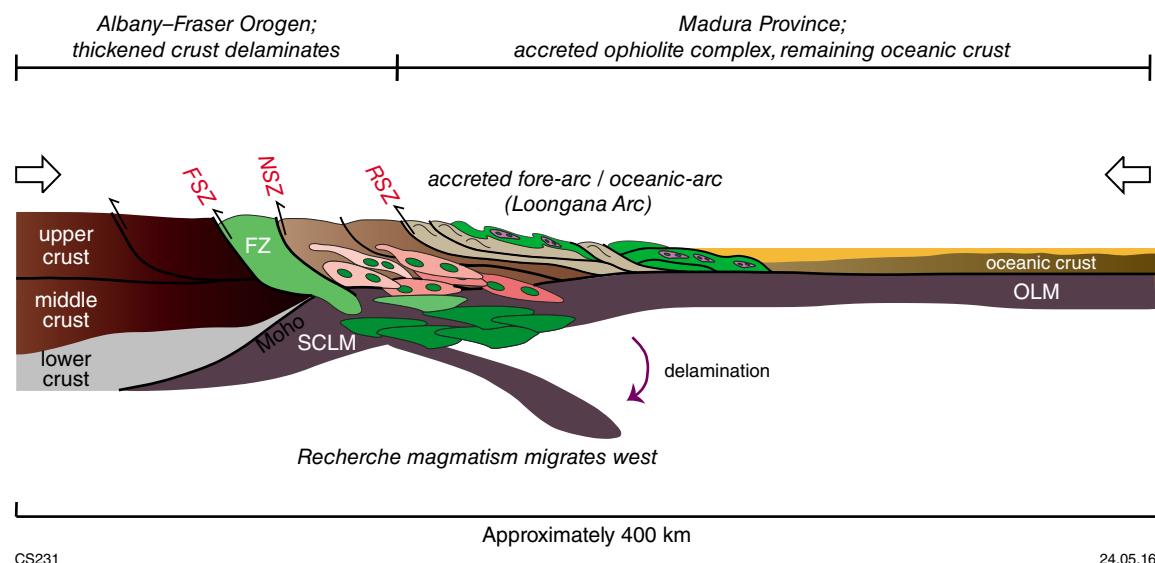


Figure 23. Schematic diagram showing the diachronous effect on magmatism associated with accretion of the Loongana Arc onto the passive margin of the Albany–Fraser Orogen. This is followed by delamination of the lower crust, with associated magmatism culminating in emplacement of the Fraser Zone gabbros at c. 1300 Ma, and a phase of compression. SCLM – subcontinental lithospheric mantle; OLM – oceanic lithospheric mantle; FSZ – Fraser Shear Zone; NSZ – Newman Shear Zone; RSZ – Rodona Shear Zone; FZ – Fraser Zone. Green indicates mafic/mantle component; pink indicates crustal melt/granitic component. Large arrows indicate approximate stress field orientation.

Summary and conclusions

Fraser Zone magmatism formed during Stage I of the Albany–Fraser Orogeny along the southeastern margin of the Yilgarn Craton, as the overthrust and strongly reworked component of that margin underwent progressive extensional collapse.

There is no evidence that the various mafic and ultramafic rocks of the Fraser Zone were derived from a different mantle-source component. Their mantle source was slightly more melt depleted than the source for N-MORB. Nor is there any evidence that the crustal component that formed the initial and main source of incompatible trace-element enrichment in these magmas differed. All magmas extracted from the mantle appear to have ponded in, or at least interacted with, the felsic basement to the Fraser Zone.

Major element trends and mineral compositions indicate that the parental magmas at Nova–Bollinger either reflect higher degree partial melts of a common mantle source, and/or that the magmas from which the Plato cumulates and the main gabbros formed had already undergone more extensive olivine and plagioclase fractionation. If the latter is true, then some magmas underwent enhanced fractional crystallization, without sulfur-saturation, before intrusion into the Fraser Zone.

The Ni-depleted compositions of olivine in Nova–Bollinger cumulates suggest that some magmas (but not those for Plato and other main gabbros) reached sulfur-

saturation before completion of olivine crystallization. This, combined with evidence for an additional sulfur-rich crustal contaminant in the Nova–Bollinger rocks, points to an intrusion history allowing an early staging chamber that was open to additional crustal contamination. This occurred at crustal depths of <20 km and was likely within deeply buried sequences of the sulfur-rich Snowys Dam Formation (i.e. within the Fraser Zone).

Irrespective of whether the intrusion history allowed assimilation and homogenization of sulfide-rich country rock and consequent widespread sulfur-saturation, the tectonic conditions accompanying final emplacement were probably critical. In the case of Nova–Bollinger, syn-magmatic tectonic activity likely facilitated the transport of sulfide-laden slurries or crystal suspensions into deformation zones where hydrodynamic sorting could lead to sulfide concentrations, and also drained the resulting cumulate assemblages of interstitial liquid. In the case of Plato, textural observations suggest final emplacement in a tectonic environment that lacked the capacity to transport a sulfide-bearing slurry.

Similarly, most intrusions of the main gabbro were of relatively evolved magmas that had undergone early olivine fractionation, and typically formed relatively thin sills of finer grained rocks that presumably crystallized rapidly enough so that effective crystal fractionation, crystal-liquid separation and cumulate formation was negligible. These thin intrusions would also have had a low capacity to assimilate potential sulfide-bearing country rocks of the Snowys Dam Formation in order to trigger

sulfur-saturation. Even if such assimilation did occur, convective homogenization and hence widespread sulfur-saturation within these bodies would be unlikely.

The mafic magmas and the processes that concentrated them within the Fraser Zone should simply be regarded as end-member components and processes within an orogen-wide system that progressively mixed mantle-derived magmas with granites of the Gora Hill Suite. Although in lower abundance, similar mafic intrusions should be expected to the east of the Fraser Zone in the eastern Nornalup Zone, where enhanced interaction with (potentially sulfur-rich) crust might also be expected.

References

- Armstrong, JT 1988, Quantitative analysis of silicates and oxide minerals: Comparison of Monte-Carlo, ZAF and Phi-Rho-Z procedures: *Microbeam Analysis*, v. 1988, p. 239–246.
- Barnes, SJ 1986, The effect of trapped liquid crystallization on cumulus mineral compositions in layered intrusions: *Contributions to Mineralogy and Petrology*, v. 93, p. 524–531.
- Barnes, S-J Maier, WD and Curl, E 2010, Composition of the marginal rocks and sills of the Rustenburg layered suite, Bushveld Complex, South Africa: implications for the formation of the PGE deposits: *Economic Geology*, v. 105, p. 1491–1511.
- Begg, GC, Hronsky, JAM, Arndt, NT, Griffin, WL, O'Reilly, SY and Hayward, N 2010, Lithospheric, cratonic and geodynamic setting of Ni–Cu–PGE sulfide deposits: *Economic Geology*, v. 105, p. 1057–1070.
- Bennett, M, Gollan, M, Staubmann, M, Bartlett, J 2014, Motive, Means, and Opportunity: Key Factors in the Discovery of the Nova-Bollinger Magmatic Nickel-Copper Sulfide Deposits in Western Australia: *Society of Economic Geologists, Special Publication 18*, p. 301–320.
- Bodorkos, S and Clark, DJ 2004, Evolution of a crustal-scale transpressive shear zone in the Albany–Fraser Orogen, SW Australia: 1. P–T conditions of Mesoproterozoic metamorphism in the Coramup Gneiss: *Journal of Metamorphic Geology*, v. 22, p. 691–711.
- Clark, DJ, Hensen, BJ and Kinny, PD 2000, Geochronological constraints for a two-stage history of the Albany–Fraser Orogen, Western Australia: *Precambrian Research*, v. 102, p. 155–183.
- Clark, C, Kirkland, CL, Spaggiari, CV, Oorschot, C, Wingate, MTD and Taylor, RJ 2014, Proterozoic granulite formation driven by mafic magmatism: An example from the Fraser Range Metamorphics, Western Australia: *Precambrian Research*, v. 240, p. 1–21.
- Condie, KC and Myers, JS 1999, Mesoproterozoic Fraser Complex: geochemical evidence for multiple subduction-related sources of lower crustal rocks in the Albany–Fraser Orogen, Western Australia: *Australian Journal of Earth Sciences*, v. 46, p. 875–882.
- De Waele, B and Pisarevsky, SA 2008, Geochronology, paleomagnetism and magnetic fabric of metamorphic rocks in the northeast Fraser Belt, Western Australia: *Australian Journal of Earth Sciences*, v. 55, p. 605–621.
- Donovan, JJ and Tingle, TN 1996, An Improved Mean Atomic Number Correction for Quantitative Microanalysis: *Journal of Microscopy*, v. 2, p. 1–7.
- Donovan, JJ, Snyder, DA and Rivers, ML 1993, An Improved Interference Correction for Trace Element Analysis: *Microbeam Analysis*, v. 2, p. 23–28.
- Doyle, MG, Fletcher, IR, Foster, J, Large, R, Mathur, R, McNaughton, NJ, Meffre, S, Muhling, JR, Phillips, D and Rasmussen, B 2015, Geochronological constraints on the Tropicana Gold Deposit and Albany–Fraser Orogen, Western Australia: *Economic Geology*, v. 110, p. 1–32.
- Fletcher, IR, Myers, JS and Ahmat, AL 1991, Isotopic evidence on the age and origin of the Fraser Complex, Western Australia: a sample of Mid-Proterozoic lower crust: *Chemical Geology: Isotope Geoscience*, v. 87, p. 197–216.
- Frost, BR, Barnes, CG, Collins, WJ, Arculus, RJ, Ellis, DJ and Frost, CD 2001, A geochemical classification for granite rocks: *Journal of Petrology*, v. 42, p. 2033–2048.
- Gale, A, Dalton, CA, Langmuir, CH, Su, Y and Schilling, J-G 2013, The mean composition of ocean ridge basalts: *Geochemistry Geophysics Geosystems*, v. 14, p. 489–518.
- Gollam, M 2012, Final drilling report 'The Eye'; Sirius Gold Pty Ltd: Geological Survey of Western Australia, Statutory mineral exploration report, A092733 (unpublished).
- Jolly, WT, Lidiak, EG, Dickin, AP and Wu, T-U 2001, Secular geochemistry of central Puerto Rican island arc lavas: constraints on Mesozoic tectonism in the eastern Greater Antilles: *Journal of Petrology*, v. 42, p. 2197–2214.
- Kirkland, CL, Spaggiari, CV, Pawley, MJ, Wingate, MTD, Smithies, RH, Howard, HM, Tyler, IM, Belousova, EA and Poujol, M 2011, On the edge: U–Pb, Lu–Hf, and Sm–Nd data suggests reworking of the Yilgarn Craton margin during formation of the Albany–Fraser Orogen: *Precambrian Research*, v. 187, p. 223–247.
- Kirkland, CL, Spaggiari, CV, Smithies, RH and Wingate, MTD 2014, Cryptic progeny of craton margins: Geochronology and Isotope Geology of the Albany–Fraser Orogen with implications for evolution of the Tropicana Zone, in *Albany–Fraser Orogen seismic and magnetotelluric (MT) workshop 2014: extended abstracts compiled by CV Spaggiari and IM Tyler*, Geological Survey of Western Australia, Record 2014/6, p. 89–101.
- Li, C, Zhang, Z, Li, W, Wang, Y, Sund, T and Ripley, EM 2015, Geochronology, petrology and Hf–S isotope geochemistry of the newly-discovered Xiarihamu magmatic Ni–Cu sulfide deposit in the Qinghai–Tibet plateau, western China: *Lithos*, v. 216–217, p. 224–240.
- Maier, WD and Barnes, S-J 2010, The Kabanga Ni sulfide deposits, Tanzania: II. Chalcophile and siderophile element geochemistry: *Mineralium Deposita*, v. 45, p. 443–460.
- Maier, WD and Eales, HV 1997, Correlation within the UG2 – Merensky Reef interval of the Western Bushveld Complex, based on geochemical, mineralogical and petrological data: *Geological Survey of South Africa, Bulletin 120*, 56p.
- Maier, WD, Howard, HM, Smithies, RH, Yang, SH, Barnes, S-J, O'Brien, H, Huhma, H and Gardoll, S 2015, Magmatic ore deposits in mafic-ultramafic intrusions of the Giles Event, Western Australia: *Ore Geology Reviews*, v. 71, p. 405–436.
- Morris, PA, Sanders, AJ, McGuinness, SA, Coker, J and King, JD 2000, Geochemical mapping of the Fraser Range region: Geological Survey of Western Australia, *Regolith Geochemical Series Explanatory Notes*, 45p.
- Mungall, J and Brenan, J 2014, Partitioning of platinum-group elements and Au between sulfide liquid and basalt and the origins of mantle-crust fractionation of the chalcophile elements: *Geochimica et Cosmochimica Acta*, v. 125, p. 265–289.
- Nelson, DR, Myers, JS and Nutman, AP 1995, Chronology and evolution of the Middle Proterozoic Albany–Fraser Orogen, Western Australia: *Australian Journal of Earth Sciences*, v. 42, p. 481–495.

- Occhipinti, SA, Doyle, M, Spaggiari, CV, Korsch, R, Cant, G, Martin, K, Kirkland, CL, Savage, J, Less, T, Bergin, L and Foz, L 2014, Interpretation of the deep seismic reflection line 12GA-T1: northeastern Albany–Fraser Orogen, *in* Albany–Fraser Orogen seismic and magnetotelluric (MT) workshop 2014: extended abstracts *compiled by* CV Spaggiari and IM Tyler: Geological Survey of Western Australia, Record 2014/6, p. 52–68.
- Oorschot, CW 2011, P-T-t evolution of the Fraser Zone, Albany–Fraser Orogen, Eastern Australia: Geological Survey of Western Australia, Record 2011/18, 101p.
- Pearce, JA, Harris, NBW and Tindle, AG 1984, Trace element discrimination diagrams for the tectonic interpretation of granitic rocks: *Journal of Petrology*, v. 25, p. 956–983.
- Raedeke, LD 1982, Petrogenesis of the Stillwater Complex: The University of Washington, Seattle, PhD thesis (unpublished).
- Ripley, EM 1999, Systematics of sulfur and oxygen isotopes in mafic igneous rocks and related Cu–Ni–PGE mineralization, *in* Dynamic processes in magmatic ore deposits and their application to mineral exploration *edited by* RR Keays, CM Lesher, PC Lightfoot and CEG Farrow: Geological Association of Canada, Short Course Notes 13, p. 133–158.
- Sinton, JM, Ford, LL, Chappell, B and McCulloch, MT 2003, Magma genesis and mantle heterogeneity in the Manus back-arc basin, Papua New Guinea: *Journal of Petrology*, v. 44, p. 159–195.
- Smithies, RH, Spaggiari, CV, Kirkland, CL, Howard, HM and Maier, WD 2013, Petrogenesis of gabbros of the Mesoproterozoic Fraser Zone: constraints on the tectonic evolution of the Albany–Fraser Orogen: Geological Survey of Western Australia, Record 2013/5, 29p.
- Smithies, RH, Spaggiari, CV, Kirkland, CL and Maier, WD 2014, Geochemistry and petrogenesis of igneous rocks in the Albany–Fraser Orogen, *in* Albany–Fraser Orogen seismic and magnetotelluric (MT) workshop 2014: extended abstracts *compiled by* CV Spaggiari and IM Tyler: Geological Survey of Western Australia, Record 2014/6, p. 77–88.
- Smithies, RH, Spaggiari, CV and Kirkland, CL 2015, Building the crust of the Albany–Fraser Orogen: constraints from granite geochemistry: Geological Survey of Western Australia, Report 150, 49p.
- Sobolev, SV, Sobolev, AV, Kuzmin, DV, Krivolutszkaya, NA, Petrunin, AG, Arndt, NT, Radko, VA and Vasiliev, YR 2011, Linking mantle plumes, large igneous provinces and environmental catastrophes: *Nature*, v. 477, p. 312–16.
- Spaggiari, CV, Bodorkos, S, Barquero-Molina, M, Tyler, IM and Wingate, MTD 2009, Interpreted bedrock geology of the south Yilgarn and central Albany–Fraser Orogen, Western Australia: Geological Survey of Western Australia, Record 2009/10, 84p.
- Spaggiari, CV, Kirkland, CL, Pawley, MJ, Smithies, RH, Wingate, MTD, Doyle, MG, Blenkinsop, TG, Clark, C, Oorschot, CW, Fox, LJ and Savage, J 2011, The geology of the east Albany–Fraser Orogen — a field guide: Geological Survey of Western Australia, Record 2011/23, 97p.
- Spaggiari, CV, Kirkland, CL, Smithies, RH and Wingate, MTD 2012, What lies beneath — interpreting the Eucla basement, *in* GSWA 2012 extended abstracts: promoting the prospectivity of Western Australia: Geological Survey of Western Australia, Record 2012/2, p. 25–27.
- Spaggiari, CV, Kirkland, CL, Smithies, RH, Occhipinti, SA and Wingate, MTD 2014a, Geological framework of the Albany–Fraser Orogen, *in* Albany–Fraser Orogen seismic and magnetotelluric (MT) workshop 2014: extended abstracts *compiled by* CV Spaggiari and IM Tyler: Geological Survey of Western Australia, Record 2014/6, p. 12–27.
- Spaggiari, CV, Occhipinti, SA, Korsch, RJ, Doublier, MP, Clark, DJ, Dentith, MC, Gessner, K, Doyle, MG, Tyler, IM, Kennett, BLN, Costelloe, RD, Fomin, T and Holzschuh, J 2014b, Interpretation of Albany–Fraser seismic lines 12GA-AF1, 12GA-AF2 and 12GA-AF3: implications for crustal architecture, *in* Albany–Fraser Orogen seismic and magnetotelluric (MT) workshop 2014: extended abstracts *compiled by* CV Spaggiari and IM Tyler: Geological Survey of Western Australia, Record 2014/6, p. 28–51.
- Spaggiari, CV, Kirkland, CL, Smithies, RH and Wingate, MTD 2014c, Tectonic links between Proterozoic sedimentary cycles, basin formation and magmatism in the Albany–Fraser Orogen, Western Australia: Geological Survey of Western Australia, Report 133, 63p.
- Spaggiari, CV, Kirkland, CL, Smithies, RH, Wingate, MTD and Belousova, E 2015a, Transformation of an Archean craton margin during Proterozoic basin formation and magmatism: the Albany–Fraser Orogen, Western Australia: *Precambrian Research*, v. 266, p. 440–466.
- Spaggiari, CV, Smithies, RH, Kirkland, CL, England, RN, Occhipinti, SA and Wingate, MTD 2015b, Eucla basement results: implications for geodynamics and mineral prospectivity: Geological Survey of Western Australia, Record 2015/10, p. 53–58.
- Spaggiari, CV and Smithies, RH (compilers) 2015, Eucla basement stratigraphic drilling results release workshop: extended abstracts: Geological Survey of Western Australia, Record 2015/10, 70p.
- Sun, S-S and McDonough, WF 1989, Chemical and isotopic systematics of oceanic basalts: implications for mantle compositions and processes, *in* *Magmatism in the Ocean Basins* *edited by* AD Saunders and MJ Norry: Geological Society, London, Special Publication 42, p. 313–345.
- Teigler, B and Eales, HV 1996, The Lower and Critical Zones of the western limb of the Bushveld Complex, as indicated by the Nooitgedacht boreholes: Geological Survey of South Africa, Bulletin 111, 126p.
- Tyler, IM, Spaggiari, CV, Occhipinti, SA, Kirkland CL and Smithies, RH 2014, The Albany–Fraser deep reflection seismic and MT survey: Implications for mineral systems, *in* Albany–Fraser Orogen seismic and magnetotelluric (MT) workshop 2014: extended abstracts *compiled by* CV Spaggiari and IM Tyler: Geological Survey of Western Australia Record 2014/6, p. 174–182.
- Venables, T 2014, Enterprise Metals Limited, Fraser Range Project, Exploration Licence 63/1281 Final Drilling Report, Co-funded Drilling Agreement DAG 2014/00384566, 25th July, 2014: WAMEX report A103177.
- Wallace, P and Carmichael, ISE 1992, Sulfur in basaltic magmas: *Geochimica et Cosmochimica Acta*, v. 56, p. 1863–1874.
- Woodhead, J, Hergt, J, Greig, A and Edwards, L 2011, Subduction zone Hf-anomalies: Mantle messenger, melting artefact or crustal process?: *Earth and Planetary Science Letters*, v. 304, p. 231–239.
- Yang, S, Maier, WD, Lahaye, Y and O'Brien, H 2013, Strontium isotope disequilibrium of plagioclase in the Upper Critical Zone of the Bushveld Complex: evidence for mixing of crystal slurries: *Contributions to Mineralogy and Petrology*, v. 166, p. 959–974.

Appendix 1

Analytical methods

Whole-rock geochemical samples other than bottom-of-hole (BOH) chips were prepared for analysis at GSWA using a jaw crusher followed by milling in either a tungsten carbide or low-Cr carbon-steel mill. All BOH chips were first washed in an ultrasonic bath, dried and the least altered or weathered chips were hand-picked prior to milling. Major and trace elements were determined at a variety of laboratories over the course of the study and all data and analytical details can be accessed from the WACHEM database (<http://geochem.dmp.wa.gov.au/geochem/>). For all laboratories, major elements were determined by wavelength-dispersive X-ray fluorescence (XRF) on fused disks and trace-element concentrations were determined by inductively coupled plasma – mass spectrometry (ICP-MS). Precision is better than 1% of the reported values for major elements and better than 10% of the reported values for trace elements. Platinum group elements were determined by ICP-MS at the University of Quebec at Chicoutimi, Canada. Analytical details are given in Barnes et al. (2010), and the data are listed in Appendix 3.

Whole-rock sulfur isotopes were determined by Rafter GNS Sciences at the New Zealand National Isotope Centre. The samples were measured in duplicate in tin capsules with equal amounts of V_2O_5 on a EuroVector Elemental Analyzer connected to a GVI IsoPrime mass spectrometer. All results are averages and standard deviations of duplicates are reported with respect to VCDT, normalized to internal standards: R18742, R2268, and R2298 with accepted $\delta^{34}S$ values of -32‰ , $+3.3\text{‰}$, and $+8.6\text{‰}$, respectively. The external precision for this instrument is better than 0.3 for $\delta^{34}S$. All data are listed in Appendix 4. Strontium and sulfur isotopic compositions of plagioclase and sulfide minerals respectively were analysed by laser ablation ICP-MS at GTK, Espoo, Finland. Analytical details are given in Yang et al. (2013), and the data are listed in Appendix 4.

All whole-rock Nd isotope analyses were determined on sample powders by isotope dilution at the University of Rennes (France) and the University of Queensland (Australia) over the course of several years. Analytical details are given in Kirkland et al. (2014), and the data are provided in Appendix 5.

The major-element compositions of plagioclase, pyroxenes and olivine were determined at two separate laboratories. All data are presented in Appendix 6. Data for samples from Nova were analysed at the CSIRO labs at Clayton, Victoria using a JEOL 8900R electron microprobe equipped with a five wavelength dispersive spectrometers and two energy dispersive spectrometers. All elements

were analysed using the $K\beta$ line except for Co which used the $K\beta$ to avoid the overlap with Fe; $K\alpha$. Standards used were San Carlos olivine $[(Mg, Fe)_2SiO_4]$, heazlewoodite $[Ni_3S_2]$, hematite $[Fe_2O_3]$, adularia $[KAlSi_3O_8]$, magalox-spinel $[MgAl_2O_4]$, albite $[NaAlSi_3O_8]$, Co metal, rhodonite $[MnSiO_3]$, rutile $[TiO_2]$, chromite $[Cr_2O_3]$, wollastonite $(CaSiO_3)$. Oxygen was calculated by stoichiometry, based on valence. Operating conditions for the microprobe were: an accelerating voltage of 20 kV and a beam current of 15 nA. To average the composition of grains, the electron beam was defocused a same amount (5 μm) for the analyses. All analysis positions were verified as being homogeneous by viewing the backscattered electron image of the area to be analysed. All elemental analyses were corrected for atomic number (Z), absorption (A) and fluorescence (F) using a Phi-Rho-Z matrix correction procedure implemented on the JEOL 8500F.

Mineral data for samples from the Plato Prospect were analysed at the Centre for Microscopy Characterisation and Analysis, The University of Western Australia, using a JEOL JXA8530F electron microprobe equipped with five tunable wavelength dispersive spectrometers. Operating conditions were 40 degrees take-off angle, and a beam energy of 15 keV. The beam current was 20 nA, and the beam was fully focused. Elements were acquired using analysing crystals LiFH for Ti $K\alpha$, Cr $K\alpha$, LiF for Fe $K\alpha$, Mn $K\alpha$, Ni $K\alpha$, PETJ for K $K\alpha$, Ca $K\alpha$, and TAP for Mg $K\alpha$, Al $K\alpha$, Na $K\alpha$, Si $K\alpha$. The standards were Cr_2O_3 for Cr $K\alpha$, Magnetite for Fe $K\alpha$, Periclase for Mg $K\alpha$, Rutile for Ti $K\alpha$, Wollastonite for Si $K\alpha$, Ca $K\alpha$, Corundum for Al $K\alpha$, Jadeite for Na $K\alpha$, Mn for Mn $K\alpha$, Orthoclase for K $K\alpha$, and Ni-Olivine for Ni $K\alpha$. The counting time was 20 seconds for Si $K\alpha$, Mg $K\alpha$, Ti $K\alpha$, Fe $K\alpha$, Mn $K\alpha$, Ca $K\alpha$, K $K\alpha$, Al $K\alpha$, Na $K\alpha$, and 50 seconds for Cr $K\alpha$ and Ni $K\alpha$. The intensity data was corrected for Time Dependent Intensity (TDI) loss (or gain) using a self-calibrated correction for Si $K\alpha$, Ti $K\alpha$, Mn $K\alpha$, K $K\alpha$, Na $K\alpha$. The MAN background correction was used throughout, with intensity data calibrated and continuum absorption corrected for Si $K\alpha$, Mg $K\alpha$, Ti $K\alpha$, Cr $K\alpha$, Fe $K\alpha$, Mn $K\alpha$, Ca $K\alpha$, K $K\alpha$, Al $K\alpha$, Na $K\alpha$, Ni $K\alpha$ (Donovan and Tingle 1996). Unknown and standard intensities were corrected for deadtime. Interference corrections were applied to Fe for interference by Mn, and to Mn for interference by Cr (Donovan et al., 1993). Detection limits ranged from 0.005 wt% for Si $K\alpha$ to 0.007 wt% for Al $K\alpha$ to 0.009 wt% for Ca $K\alpha$ to 0.012 wt% for Ti $K\alpha$ to 0.026 wt% for Fe $K\alpha$. Oxygen was calculated by cation stoichiometry and included in the matrix correction. The ZAF correction procedure utilized was Armstrong/Love Scott (Armstrong, 1988).

Appendix 2

Whole-rock major and trace-element geochemical data

Table 2.1. Whole-rock major and trace element geochemical data from Nova-Bollinger

GSWA No.	Drillhole	depth interval in m		SiO ₂ wt%	TiO ₂	Al ₂ O ₃	Fe ₂ O ₃ T	MgO	MnO	CaO	K ₂ O	Na ₂ O	P ₂ O ₅	LOI	Total
		From	To												
201233	SFRD0017	66.6	66.9	49.50	0.20	15.60	8.51	14.85	0.15	9.83	0.09	1.24	0.00	0.29	99.97
201234	SFRD0017	77	77.2	47.90	0.25	13.00	11.06	15.25	0.17	9.19	0.11	1.16	0.01	0.76	98.10
201235	SFRD0017	87.5	87.7	48.60	0.22	12.20	9.55	20.10	0.17	7.93	0.06	0.86	0.00	0.32	99.69
201236	SFRD0017	95.8	96	43.80	0.15	8.27	13.39	27.60	0.19	5.68	0.06	0.65	0.00	0.46	99.79
201237	SFRD0017	115.6	115.8	40.00	0.12	5.69	13.06	31.10	0.19	3.89	0.05	0.45	0.01	4.68	94.56
201238	SFRD0017	129.5	129.7	48.40	0.18	16.50	5.52	13.65	0.11	13.10	0.08	1.06	0.00	0.38	98.60
201239	SFRD0017	135.5	135.8	49.10	0.39	7.29	8.91	15.15	0.16	16.15	0.10	0.68	0.01	1.14	97.94
201240	SFRD0017	141.6	141.8	50.70	0.19	13.15	8.60	18.45	0.16	7.54	0.08	0.87	0.00	0.43	99.74
201241	SFRD0017	169	169.3	38.10	0.12	5.16	12.46	31.50	0.18	3.23	0.07	0.40	0.01	8.35	91.23
201242	SFRD0017	191.4	191.6	39.90	0.14	6.15	12.34	30.50	0.18	4.04	0.06	0.50	0.01	6.07	93.82
201243	SFRD0017	203.5	203.7	39.80	0.17	5.22	14.94	30.70	0.19	3.26	1.01	0.30	0.01	2.16	95.60
201244	SFRD0017	222.5	222.7	45.50	0.27	16.45	11.46	9.43	0.11	10.90	0.13	1.55	0.00	2.62	95.80
201245	SFRD0017	231.1	231.5	50.30	0.21	18.40	6.88	10.90	0.13	11.00	0.17	1.79	0.01	0.31	99.79
201246	SFRD0017	239.2	239.4	49.80	0.22	18.30	6.20	11.00	0.12	11.45	0.35	1.86	0.00	0.61	99.30
201247	SFRD0017	251	251.4	43.60	0.16	7.64	12.78	29.20	0.19	5.23	0.08	0.64	0.01	1.08	99.53
201248	SFRD0017	259.7	259.9	47.40	0.29	16.05	9.45	11.55	0.13	11.85	0.13	1.72	0.01	0.88	98.58
201249	SFRD0017	273	273.3	43.10	0.19	5.81	13.76	33.10	0.21	3.84	0.09	0.50	0.03	0.73	100.63
201250	SFRD0017	283	283.2	41.50	0.15	5.13	14.24	33.70	0.21	3.66	0.07	0.43	0.02	1.15	99.11
201255	SFRD0017	56.7	57	49.00	0.31	16.65	8.11	9.43	0.13	12.25	0.19	2.08	0.00	1.17	98.15
206721	SFRD0017	52.9	53	46.34	0.13	14.88	10.96	16.09	0.17	9.90	0.08	1.16	0.01	0.05	99.77
206722	SFRD0017	57.4	57.5	50.34	0.30	17.36	7.30	9.04	0.13	12.36	0.18	2.19	0.02	0.51	99.73
206723	SFRD0017	91.5	91.6	49.25	1.11	15.62	12.70	8.40	0.22	10.57	0.27	2.01	0.08	0.08	100.31
206724	SFRD0017	145.9	146	41.25	0.13	6.87	12.18	28.39	0.18	4.66	0.07	0.58	0.02	4.80	99.13
206725	SFRD0017	155.1	155.2	40.77	0.09	6.22	13.62	29.83	0.18	3.58	0.14	0.56	0.02	4.19	99.20
206726	SFRD0017	221.1	221.2	39.88	0.09	7.16	12.85	30.04	0.18	3.78	0.04	0.63	0.02	4.04	98.71
206727	SFRD0017	262.4	262.5	49.70	0.27	16.85	7.97	10.92	0.14	11.55	0.17	1.73	0.02	0.65	99.97
206728	SFRD0017	278.7	278.8	42.07	0.16	5.60	13.86	32.25	0.20	3.87	0.08	0.54	0.04	0.41	99.08

Table 2.1. continued

GSWA No.	Drillhole	Ag (ppm)	As	Au (ppb)	Ba	Cd	Ce	Co	Cr	Cs	Cu	Dy	Er	Eu	Ga
201233	SFRD0017	n.d.	n.d.	10	41.9	-0.5	2.0	84	1040	0.1	164	0.7	0.5	0.3	11.6
201234	SFRD0017	n.d.	n.d.	80	43.9	-0.5	2.8	136	840	0.1	857	1.1	0.7	0.4	10.9
201235	SFRD0017	n.d.	n.d.	30	34.2	-0.5	2.1	98	2150	0.1	339	0.7	0.5	0.3	10.2
201236	SFRD0017	n.d.	n.d.	30	32.0	-0.5	2.1	142	1570	0.1	375	0.7	0.5	0.2	7.6
201237	SFRD0017	n.d.	n.d.	10	23.0	-0.5	2.2	123	1410	0.1	161	0.5	0.4	0.2	5.3
201238	SFRD0017	n.d.	n.d.	10	28.5	-0.5	2.1	65	3080	0.1	161	0.9	0.5	0.3	10.6
201239	SFRD0017	n.d.	n.d.	70	23.6	-0.5	5.1	108	970	0.1	677	2.1	1.3	0.5	7.9
201240	SFRD0017	n.d.	n.d.	30	32.3	-0.5	2.0	98	1640	0.1	460	0.6	0.5	0.2	10.0
201241	SFRD0017	n.d.	n.d.	10	27.8	-0.5	2.5	121	860	0.1	88	0.5	0.4	0.2	5.0
201242	SFRD0017	n.d.	5	10	28.5	-0.5	2.6	119	840	0.1	66	0.6	0.4	0.2	5.8
201243	SFRD0017	n.d.	n.d.	30	36.7	-0.5	5.2	148	5310	3.2	362	0.8	0.5	0.2	7.2
201244	SFRD0017	2.6	n.d.	370	45.3	-0.5	2.9	200	550	0.1	4700	1.3	0.8	0.5	12.2
201245	SFRD0017	n.d.	n.d.	10	50.6	-0.5	3.0	61	450	0.1	74	0.8	0.6	0.4	12.9
201246	SFRD0017	n.d.	n.d.	10	42.7	-0.5	3.0	61	440	0.2	123	1.0	0.6	0.4	12.7
201247	SFRD0017	n.d.	n.d.	10	32.3	-0.5	2.9	119	1740	0.2	83	0.6	0.4	0.2	6.6
201248	SFRD0017	n.d.	n.d.	70	68.8	-0.5	4.6	136	580	0.1	642	1.5	0.9	0.5	12.8
201249	SFRD0017	n.d.	n.d.	10	38.6	-0.5	4.0	138	1810	0.1	85	0.7	0.5	0.2	5.8
201250	SFRD0017	n.d.	n.d.	10	32.5	-0.5	3.1	132	1650	0.1	106	0.6	0.4	0.2	5.2
201255	SFRD0017	0.50	n.d.	80	61.9	-0.5	3.4	106	250	0.3	899	1.5	0.9	0.5	13.9
206721	SFRD0017	0.06	-0.5	3	42.4	0.1	1.5	81	253	-0.1	97.1	0.6	0.4	0.3	10.8
206722	SFRD0017	0.25	-0.5	3	62.8	0.2	3.3	67	213	0.2	497.8	1.3	0.9	0.4	13.7
206723	SFRD0017	0.05	-0.5	-1	111.1	0.2	13.6	58	113	0.3	75	3.1	1.9	1.0	16.8
206724	SFRD0017	0.06	0.5	-1	23.5	0.1	1.9	118	1281	0.2	117.2	0.6	0.4	0.2	5.7
206725	SFRD0017	0.08	3.5	1	33.6	0.1	2.7	128	1130	2.2	169.1	0.5	0.3	0.2	5.5
206726	SFRD0017	0.06	-0.5	2	18.6	0.1	1.1	118	3623	0.2	94.3	0.3	0.2	0.1	6.4
206727	SFRD0017	0.20	-0.5	2	72.5	0.2	3.8	66	388	0.2	331	1.3	0.8	0.5	12.6
206728	SFRD0017	0.05	-0.5	-1	33.6	0.1	3.6	136	1221	0.2	92.3	0.6	0.4	0.2	5.0

Table 2.1. continued

GSWA No.	Drillhole	Gd	Hf	Ho	La	Lu	Nb	Nd	Ni	Pb	Pd (ppb)	Pr	Pt (ppb)	Rb	Re (ppb)
201233	SFRD0017	0.6	0.2	0.2	1.5	0.1	-0.2	1.4	339	-2	n.a.	0.3	1	1.2	n.a.
201234	SFRD0017	1.0	0.3	0.2	1.8	0.1	-0.2	2.2	1430	6	0.4	0.4	2.9	1.9	n.a.
201235	SFRD0017	0.7	0.2	0.2	1.6	0.1	-0.2	1.5	700	4	0.1	0.3	2.5	1.3	n.a.
201236	SFRD0017	0.6	0.2	0.2	1.6	0.1	-0.2	1.4	1040	4	0.1	0.3	1.5	1.4	n.a.
201237	SFRD0017	0.5	0.2	0.1	1.6	0.1	-0.2	1.4	882	-2	0.1	0.3	0.5	1.6	n.a.
201238	SFRD0017	0.8	0.2	0.2	1.5	0.1	-0.2	1.6	391	-2	n.a.	0.3	0.9	2.0	n.a.
201239	SFRD0017	2.0	0.6	0.4	2.5	0.2	0.3	4.3	1040	4	0.3	0.9	1.8	2.7	n.a.
201240	SFRD0017	0.5	0.2	0.1	1.6	0.1	-0.2	1.2	796	-2	0.1	0.3	1.6	1.7	n.a.
201241	SFRD0017	0.5	0.2	0.1	1.8	0.1	0.2	1.5	761	-2	0.1	0.3	0.5	2.5	n.a.
201242	SFRD0017	0.6	0.2	0.1	1.8	0.1	0.5	1.6	688	-2	n.a.	0.4	0.5	2.1	n.a.
201243	SFRD0017	0.8	0.3	0.2	2.8	0.1	0.6	2.7	1240	-2	0.2	0.7	2.2	47.0	n.a.
201244	SFRD0017	1.3	0.4	0.3	1.7	0.1	-0.2	2.5	2930	13	0.6	0.5	2.4	2.3	n.a.
201245	SFRD0017	0.8	0.2	0.2	2.0	0.1	0.2	2.0	145	3	n.a.	0.4	0	2.1	n.a.
201246	SFRD0017	0.9	0.3	0.2	1.9	0.1	-0.2	2.2	181	2	n.a.	0.5	0.6	4.4	n.a.
201247	SFRD0017	0.6	0.2	0.1	1.9	0.1	0.2	1.9	684	-2	n.a.	0.4	1.5	2.5	n.a.
201248	SFRD0017	1.5	0.4	0.3	2.6	0.1	-0.2	3.8	1100	8	0.3	0.7	2.5	1.5	n.a.
201249	SFRD0017	0.7	0.3	0.2	2.5	0.1	0.4	2.5	845	6	n.a.	0.6	0.8	2.9	n.a.
201250	SFRD0017	0.6	0.2	0.1	2.1	0.1	0.3	1.9	810	-2	n.a.	0.5	0.6	2.4	n.a.
201255	SFRD0017	1.4	0.4	0.3	2.0	0.1	0.2	2.8	1360	4	0.3	0.5	1.9	3.0	n.a.
206721	SFRD0017	0.6	0.7	0.2	0.7	-0.1	0.2	1.2	315.3	1.2	-1	0.2	-1	0.5	n.a.
206722	SFRD0017	1.2	0.8	0.3	1.3	0.1	0.3	2.7	728.6	3.4	2	0.5	2	2.1	n.a.
206723	SFRD0017	2.7	1.4	0.7	5.5	0.3	1.6	9.2	78.8	2.8	-1	1.9	-1	4.0	n.a.
206724	SFRD0017	0.5	0.6	0.1	0.8	-0.1	0.2	1.3	766.3	1.1	-1	0.3	-1	1.3	n.a.
206725	SFRD0017	0.5	0.6	0.1	1.3	-0.1	0.4	1.2	866.8	3.4	-1	0.3	-1	4.5	n.a.
206726	SFRD0017	0.3	0.5	-0.1	0.6	-0.1	0.1	0.7	1348.1	0.9	7	0.2	2	1.0	n.a.
206727	SFRD0017	1.1	0.4	0.2	1.5	-0.1	0.2	2.6	536	3.2	1	0.5	-1	1.8	n.a.
206728	SFRD0017	0.7	0.3	0.1	1.5	-0.1	0.4	2.2	783.9	2	-1	0.5	-1	2.0	n.a.

Table 2.1. continued

GSWA No.	Drillhole	Sc	Sm	SO ₃ (wt%)	Sr	Ta	Tb	Th	Tm	U	V	Y	Yb	Zn	Zr
201233	SFRD0017	26	0.4	0.51	176.0	-0.1	0.1	-0.1	0.1	-0.1	134	4.3	0.5	55.0	4
201234	SFRD0017	32	0.7	2.69	155.5	-0.1	0.2	0.1	0.1	0.1	185	6.5	0.7	62.0	7
201235	SFRD0017	27	0.4	1.05	133.5	-0.1	0.1	0.1	0.1	0.1	159	4.7	0.5	45.0	6
201236	SFRD0017	20	0.4	1.31	101.5	-0.1	0.1	0.1	0.1	-0.1	109	4.1	0.4	54.0	5
201237	SFRD0017	14	0.4	0.59	58.4	-0.1	0.1	0.1	0.1	0.1	71	3.4	0.3	59.0	5
201238	SFRD0017	29	0.6	0.37	165.5	-0.1	0.1	0.1	0.1	0.1	148	4.9	0.5	28.0	6
201239	SFRD0017	52	1.4	2.71	63.2	0.1	0.3	0.3	0.2	0.1	551	11.9	1.1	37.0	16
201240	SFRD0017	26	0.4	1.24	126.0	-0.1	0.1	0.1	0.1	0.1	146	4.0	0.5	49.0	6
201241	SFRD0017	12	0.4	0.96	55.0	0.1	0.1	0.1	0.1	0.1	55	3.2	0.3	56.0	7
201242	SFRD0017	14	0.5	0.61	67.6	-0.1	0.1	0.2	0.1	0.1	60	3.7	0.4	53.0	7
201243	SFRD0017	14	0.7	0.95	23.5	0.1	0.1	0.7	0.1	0.6	115	5.1	0.5	61.0	10
201244	SFRD0017	31	0.9	7.48	187.5	-0.1	0.2	0.1	0.1	-0.1	169	7.2	0.7	62.0	9
201245	SFRD0017	23	0.6	0.18	211.0	-0.1	0.1	0.1	0.1	-0.1	132	4.9	0.5	50.0	7
201246	SFRD0017	23	0.7	0.31	208.0	0.1	0.2	0.1	0.1	0.1	136	5.7	0.6	41.0	6
201247	SFRD0017	17	0.5	0.30	104.5	-0.1	0.1	0.1	0.1	0.1	83	3.7	0.4	58.0	7
201248	SFRD0017	33	1.1	3.42	274.0	-0.1	0.2	0.1	0.1	0.1	185	8.5	0.8	47.0	10
201249	SFRD0017	16	0.6	0.28	79.5	0.1	0.1	0.3	0.1	0.1	81	4.1	0.4	67.0	11
201250	SFRD0017	13	0.5	0.35	71.7	0.1	0.1	0.2	0.1	0.1	70	3.5	0.4	58.0	9
201255	SFRD0017	38	1.0	2.68	208.0	0.1	0.2	0.1	0.2	0.1	187	8.6	0.9	42.0	10
206721	SFRD0017	20	0.3	0.42	182.6	-0.1	-0.1	-0.1	-0.1	-0.1	83	3.5	0.3	42.0	2
206722	SFRD0017	32	0.9	1.53	213.9	-0.1	0.2	0.1	0.1	-0.1	150	7.5	0.8	38.0	8
206723	SFRD0017	38	2.5	0.47	231.8	0.2	0.5	0.4	0.3	0.1	293	16.3	1.8	92.0	34
206724	SFRD0017	15	0.4	0.57	51.7	-0.1	-0.1	-0.1	-0.1	-0.1	57	3.1	0.3	45.0	5
206725	SFRD0017	10	0.4	0.52	66.3	0.2	-0.1	1.1	-0.1	1.5	41	2.5	0.3	39.0	4
206726	SFRD0017	-10	0.2	0.37	68.7	-0.1	-0.1	-0.1	-0.1	-0.1	49	1.5	0.2	42.0	2
206727	SFRD0017	30	0.9	1.25	259.3	-0.1	0.2	-0.1	0.1	-0.1	139	6.3	0.7	39.0	8
206728	SFRD0017	14	0.5	0.27	77.8	-0.1	-0.1	0.2	-0.1	-0.1	52	3.2	0.4	59.0	10

NOTES: n.d. = not detected n.a. = not analysed

Table 2.2. Whole-rock major and trace-element geochemical data from Plato

GSWA No.	Drillhole	depth interval in m From To	SiO ₂	TiO ₂	Al ₂ O ₃	Fe ₂ O ₃ T	MgO	MnO	CaO	K ₂ O	Na ₂ O	P ₂ O ₅	LOI	Total
216335	PLDT006	441.16	61.75	1.14	15.38	8.85	1.70	0.22	4.78	2.71	2.76	0.32	0.14	99.75
216336	PLDT006	372.19	49.16	1.67	15.47	13.32	7.14	0.23	9.79	0.65	2.34	0.29	-0.25	99.81
216337	PLDT006	339.9	50.66	1.39	15.27	12.03	7.36	0.22	9.79	0.69	2.32	0.21	-0.15	99.79
216338	PLDT006	322.39	50.48	1.04	16.77	9.79	8.28	0.18	9.78	0.62	2.42	0.15	0.01	99.52
216377	PLDT006	412.1	62.16	1.19	14.82	9.43	1.97	0.23	4.54	2.93	2.74	0.32	-0.29	100.04
216339	PLDT005	307.09	57.92	1.57	14.17	13.21	3.23	0.33	5.20	1.75	2.55	0.45	-0.49	99.89
216340	PLDT005	358.92	50.32	1.93	14.34	14.51	5.73	0.25	9.50	0.89	2.55	0.30	-0.39	99.93
216341	PLDT005	360.58	55.72	1.59	15.96	13.14	3.06	0.27	6.06	1.38	2.91	0.47	-0.47	100.09
216342	PLDT001	299.68	51.55	0.65	9.06	14.39	17.65	0.26	5.38	0.28	1.07	0.08	-0.41	99.96
216343	PLDT001	343.28	51.09	0.71	11.99	12.30	14.63	0.22	6.77	0.40	1.50	0.13	-0.15	99.59
216344	PLDT001	367.59	51.41	0.80	9.05	13.85	17.58	0.26	5.49	0.36	1.12	0.16	-0.29	99.79
216345	PLDT001	346.63	51.14	0.82	8.73	14.24	17.32	0.26	5.79	0.39	1.07	0.16	-0.13	99.79
216346	PLDT001	392.7	51.47	0.70	8.61	13.92	18.21	0.26	5.26	0.31	1.05	0.12	-0.39	99.52
216347	PLDT001	415.31	50.70	1.32	8.45	14.56	17.75	0.26	5.30	0.34	1.06	0.13	-0.14	99.73
216348	PLDT001	429	50.83	1.10	9.01	14.61	17.19	0.27	5.38	0.38	1.11	0.15	-0.32	99.71
216349	PLDT001	448.31	50.83	0.79	17.96	8.52	9.79	0.15	8.65	0.53	2.27	0.21	0.04	99.74
216350	PLDT001	459.05	51.24	0.67	16.54	10.30	8.19	0.20	10.06	0.46	2.38	0.06	-0.19	99.91
216351	PLDT003	271.6	43.29	0.50	6.00	17.60	26.95	0.25	4.11	0.17	0.79	0.12	-0.69	99.09
216352	PLDT003	297.9	42.63	0.41	6.86	17.35	27.55	0.24	3.66	0.18	0.97	0.10	-0.73	99.22
216353	PLDT003	317.56	42.92	0.95	4.45	18.14	28.83	0.26	2.96	0.30	0.61	0.25	-0.34	99.33
216354	PLDT003	325.7	44.66	1.14	7.28	16.63	23.76	0.24	4.31	0.36	1.10	0.29	-0.17	99.60
216355	PLDT003	348.41	51.11	0.68	17.08	8.66	9.00	0.17	10.56	0.39	2.28	0.09	-0.06	99.96
216356	PLDT003	369.4	49.61	1.10	16.41	11.90	8.33	0.20	10.08	0.43	2.22	0.09	-0.14	100.23
216357	PLDT003	384.18	56.56	0.48	21.87	4.75	1.40	0.11	8.16	1.55	4.59	0.14	0.07	99.68
216358	PLDT003	389.93	51.21	1.02	15.72	11.65	7.23	0.19	9.79	0.74	2.46	0.12	-0.18	99.95
216359	PLDT003	409.03	57.37	1.27	16.55	10.54	3.01	0.24	6.08	1.42	3.34	0.34	-0.33	99.83
216360	PLDT003	440.11	49.75	1.66	15.24	13.50	7.05	0.23	9.96	0.57	2.33	0.28	-0.32	100.25

Table 2.2. continued

GSWA No.	Drillhole	Ag	As	Au (ppb)	Ba	Cd	Ce	Co	Cr	Cs	Cu	Dy	Er	Eu	Ga
216335	PLDT006	0.03	-0.5	-1	1397.5	0.1	45.6	16	45	0.2	28.8	3.2	2.0	2.7	21.3
216336	PLDT006	0.01	-0.5	-1	336.9	0.1	42.0	43	275	0.2	45.6	6.5	3.7	1.9	19.0
216337	PLDT006	0.02	-0.5	-1	328.7	0.1	36.8	43	267	0.2	55.7	5.8	3.3	1.6	18.2
216338	PLDT006	0.03	0.9	-1	246.9	0.1	26.6	38	452	0.6	50.3	4.0	2.5	1.4	18.3
216377	PLDT006	0.02	-0.5	-1	1190.7	0.1	65.3	19	30	0.5	15.6	5.2	2.8	2.5	22.1
216339	PLDT005	-0.01	-0.5	1	659.4	0.1	71.5	29	81	0.5	26.4	6.5	3.8	2.3	20.6
216340	PLDT005	0.03	-0.5	-1	404.0	0.1	51.1	44	79	0.1	45.4	8.4	5.1	2.2	19.7
216341	PLDT005	0.03	-0.5	-1	606.3	0.2	74.1	28	76	0.3	28.8	6.5	3.3	2.5	22.8
216342	PLDT001	0.03	-0.5	-1	146.7	0.1	13.9	70	1796	0.2	53.6	2.2	1.5	0.7	12.2
216343	PLDT001	0.04	-0.5	-1	209.7	0.1	22.9	59	1323	0.3	77.1	3.1	1.7	1.1	12.7
216344	PLDT001	0.02	-0.5	-1	195.5	0.1	25.6	68	1996	0.2	40.2	3.3	2.2	0.9	12.0
216345	PLDT001	0.07	0.8	-1	216.0	0.1	27.9	71	1611	0.3	62.8	3.6	2.3	1.1	11.7
216346	PLDT001	0.04	-0.5	-1	169.6	0.1	19.7	70	1719	0.2	54.2	2.6	1.8	0.9	10.1
216347	PLDT001	0.03	-0.5	-1	189.2	0.1	23.1	70	1600	0.3	48	2.9	1.9	0.8	11.4
216348	PLDT001	0.06	0.6	-1	201.2	0.1	25.0	70	1568	0.2	46.7	3.4	2.0	0.8	11.9
216349	PLDT001	0.03	0.7	-1	283.2	0.1	30.2	40	810	0.3	34.3	3.2	1.9	1.0	14.7
216350	PLDT001	0.05	-0.5	-1	238.4	0.1	13.7	46	299	-0.1	50.5	2.7	1.7	1.2	18.8
216351	PLDT003	-0.01	-0.5	1	101.8	0.1	13.1	124	1250	0.1	45.9	2.0	1.2	0.6	7.4
216352	PLDT003	0.17	-0.5	2	115.6	0.1	12.0	129	1234	0.1	44.4	1.5	0.9	0.5	7.9
216353	PLDT003	0.05	0.7	3	193.3	0.1	33.9	138	1801	0.2	102.2	4.0	2.4	1.3	8.2
216354	PLDT003	0.03	1.1	1	235.8	0.1	37.8	115	1526	0.2	100.4	4.6	2.4	1.5	10.6
216355	PLDT003	0.02	-0.5	-1	184.3	0.1	18.8	42	351	0.1	51.5	3.3	1.7	1.1	16.5
216356	PLDT003	0.13	-0.5	-1	197.3	0.1	19.1	51	281	0.2	55.5	3.7	2.3	1.3	18.2
216357	PLDT003	0.05	0.9	1	658.0	0.1	37.8	12	35	0.3	24.9	2.4	1.3	4.0	27.7
216358	PLDT003	-0.01	0.6	-1	256.9	0.1	28.3	57	234	0.3	51.9	4.1	2.4	1.4	17.7
216359	PLDT003	0.02	4.1	-1	806.9	0.1	58.6	27	61	0.4	26.6	3.9	2.3	2.9	23.5
216360	PLDT003	0.03	0.5	-1	317.9	0.2	44.9	51	240	0.2	53	7.1	3.8	1.9	20.5

Table 2.2. continued

GSWA No.	Drillhole	Gd	Hf	Ho	La	Lu	Nb	Nd	Ni	Pb	Pd (ppb)	Pr	Pt (ppb)	Rb	Re (ppb)
216335	PLDT006	4.3	6.0	0.7	23.4	0.3	7.9	24.4	11.6	13.7	-1	5.8	-1	41.7	-0.2
216336	PLDT006	6.2	4.7	1.5	18.7	0.5	7.5	25.9	74.2	5.7	-1	5.7	-1	14.4	-0.2
216337	PLDT006	5.3	4.2	1.2	16.6	0.5	6.4	21.6	80.3	7.2	-1	4.8	-1	8.6	-0.2
216338	PLDT006	4.2	3.0	0.8	11.8	0.4	3.8	15.8	104.7	4.7	-1	3.6	-1	14.9	-0.2
216377	PLDT006	6.5	8.4	1.1	32.8	0.5	13.0	33.1	12.1	16.8	-1	7.6	-1	59.5	-0.2
216339	PLDT005	7.5	7.5	1.3	34.1	0.5	16.5	39.5	26.5	12.6	-1	9.1	-1	31.5	-0.2
216340	PLDT005	7.6	5.5	1.7	22.4	0.8	9.1	29.7	39.6	8.8	-1	6.8	-1	10.9	-0.2
216341	PLDT005	7.4	12.8	1.3	37.8	0.5	13.8	39.5	23.3	11.1	-1	9.2	-1	21.0	-0.2
216342	PLDT001	2.2	1.7	0.5	6.6	0.3	2.1	7.9	422.3	3.4	-1	1.8	-1	5.7	-0.2
216343	PLDT001	2.6	2.4	0.6	10.4	0.3	3.6	12.4	392.9	5	-1	2.8	-1	9.9	-0.2
216344	PLDT001	3.4	3.0	0.7	11.7	0.3	4.3	15.0	374	3.8	-1	3.1	-1	9.2	-0.2
216345	PLDT001	3.4	2.4	0.7	12.7	0.3	4.3	16.5	406.3	4.6	-1	3.6	-1	10.6	-0.2
216346	PLDT001	2.7	2.4	0.6	9.6	0.3	2.6	10.1	409	4	-1	2.4	-1	7.3	-0.2
216347	PLDT001	3.0	2.1	0.6	10.2	0.3	4.6	12.3	401	3.7	-1	3.0	-1	10.1	-0.2
216348	PLDT001	2.9	2.3	0.7	12.0	0.3	4.6	15.3	356.2	3.8	-1	3.2	-1	8.3	-0.2
216349	PLDT001	3.3	3.1	0.6	13.3	0.3	5.3	16.9	232.2	4.9	-1	3.9	-1	10.9	-0.2
216350	PLDT001	2.5	1.3	0.6	6.9	0.3	1.3	8.5	123.9	3.3	-1	1.8	-1	3.4	-0.2
216351	PLDT003	2.1	1.2	0.4	6.2	0.2	2.1	8.8	1168.3	2.2	2	1.9	2	3.5	-0.2
216352	PLDT003	1.7	1.9	0.3	5.6	0.1	1.9	6.4	1324.2	2.7	3	1.6	3	3.3	-0.2
216353	PLDT003	4.7	3.0	0.9	15.1	0.3	6.3	19.6	1379.1	4.5	4	4.5	3	8.2	-0.2
216354	PLDT003	4.2	2.6	0.9	16.8	0.4	6.7	20.3	1069.2	4.4	4	4.9	4	8.7	-0.2
216355	PLDT003	2.8	1.5	0.6	9.7	0.3	2.4	11.2	161.5	3	-1	2.4	-1	4.5	-0.2
216356	PLDT003	3.7	1.8	0.8	9.0	0.4	2.2	12.5	137.2	3.8	-1	2.8	-1	3.3	-0.2
216357	PLDT003	2.6	2.1	0.5	22.9	0.2	3.4	17.0	18	13.4	-1	4.3	-1	15.8	-0.2
216358	PLDT003	4.1	2.7	1.0	13.5	0.4	4.1	16.0	111.9	6.6	-1	3.6	-1	13.3	-0.2
216359	PLDT003	4.9	4.3	0.9	30.9	0.3	11.3	27.2	25.2	11.5	-1	7.0	-1	21.3	-0.2
216360	PLDT003	6.7	4.7	1.6	19.5	0.6	7.2	27.1	81.3	6.8	-1	6.0	-1	6.9	0.2

Table 2.2. continued

GSWA No.	Drillhole	Sc	Sm	SO ₃ (wt%)	Ta	Tb	Th	Tm	U	V	Y	Yb	Zn	Zr
216335	PLDT006	16	4.7	0.11	249.0	0.6	0.6	0.3	0.2	102	18.1	1.9	95.0	247
216336	PLDT006	36	6.2	0.32	215.7	0.5	0.7	0.5	0.3	245	34.0	3.7	102.0	181
216337	PLDT006	37	5.8	0.29	210.4	0.4	1.0	0.4	0.3	222	29.8	3.3	96.0	151
216338	PLDT006	31	3.6	0.23	216.2	0.3	0.6	0.3	0.4	178	21.7	2.2	72.0	116
216377	PLDT006	20	6.8	0.12	240.6	0.7	0.9	0.3	0.4	106	26.4	2.6	95.0	356
216339	PLDT005	30	8.2	0.20	227.1	1.0	1.1	0.4	0.5	178	34.3	3.3	150.0	292
216340	PLDT005	43	7.5	0.36	194.7	0.6	0.8	0.6	0.4	306	44.0	4.5	115.0	213
216341	PLDT005	24	7.8	0.18	228.8	0.8	1.1	0.5	0.9	183	32.0	3.7	144.0	474
216342	PLDT001	35	1.9	0.20	115.7	3.8	0.3	0.2	0.2	167	13.4	1.8	117.0	63
216343	PLDT001	32	2.9	0.27	172.5	0.3	0.5	0.2	0.9	155	16.4	1.9	101.0	95
216344	PLDT001	37	3.0	0.14	116.8	0.3	0.5	0.2	0.3	184	18.2	2.1	106.0	140
216345	PLDT001	38	4.3	0.22	116.5	0.4	0.6	0.3	0.3	187	19.7	2.3	120.0	96
216346	PLDT001	37	2.3	0.20	106.2	0.2	0.4	0.2	0.2	175	14.6	1.9	112.0	95
216347	PLDT001	37	3.2	0.23	111.4	0.3	0.5	0.3	0.3	203	16.8	2.1	112.0	82
216348	PLDT001	36	3.4	0.22	116.7	0.3	0.6	0.2	0.2	196	16.8	2.2	114.0	92
216349	PLDT001	23	3.5	0.12	254.9	0.3	0.5	0.2	0.3	123	17.2	1.8	74.0	140
216350	PLDT001	34	2.3	0.20	242.6	0.2	0.4	0.2	-0.1	177	14.7	1.6	79.0	40
216351	PLDT003	21	2.1	0.18	93.7	0.2	0.3	0.1	0.2	102	11.2	1.1	93.0	51
216352	PLDT003	14	1.4	0.17	111.3	0.2	0.2	-0.1	0.1	78	8.1	1.0	95.0	90
216353	PLDT003	21	4.3	0.32	55.3	0.5	0.7	0.3	0.3	134	20.8	2.3	111.0	128
216354	PLDT003	23	4.5	0.29	112.7	0.4	0.8	0.2	0.2	144	22.2	2.1	111.0	115
216355	PLDT003	31	2.6	0.15	257.5	0.1	0.5	0.1	0.1	152	16.1	1.8	59.0	55
216356	PLDT003	31	3.5	0.26	234.5	0.1	0.7	0.3	-0.1	207	19.6	2.1	91.0	53
216357	PLDT003	-10	2.9	0.12	407.6	0.1	0.4	-0.1	0.2	50	12.5	1.3	48.0	87
216358	PLDT003	32	4.1	0.24	220.2	0.3	0.7	0.3	0.3	185	23.6	2.4	89.0	107
216359	PLDT003	19	5.4	0.20	300.3	0.6	0.7	0.3	0.4	173	21.6	2.2	111.0	178
216360	PLDT003	37	7.2	0.31	220.2	0.5	1.2	0.5	0.4	244	37.2	3.7	108.0	184

Appendix 3

Platinum group elements data (ppb)

<i>Sample No.</i>	<i>Os</i>	<i>Ir</i>	<i>Ru</i>	<i>Rh</i>	<i>Pt</i>	<i>Pd</i>	<i>Au</i>
Regional Fraser gabbro							
183668	0.16	0.10	0.18	<0.08	0.74	<0.47	<0.48
183652	<0.065	0.06	0.18	<0.08	1.31	<0.47	0.67
183643	<0.065	0.11	0.27	0.32	8.00	10.21	3.43
183629	<0.065	0.05	<0.12	<0.08	0.68	<0.47	1.43
183632	<0.065	<0.025	<0.12	<0.08	0.32	<0.47	0.59
183669	<0.065	<0.025	<0.12	<0.08	0.80	<0.47	0.48
183675	<0.065	<0.025	<0.12	<0.08	0.36	<0.47	<0.48
183660	<0.065	<0.025	<0.12	<0.08	0.27	<0.47	<0.48
183662	<0.065	<0.025	<0.12	<0.08	0.42	<0.47	<0.48
Nova–Bollinger (SFRD0017)							
201255	0.21	0.07	0.14	0.11	4.87	3.42	6.21
201234	0.17	0.12	0.24	0.13	2.16	3.95	6.71
201235	0.08	0.03	<0.12	<0.08	2.41	0.97	1.55
201243	<0.065	0.04	0.23	<0.08	6.49	2.20	3.80
201244	0.51	0.31	0.62	0.45	4.20	7.62	54.62
201248	0.10	0.35	0.32	0.37	9.04	9.89	2.89
201250	<0.065	<0.025	<0.12	<0.08	1.88	<0.47	0.59

Appendix 4

S and Sr isotope data

<i>Sample No.</i>	<i>n</i>	$\delta^{34}\text{S}\text{‰ CDT}$	<i>2s</i>	<i>n</i>	$^{87}\text{Rb}/^{86}\text{Sr}$	$^{87}\text{Sr}/^{86}\text{Sr}$	$^{87}\text{Sr}/^{86}\text{Sr}_{(1300\text{Ma})}$	<i>2s</i>
Mount Malcom								
183654	4	0.1	0.1					
183651	6	0.0	0.2					
183643	4	0.4	0.1	7	0.003	0.70529	0.70524	0.00037
183652	4	0.3	0.4	5	0.035	0.70545	0.70481	0.00040
183629	4	0.2	0.3	6	0.005	0.70483	0.70474	0.00013
Nova–Bollinger (SFRD0017)								
201253	7	0.9	0.2					
201251	5	3.7	0.1	7	0.007	0.70582	0.70569	0.00027
201254	5	1.6	0.5	7	0.002	0.70421	0.70418	0.00013
201255	4	3.3	0.2	7	0.002	0.70568	0.70565	0.00021
201239	7	4.2	0.3	8	0.002	0.70601	0.70599	0.00033
201252	10	3.9	0.1	9	0.002	0.70670	0.70666	0.00014
201236	4	3.1	0.2					
Sunline (Snowys Dam Fm.)								
206712	1	3.6	0.3					
206709	1	5.2	0.3					

NOTE: n = number of analyses

Appendix 5

Nd isotope data

	Sample No.	$^{147}\text{Sm}/^{144}\text{Nd}$	$^{143}\text{Nd}/^{144}\text{Nd}$ (Std cor)	$^{143}\text{Nd}/^{144}\text{Nd}_{(1300\text{Ma})}$	$\epsilon_{\text{Nd}} (1300\text{Ma})$
Regional main gabbro	183663	0.147252	0.512198	0.510941	-0.58
	194718	0.139495	0.511975	0.510784	-3.65
	183652	0.163111	0.512365	0.510973	0.04
	183668	0.152538	0.512182	0.510879	-1.79
	183659	0.131009	0.512001	0.510882	-1.72
Group 1 hybrid	183643	0.144362	0.512119	0.510886	-1.65
	183626	0.144740	0.512166	0.510930	-0.79
	183660	0.136431	0.512029	0.510864	-2.09
	183661	0.150212	0.512207	0.510924	-0.90
Group 2 hybrid	183658	0.136364	0.511984	0.510820	-2.95
Nova–Bollinger (SFRD0017)	201243	0.155946	0.512324	0.510992	0.43
	201235	0.195152	0.512600	0.510934	-0.72
	201255	0.207088	0.512673	0.510905	-1.29

Appendix 6

Mineral compositions

Olivine compositions		Depth	SiO ₂	TiO ₂	Al ₂ O ₃	Cr ₂ O ₃	FeO	MnO	MgO	NiO	CoO	CaO	Na ₂ O	K ₂ O	TOTAL
Nova–Bollinger SFRD0017															
SFRD0017-049.8	49.8	38.94	0.01	-0.01	0.00	0.00	19.40	0.25	41.22	0.14	-0.01	0.00	0.01	0.01	99.97
SFRD0017-049.8	49.8	39.26	0.00	-0.02	0.00	0.00	18.45	0.22	41.99	0.14	-0.03	0.00	0.01	0.00	100.02
SFRD0017-049.8	49.8	38.79	-0.01	0.03	-0.02	0.00	17.94	0.22	42.41	0.13	-0.07	0.03	0.02	-0.01	99.46
SFRD0017-049.8	49.8	39.00	0.01	0.01	0.01	0.00	18.58	0.19	41.95	0.13	0.02	0.03	-0.01	-0.01	99.92
SFRD0017-049.8	49.8	38.98	0.00	0.00	0.01	0.00	18.84	0.29	42.02	0.12	-0.11	0.03	-0.01	0.02	100.20
SFRD0017-049.8	49.8	39.16	0.00	0.00	0.00	0.00	18.57	0.22	42.44	0.16	0.00	0.00	0.03	0.02	100.59
SFRD0017-049.8	49.8	39.36	0.00	0.01	0.00	0.00	18.69	0.25	41.61	0.14	-0.07	0.00	0.05	0.00	100.04
SFRD0017-087.5	87.5	39.14	0.01	0.00	-0.01	0.00	17.98	0.19	42.10	0.15	0.02	0.01	0.00	0.00	99.60
SFRD0017-087.5	87.5	39.16	0.00	0.04	-0.05	0.00	18.31	0.25	42.08	0.15	-0.06	0.02	0.04	-0.02	99.93
SFRD0017-087.5	87.5	39.32	0.00	0.02	0.00	0.00	18.25	0.28	41.94	0.12	0.01	0.01	-0.01	0.01	99.96
SFRD0017-115.6	115.6	39.07	0.00	0.00	-0.01	0.00	17.16	0.18	43.02	0.14	0.01	0.02	0.00	0.00	99.59
SFRD0017-115.6	115.6	39.21	0.00	0.03	-0.02	0.00	17.14	0.32	43.10	0.12	-0.03	0.00	-0.02	0.00	99.86
SFRD0017-115.6	115.6	39.22	0.00	-0.01	0.01	0.00	17.13	0.30	43.13	0.14	0.05	0.00	0.01	0.00	99.98
SFRD0017-115.6	115.6	39.30	-0.01	0.05	0.01	0.00	16.98	0.27	42.81	0.12	-0.01	-0.02	0.04	0.00	99.53
SFRD0017-115.6	115.6	39.24	0.00	-0.02	0.01	0.00	16.70	0.27	42.65	0.11	0.02	0.00	0.03	-0.01	99.01
SFRD0017-115.6	115.6	39.46	-0.01	0.04	0.02	0.00	16.83	0.27	42.66	0.14	0.05	-0.02	0.03	-0.01	99.45
SFRD0017-115.6	115.6	39.13	0.01	-0.02	-0.02	0.00	17.10	0.26	42.83	0.15	-0.02	0.02	0.03	0.02	99.48
SFRD0017-115.6	115.6	39.06	0.00	0.02	-0.01	0.00	16.95	0.28	42.91	0.10	0.00	0.02	0.02	-0.01	99.33
SFRD0017-115.6	115.6	39.01	-0.01	0.00	0.01	0.00	17.01	0.24	42.89	0.14	0.01	0.02	-0.05	-0.01	99.26
SFRD0017-115.6	115.6	39.12	0.02	0.00	0.00	0.00	17.22	0.28	43.12	0.13	0.05	-0.01	0.04	0.00	99.97
SFRD0017-115.6	115.6	39.16	0.00	0.06	-0.03	0.00	16.64	0.29	42.79	0.11	-0.01	0.03	0.01	0.01	99.07
SFRD0017-169.0	169	39.22	0.02	0.03	-0.02	0.00	16.22	0.28	43.26	0.12	-0.06	0.02	0.02	0.00	99.12
SFRD0017-169.0	169	39.37	0.02	0.00	0.00	0.00	16.56	0.26	44.11	0.13	-0.07	0.01	0.02	0.03	100.45
SFRD0017-169.0	169	39.67	-0.01	0.02	0.02	0.00	15.94	0.25	43.59	0.14	-0.09	0.04	0.03	-0.01	99.59
SFRD0017-169.0	169	39.47	-0.02	0.01	0.01	0.00	16.09	0.23	43.68	0.12	-0.04	-0.01	-0.05	0.00	99.49
SFRD0017-169.0	169	39.39	-0.01	0.01	0.03	0.00	16.32	0.18	43.86	0.13	-0.10	0.00	0.03	0.00	99.84
SFRD0017-169.0	169	39.29	0.00	0.02	0.03	0.00	16.37	0.22	43.68	0.16	-0.03	0.01	0.02	0.01	99.78

Olivine compositions (continued)

	Depth	SiO ₂	TiO ₂	Al ₂ O ₃	Cr ₂ O ₃	FeO	MnO	MgO	NiO	CoO	CaO	Na ₂ O	K ₂ O	TOTAL
SFRD0017-169.0	169	39.94	0.01	-0.01	-0.01	16.35	0.27	43.49	0.11	0.03	0.01	-0.01	0.01	100.20
SFRD0017-169.0	169	39.38	0.01	0.02	-0.01	16.67	0.18	43.19	0.11	-0.01	0.00	-0.01	-0.01	99.51
SFRD0017-169.0	169	39.44	0.01	0.04	0.00	16.38	0.26	44.03	0.10	-0.04	0.03	-0.04	0.00	100.20
SFRD0017-221.1	221.1	39.27	0.01	0.00	-0.02	15.90	0.29	43.73	0.23	-0.02	0.00	0.01	0.02	99.41
SFRD0017-221.1	221.1	39.60	0.02	-0.03	0.00	16.54	0.11	43.84	0.22	-0.06	-0.01	0.02	0.01	100.26
SFRD0017-221.1	221.1	39.41	0.02	0.00	-0.02	16.63	0.24	43.31	0.23	-0.06	0.01	0.00	0.00	99.78
SFRD0017-221.1	221.1	39.18	0.00	0.02	-0.02	16.47	0.23	43.53	0.21	-0.06	-0.01	0.00	0.00	99.55
SFRD0017-221.1	221.1	39.22	0.01	0.02	0.02	16.23	0.22	43.67	0.23	0.01	-0.01	0.03	0.00	99.64
SFRD0017-221.1	221.1	39.00	0.02	-0.02	-0.02	16.18	0.26	43.52	0.20	0.00	-0.01	0.00	0.00	99.14
SFRD0017-221.1	221.1	39.44	0.01	0.02	-0.04	15.95	0.32	43.69	0.22	-0.07	-0.01	-0.03	-0.02	99.47
SFRD0017-221.1	221.1	39.54	0.02	0.00	0.03	16.34	0.29	43.32	0.21	-0.04	0.04	0.01	-0.01	99.75
SFRD0017-221.1	221.1	39.38	0.00	-0.02	-0.04	16.37	0.27	43.72	0.21	-0.04	0.00	0.02	-0.02	99.85
SFRD0017-221.1	221.1	39.98	0.01	0.00	0.02	16.46	0.30	43.38	0.23	0.05	0.04	0.02	-0.01	100.47
SFRD0017-273.0	273	39.62	0.00	-0.01	-0.01	16.88	0.23	43.55	0.14	-0.01	0.02	0.00	0.00	100.41
SFRD0017-273.0	273	39.51	0.00	-0.02	0.01	17.29	0.24	43.10	0.12	-0.04	0.03	-0.01	-0.01	100.23
SFRD0017-273.0	273	39.43	0.01	-0.02	-0.02	16.72	0.27	43.17	0.15	-0.04	0.01	0.00	-0.03	99.64
SFRD0017-273.0	273	39.50	0.00	0.01	0.01	16.69	0.27	43.30	0.12	-0.04	0.04	-0.01	0.02	99.91
SFRD0017-273.0	273	39.74	0.00	-0.03	-0.02	17.06	0.20	43.50	0.14	0.01	-0.01	0.01	0.01	100.60
SFRD0017-273.0	273	39.26	0.00	-0.01	-0.03	17.07	0.25	43.17	0.15	0.00	0.03	-0.01	0.00	99.88
SFRD0017-273.0	273	39.29	-0.01	0.01	-0.02	16.97	0.28	43.12	0.14	-0.06	0.01	0.01	0.01	99.75
SFRD0017-273.0	273	39.58	0.00	-0.01	0.00	16.94	0.24	43.59	0.13	0.02	0.02	-0.02	0.00	100.49
SFRD0017-273.0	273	39.55	0.00	0.03	0.00	16.82	0.22	43.23	0.13	0.03	0.00	-0.01	0.01	100.02
SFRD0017-273.0	273	39.41	0.00	-0.01	0.00	16.87	0.26	43.36	0.14	-0.01	0.01	0.04	0.00	100.08
SFRD0017-273.0	273	39.04	-0.01	0.00	-0.01	17.04	0.24	43.36	0.13	-0.05	0.02	-0.01	0.01	99.76
SFRD0017-273.0	273	39.49	0.00	-0.01	0.00	17.18	0.26	43.18	0.16	-0.05	-0.01	0.01	0.02	100.23
SFRD0017-278.7	278.7	39.30	0.01	0.00	0.02	16.76	0.23	43.58	0.12	-0.01	0.02	-0.01	0.00	100.02
SFRD0017-278.7	278.7	39.30	0.02	0.03	0.00	16.50	0.19	43.56	0.14	-0.03	-0.01	-0.02	0.00	99.69
SFRD0017-278.7	278.7	39.36	0.01	0.00	0.02	16.79	0.25	43.39	0.13	-0.05	-0.01	-0.01	0.03	99.90
SFRD0017-278.7	278.7	38.88	0.02	0.00	0.03	17.01	0.30	43.45	0.11	-0.07	0.04	0.02	-0.01	99.78
SFRD0017-278.7	278.7	39.32	0.02	0.00	0.00	16.59	0.31	43.39	0.13	-0.06	0.02	0.01	0.00	99.74
SFRD0017-278.7	278.7	39.20	0.03	0.01	0.00	16.64	0.27	43.51	0.12	-0.03	0.02	-0.01	-0.02	99.73
SFRD0017-278.7	278.7	39.17	0.02	0.02	0.01	17.02	0.24	43.67	0.12	-0.03	0.02	-0.01	0.00	100.25

Olivine compositions (continued)

	Depth	SiO ₂	TiO ₂	Al ₂ O ₃	Cr ₂ O ₃	FeO	MnO	MgO	NiO	CoO	CaO	Na ₂ O	K ₂ O	TOTAL
SFRD0017-278.7	278.7	39.13	-0.01	0.03	0.00	16.75	0.24	43.70	0.12	-0.06	0.01	0.04	0.00	99.95
SFRD0017-278.7	278.7	39.39	0.01	0.03	-0.01	16.49	0.24	43.83	0.13	-0.08	0.02	0.02	0.01	100.08
Plato PLDT003	317.56													
216353_ol_6		38.46	0.00	0.00	0.00	21.34	0.28	38.91	0.21		0.01	0.00	0.01	99.23
216353_ol_9		38.47	0.00	0.00	0.00	21.08	0.28	38.42	0.22		0.00	0.01	0.02	98.50
216353_ol_10		38.62	0.01	0.00	0.00	21.53	0.21	38.32	0.24		0.01	0.00	0.00	98.94
216353_ol_11		38.38	0.00	0.00	0.00	21.68	0.22	38.37	0.24		0.01	0.00	0.01	98.91
216353_ol_13		38.09	0.01	0.00	0.00	21.31	0.32	38.38	0.27		0.02	0.04	0.02	98.46
216353_ol_14		38.05	0.00	0.00	0.00	21.52	0.31	38.32	0.20		0.00	0.00	0.00	98.42
216353_ol_15		38.25	0.03	0.00	0.00	21.57	0.26	38.36	0.26		0.01	0.00	0.00	98.75
216353_ol_22		38.45	0.00	0.00	0.00	21.79	0.23	37.96	0.25		0.02	0.00	0.00	98.70
216353_ol_23		38.32	0.00	0.00	0.00	21.49	0.22	38.22	0.25		0.00	0.01	0.00	98.51
216353_ol_28		38.58	0.02	0.00	0.00	21.42	0.35	38.33	0.23		0.01	0.00	0.00	98.93
216353_ol_29		38.44	0.00	0.00	0.01	21.16	0.34	38.26	0.25		0.01	0.01	0.01	98.50
216353_ol_30		38.27	0.00	0.00	0.00	21.62	0.32	38.07	0.26		0.03	0.00	0.01	98.57
216353_ol_40		38.57	0.00	0.00	0.00	21.18	0.28	38.14	0.22		0.00	0.05	0.01	98.45
216353_ol_41		38.07	0.00	0.00	0.00	21.47	0.26	38.17	0.24		0.00	0.01	0.01	98.25
216353_ol_42		37.65	0.03	0.00	0.01	21.41	0.36	37.99	0.22		0.00	0.00	0.00	97.67
216353_ol_45		38.58	0.00	0.00	0.00	21.02	0.25	37.54	0.24		0.01	0.00	0.00	97.63
216353_ol_46		38.37	0.02	0.00	0.00	20.87	0.32	37.93	0.25		0.00	0.01	0.00	97.78
216353_ol_47		39.01	0.02	0.00	0.01	21.10	0.30	38.22	0.24		0.01	0.03	0.00	98.93
216353_ol_48		38.33	0.08	0.00	0.01	21.73	0.38	38.12	0.28		0.01	0.02	0.00	98.96
216353_ol_49		38.81	0.00	0.00	0.00	21.40	0.35	38.17	0.23		0.01	0.00	0.00	98.97
216353_ol_50		38.42	0.00	0.00	0.00	21.16	0.23	37.92	0.26		0.01	0.01	0.00	98.00
216353_ol_58		38.47	0.00	0.00	0.01	21.62	0.22	38.33	0.24		0.01	0.02	0.00	98.92

Orthopyroxene compositions

	Depth	SiO ₂	TiO ₂	Al ₂ O ₃	Cr ₂ O ₃	FeO	MnO	MgO	NiO	CoO	CaO	Na ₂ O	K ₂ O	TOTAL
Nova–Bollinger SFRD0017														
SFRD0017-049.8	49.8	54.709999	0.01	2.65	0.02	12.06	0.24	29.57	-0.02	-0.04	0.43	-0.01	0.01	99.64
SFRD0017-049.8	49.8	54.110001	0.03	3.83	0.02	11.58	0.28	29.52	0.01	-0.02	0.36	0.00	0.01	99.72
SFRD0017-049.8	49.8	54.080002	0.07	2.64	0.14	11.70	0.19	29.76	0.02	0.00	0.38	0.00	0.01	99.00
SFRD0017-049.8	49.8	54.130001	0.03	3.39	0.00	11.34	0.28	29.68	0.04	-0.03	0.42	-0.03	0.01	99.25
SFRD0017-049.8	49.8	54.049999	0.05	3.34	0.07	11.68	0.25	29.50	0.00	-0.05	0.26	0.03	0.00	99.18
SFRD0017-049.8	49.8	54.380001	0.03	3.18	-0.01	11.48	0.25	29.59	0.04	-0.02	0.37	0.00	0.01	99.30
SFRD0017-049.8	49.8	54.52	0.00	2.66	-0.01	11.36	0.31	29.46	0.04	0.00	0.36	-0.05	0.00	98.66
SFRD0017-049.8	49.8	54.209999	0.03	3.22	0.02	11.70	0.25	29.27	0.03	-0.05	0.38	0.01	0.01	99.08
SFRD0017-057.4	57.4	53	0.25	2.80	0.06	17.07	0.35	24.90	0.04	0.00	1.20	0.08	0.06	99.82
SFRD0017-057.4	57.4	53.32	0.16	2.37	0.04	18.01	0.42	24.86	0.03	-0.02	0.88	0.00	0.04	100.11
SFRD0017-057.4	57.4	53.09	0.20	2.73	0.01	16.70	0.34	24.57	0.01	0.01	2.11	0.10	0.01	99.89
SFRD0017-057.4	57.4	53.549999	0.14	2.21	0.05	17.62	0.40	25.38	-0.01	-0.06	0.64	0.01	0.01	99.94
SFRD0017-057.4	57.4	53.639999	0.12	2.20	0.05	17.09	0.38	25.05	0.02	-0.08	1.18	0.04	0.04	99.73
SFRD0017-057.4	57.4	53.009998	0.15	2.42	0.04	17.24	0.44	25.27	0.02	-0.05	1.32	-0.02	0.02	99.86
SFRD0017-087.5	87.5	54.099998	0.07	2.99	0.25	12.55	0.26	28.66	0.02	-0.01	0.41	-0.01	-0.01	99.28
SFRD0017-087.5	87.5	53.91	0.03	4.03	0.01	11.69	0.30	29.16	-0.01	-0.04	0.21	0.00	0.00	99.31
SFRD0017-087.5	87.5	54.57	0.02	3.21	0.01	11.58	0.22	29.37	0.01	-0.07	0.50	0.01	0.01	99.45
SFRD0017-087.5	87.5	54.25	0.04	3.31	0.05	11.47	0.26	29.38	0.05	-0.08	0.35	-0.01	0.01	99.08
SFRD0017-087.5	87.5	54.540001	0.03	3.57	0.07	11.63	0.24	29.02	-0.01	-0.04	0.40	0.03	-0.01	99.47
SFRD0017-087.5	87.5	54.060001	0.03	3.78	0.00	11.61	0.29	29.51	0.01	-0.03	0.27	-0.01	-0.01	99.52
SFRD0017-115.6	115.6	54.470001	0.01	3.07	0.01	10.51	0.34	29.88	0.03	-0.13	0.31	0.06	0.01	98.57
SFRD0017-115.6	115.6	53.73	0.14	3.09	0.63	10.11	0.22	28.91	0.02	-0.10	1.86	0.06	0.01	98.66
SFRD0017-115.6	115.6	54.810001	0.01	2.79	0.09	10.71	0.31	30.09	0.02	0.00	0.44	-0.01	0.00	99.27
SFRD0017-129.5	129.5	54.450001	0.04	3.68	0.34	12.06	0.28	28.76	0.01	-0.01	0.48	0.03	0.00	100.12
SFRD0017-129.5	129.5	54.450001	0.03	3.57	0.34	12.03	0.23	29.26	0.02	-0.06	0.39	0.03	0.01	100.30
SFRD0017-129.5	129.5	54.110001	0.03	3.59	0.37	12.40	0.21	28.57	0.01	-0.09	0.31	-0.01	0.00	99.50
SFRD0017-129.5	129.5	54.110001	0.03	3.59	0.27	11.68	0.29	29.23	0.03	-0.08	0.42	0.03	0.00	99.60
SFRD0017-129.5	129.5	53.32	0.01	3.12	0.29	12.06	0.33	29.29	0.02	-0.03	0.47	0.04	0.01	98.93
SFRD0017-169.0	169	55.009998	0.01	3.25	0.00	10.56	0.25	29.96	0.02	0.01	0.36	0.02	0.00	99.45
SFRD0017-169.0	169	54.91	0.02	3.41	0.05	10.18	0.25	30.67	0.02	-0.09	0.40	0.05	0.01	99.88
SFRD0017-221.1	221.1	54.970001	0.00	2.52	0.17	10.43	0.24	30.43	0.04	-0.03	0.41	0.02	0.01	99.20

Orthopyroxene compositions (continued)

	Depth	SiO ₂	TiO ₂	Al ₂ O ₃	Cr ₂ O ₃	FeO	MnO	MgO	NiO	CoO	CaO	Na ₂ O	K ₂ O	TOTAL
SFRD0017-221.1	221.1	54.490002	0.17	2.61	0.57	10.32	0.20	29.98	0.05	-0.07	0.72	0.07	0.00	99.10
SFRD0017-231.1	231.1	54.049999	0.06	1.51	0.07	17.23	0.43	25.87	0.01	-0.04	0.39	0.02	-0.01	99.58
SFRD0017-231.1	231.1	54.470001	0.05	1.75	0.07	16.44	0.35	26.06	0.00	0.03	0.36	0.04	-0.01	99.62
SFRD0017-231.1	231.1	54.23	0.16	1.84	0.06	16.45	0.36	26.01	0.02	-0.03	0.89	0.04	0.08	100.11
SFRD0017-231.1	231.1	54.200001	0.07	1.59	0.08	17.11	0.39	26.43	0.02	-0.06	0.36	-0.03	-0.01	100.16
SFRD0017-231.1	231.1	54.27	0.07	1.53	0.04	16.55	0.42	26.41	0.00	-0.05	0.43	0.02	0.01	99.70
SFRD0017-273.0	273	54.139999	0.03	2.90	0.24	10.98	0.32	30.00	0.01	-0.05	0.40	0.08	0.05	99.10
SFRD0017-273.0	273	54.73	0.05	3.39	0.21	10.36	0.30	29.59	0.02	-0.01	1.16	0.04	0.00	99.84
SFRD0017-273.0	273	55.139999	0.04	2.69	0.11	10.64	0.26	30.38	0.03	-0.05	0.78	0.06	0.00	100.08
SFRD0017-273.0	273	54.73	0.08	2.85	0.19	10.69	0.29	30.04	0.02	-0.05	0.46	0.01	0.02	99.33
SFRD0017-273.0	273	54.73	0.14	3.03	0.31	9.92	0.26	28.74	0.01	-0.07	2.20	0.09	0.00	99.37
SFRD0017-278.7	278.7	54.799999	0.04	3.15	0.07	11.01	0.24	30.25	0.00	-0.01	0.33	0.00	0.01	99.91
SFRD0017-278.7	278.7	53.759998	0.14	3.50	0.43	10.21	0.22	29.49	0.03	-0.05	1.52	0.06	0.02	99.32
SFRD0017-278.7	278.7	54.630001	0.02	3.29	0.12	10.69	0.30	30.12	0.03	0.00	0.42	0.03	0.00	99.65
Plato PLDT003	317.56													
216353_opx_19		38.37	0.00	0.00	0.00	21.13	0.34	38.76	0.24		0.00	0.00	0.01	98.86
216353_opx_16		53.89	0.25	2.68	0.16	13.16	0.21	27.65	0.07		0.45	0.01	0.01	98.55
216353_opx_17		53.71	0.11	2.95	0.19	13.55	0.32	27.59	0.06		0.36	0.01	0.00	98.85
216353_opx_18		53.84	0.18	2.74	0.18	13.57	0.25	27.61	0.05		0.45	0.00	0.01	98.88
216353_opx_2		54.06	0.19	3.21	0.26	12.83	0.26	27.29	0.05		1.35	0.03	0.00	99.54
216353_opx_20		54.41	0.15	2.70	0.15	13.54	0.31	27.53	0.05		0.39	0.03	0.00	99.25
216353_opx_21		53.47	0.15	2.83	0.24	13.49	0.29	27.59	0.02		0.45	0.02	0.00	98.56
216353_opx_26		50.61	0.15	5.30	1.50	15.02	0.22	26.48	0.08		0.60	0.01	0.00	99.96
216353_opx_3		54.20	0.14	2.69	0.20	13.25	0.34	27.80	0.05		0.46	0.00	0.00	99.14
216353_opx_31		54.11	0.16	2.52	0.19	13.28	0.21	27.39	0.06		0.61	0.00	0.00	98.53
216353_opx_32		53.42	0.23	2.72	0.25	12.84	0.22	26.47	0.05		2.27	0.04	0.00	98.49
216353_opx_33		52.97	0.20	2.72	0.23	13.27	0.16	26.82	0.02		1.34	0.02	0.03	97.78
216353_opx_34		53.47	0.27	2.72	0.23	12.76	0.22	26.62	0.05		1.82	0.05	0.00	98.20
216353_opx_35		53.82	0.24	2.94	0.24	12.48	0.25	26.23	0.04		2.42	0.08	0.02	98.76
216353_opx_36		53.62	0.12	2.75	0.22	13.83	0.40	27.48	0.05		0.45	0.00	0.01	98.93
216353_opx_43		41.96	1.03	3.93	3.42	28.18	0.36	23.05	0.18		0.48	0.06	0.00	102.66

Orthopyroxene compositions (continued)

Depth	SiO ₂	TiO ₂	Al ₂ O ₃	Cr ₂ O ₃	FeO	MnO	MgO	NiO	CoO	CaO	Na ₂ O	K ₂ O	TOTAL
216353_opx_44	53.59	0.37	3.06	0.30	10.48	0.23	23.37	0.05		7.57	0.24	0.00	99.26
216353_opx_51	53.27	0.19	2.66	0.23	13.25	0.32	27.06	0.04		0.71	0.03	0.02	97.78
216353_opx_53	54.30	0.12	2.41	0.20	13.44	0.24	27.35	0.04		0.61	0.03	0.00	98.75
Plato PLDT001	415.31												
216347_opx_14	52.91	0.08	1.55	0.19	17.59	0.40	24.55	0.03		0.33	0.01	0.00	97.64
216347_opx_15	53.47	0.14	2.14	0.34	17.68	0.53	24.25	0.04		0.54	0.00	0.00	99.14
216347_opx_25	53.38	0.07	2.06	0.35	16.76	0.48	23.73	0.03		2.24	0.07	0.01	99.17
216347_opx_26	53.43	0.08	1.98	0.30	17.24	0.34	24.98	0.05		0.38	0.00	0.01	98.79
216347_opx_27	52.75	0.09	1.85	0.27	17.14	0.44	24.66	0.05		0.45	0.03	0.01	97.73
216347_opx_28	52.78	0.06	2.00	0.30	16.70	0.54	24.38	0.05		1.22	0.01	0.01	98.06
216347_opx_29	53.16	0.11	2.05	0.28	17.44	0.28	24.52	0.04		0.32	0.00	0.00	98.19
216347_opx_30	52.48	0.08	2.22	0.32	16.31	0.31	23.87	0.03		1.88	0.03	0.00	97.54
216347_opx_31	53.27	0.18	2.00	0.27	17.78	0.40	24.66	0.04		0.37	0.03	0.00	99.00
216347_opx_32	53.45	0.12	1.79	0.24	17.44	0.34	24.68	0.06		0.51	0.02	0.02	98.66
216347_opx_33	54.14	0.11	1.97	0.27	17.12	0.40	24.63	0.05		0.90	0.05	0.00	99.62
216347_opx_34	54.08	0.12	1.87	0.26	17.37	0.35	24.94	0.08		0.32	0.00	0.00	99.40
216347_opx_35	52.87	0.11	1.95	0.27	17.38	0.40	24.80	0.05		0.36	0.00	0.02	98.20
216347_opx_41	52.64	0.16	1.68	0.21	16.59	0.26	23.68	0.04		2.38	0.05	0.00	97.70
216347_opx_7	52.72	0.08	1.87	0.23	18.05	0.48	24.07	0.05		0.73	0.00	0.00	98.28
216347_opx_8	52.71	0.17	1.96	0.26	18.20	0.40	23.83	0.05		0.45	0.00	0.00	98.03
216347_opx_9	52.53	0.06	1.68	0.15	18.33	0.31	24.05	0.07		0.32	0.01	0.01	97.53

Clinopyroxene compositions

Depth	SiO ₂	TiO ₂	Al ₂ O ₃	Cr ₂ O ₃	FeO	MnO	MgO	NiO	CoO	CaO	Na ₂ O	K ₂ O	TOTAL
Nova-Bollinger SFRD0017													
SFRD0017-049.8	49.8	51.92	0.04	3.93	0.01	4.13	15.24	-0.01	0.02	22.48	0.71	-0.01	98.60
SFRD0017-049.8	49.8	52.25	0.06	4.08	0.04	3.65	15.14	0.00	-0.01	22.65	0.67	0.03	98.67
SFRD0017-049.8	49.8	52.39	0.05	4.14	0.00	3.91	15.01	0.02	0.01	22.49	0.69	-0.01	98.86
SFRD0017-057.4	57.4	51.78	0.39	2.95	0.06	6.47	14.82	0.04	0.01	22.13	0.44	0.00	99.32
SFRD0017-057.4	57.4	51.64	0.45	3.07	0.09	5.63	14.38	0.01	-0.05	23.05	0.52	-0.02	98.91

Clinopyroxene compositions (continued)

	Depth	SiO ₂	TiO ₂	Al ₂ O ₃	Cr ₂ O ₃	FeO	MnO	MgO	NiO	CoO	CaO	Na ₂ O	K ₂ O	TOTAL
SFRD0017-057.4	57.4	51.83	0.41	3.19	0.06	7.31	0.16	15.68	0.02	-0.06	19.92	0.49	0.03	99.04
SFRD0017-057.4	57.4	52.25	0.31	2.74	0.04	7.57	0.24	15.90	-0.01	-0.01	19.68	0.40	0.00	99.11
SFRD0017-115.6	115.6	50.51	0.50	5.24	1.27	5.12	0.00	17.01	0.01	-0.02	18.37	0.68	-0.01	98.68
SFRD0017-115.6	115.6	51.86	0.30	4.22	0.81	4.10	0.08	16.64	0.00	-0.06	20.00	0.79	0.01	98.75
SFRD0017-115.6	115.6	52.94	0.08	3.90	0.08	3.48	0.13	15.32	0.01	0.00	22.84	0.72	-0.01	99.49
SFRD0017-129.5	129.5	53.01	0.10	3.38	0.50	6.22	0.19	19.20	0.00	-0.06	16.84	0.36	0.00	99.74
SFRD0017-129.5	129.5	48.83	0.13	6.63	1.72	5.91	0.13	16.35	0.02	0.01	19.05	0.41	0.00	99.20
SFRD0017-129.5	129.5	52.69	0.14	3.43	0.44	3.47	0.13	15.34	0.01	-0.07	23.40	0.52	0.01	99.51
SFRD0017-129.5	129.5	52.53	0.14	3.56	0.58	3.77	0.11	14.92	0.00	-0.03	23.62	0.62	0.01	99.83
SFRD0017-129.5	129.5	52.47	0.17	3.55	0.65	3.86	0.09	15.05	0.01	-0.06	23.27	0.55	0.01	99.62
SFRD0017-135.5	135.5	53.00	0.24	1.76	0.13	5.01	0.15	15.11	0.04	-0.08	23.28	0.30	-0.01	98.94
SFRD0017-135.5	135.5	52.43	0.29	2.17	0.14	5.35	0.16	15.23	-0.02	-0.09	22.64	0.40	0.01	98.71
SFRD0017-135.5	135.5	52.92	0.29	2.19	0.13	5.08	0.20	15.06	0.00	-0.04	23.21	0.34	0.00	99.38
SFRD0017-135.5	135.5	52.70	0.28	2.07	0.10	5.31	0.15	15.25	0.00	0.00	22.47	0.35	-0.02	98.65
SFRD0017-135.5	135.5	53.32	0.23	2.02	0.16	5.15	0.24	15.06	0.00	-0.06	22.79	0.38	0.01	99.29
SFRD0017-135.5	135.5	52.82	0.24	1.98	0.16	5.14	0.20	15.11	0.01	-0.07	22.90	0.30	0.00	98.79
SFRD0017-169.0	169	50.54	0.32	5.40	1.19	5.14	0.06	17.95	-0.01	-0.07	17.60	0.73	0.02	98.87
SFRD0017-231.1	231.1	52.37	0.21	2.16	0.08	5.56	0.20	14.69	-0.01	-0.09	23.18	0.38	0.01	98.74
SFRD0017-273.0	273	49.46	0.46	7.42	1.54	4.84	0.11	15.36	0.00	-0.03	19.31	0.98	-0.01	99.45
SFRD0017-273.0	273	51.78	0.41	4.63	0.95	4.66	0.14	16.83	0.01	-0.07	19.41	0.86	0.00	99.62
SFRD0017-278.7	278.7	52.65	0.16	4.06	0.09	3.30	0.06	15.01	0.01	-0.01	22.74	0.91	0.01	98.99
Plato PLDT001	415.31													
216347_cpx_3		51.20	0.40	2.69	0.41	6.62	0.09	13.91	0.04		22.61	0.51	0.01	98.50
216347_cpx_36		49.62	0.54	4.29	0.52	8.03	0.17	13.64	0.02		20.57	0.51	0.00	97.91
216347_cpx_37		50.68	0.63	4.17	0.50	6.81	0.20	13.12	0.04		22.60	0.48	0.00	99.23
216347_cpx_38		51.15	0.56	3.73	0.45	7.13	0.26	13.97	0.02		21.28	0.44	0.00	99.00
216347_cpx_39		52.49	0.37	2.84	0.35	7.14	0.13	14.55	0.03		21.06	0.44	0.00	99.40
216347_cpx_40		50.84	0.40	2.86	0.26	6.66	0.21	14.03	0.03		22.12	0.46	0.01	97.87
216347_cpx_42a		51.00	0.55	4.00	0.46	6.56	0.34	13.58	0.01		22.07	0.47	0.01	99.05
216347_cpx_42b		51.35	0.70	4.23	0.47	6.72	0.18	13.15	0.02		22.96	0.55	0.01	100.34
216347_cpx_42d		49.66	0.66	4.13	0.50	6.73	0.21	12.98	0.04		22.70	0.57	0.00	98.18
216347_cpx_42f		51.16	0.60	4.00	0.48	6.42	0.16	13.38	0.01		22.89	0.49	0.02	99.63

Plagioclase compositions

	Depth	SiO ₂	TiO ₂	Al ₂ O ₃	Cr ₂ O ₃	FeO	MnO	MgO	NiO	CoO	CaO	Na ₂ O	K ₂ O	TOTAL
Nova-Bollinger SFRD0017														
SFRD0017-057.4	57.4	51.66	0.01	30.28	0.01	0.01	0.02	-0.02	0.00	-0.05	13.28	3.93	0.16	99.28
SFRD0017-057.4	57.4	51.62	0.03	30.37	0.03	0.01	0.02	0.02	0.01	-0.07	13.41	4.00	0.08	99.53
SFRD0017-129.5	129.5	46.05	0.00	34.60	0.01	0.10	0.02	-0.05	0.01	-0.05	17.96	1.44	0.01	100.11
SFRD0017-129.5	129.5	44.95	-0.01	34.67	0.00	0.00	0.04	-0.05	0.01	-0.04	18.69	1.12	0.00	99.38
SFRD0017-129.5	129.5	45.60	0.00	34.43	0.02	0.05	0.00	-0.05	-0.01	-0.03	17.99	1.37	0.01	99.38
SFRD0017-129.5	129.5	45.86	0.00	34.63	0.02	0.07	0.03	-0.03	-0.01	-0.05	18.12	1.30	0.01	99.94
SFRD0017-129.5	129.5	45.61	0.00	34.28	0.02	0.06	0.01	-0.03	0.00	-0.04	18.01	1.37	0.00	99.28
SFRD0017-135.5	135.5	47.52	0.00	32.82	0.01	0.06	0.01	0.00	-0.03	-0.03	16.81	2.26	0.02	99.47
SFRD0017-135.5	135.5	47.31	0.00	32.66	-0.02	0.01	0.02	-0.04	-0.02	-0.14	16.57	2.39	0.01	98.76
SFRD0017-231.1	231.1	49.50	0.02	31.26	0.00	0.05	-0.01	0.00	0.01	-0.10	14.81	3.15	0.12	98.80
SFRD0017-231.1	231.1	49.36	0.01	31.74	-0.01	0.01	-0.01	0.00	-0.01	-0.13	15.25	3.00	0.05	99.26
SFRD0017-231.1	231.1	50.22	0.02	30.82	0.02	0.10	-0.01	0.13	0.01	-0.01	14.47	3.26	0.06	99.10
SFRD0017-231.1	231.1	49.72	0.01	31.28	0.02	0.06	0.03	-0.03	-0.03	-0.07	14.86	3.10	0.10	99.06
Plato PLDT003														
216353_pl_12	317.56	55.01	0.08	27.46	0.00	0.06	0.00	0.01	0.00		10.93	5.44	0.14	99.13
216353_pl_24		53.90	0.06	28.19	0.01	0.05	0.00	0.00	0.00		11.79	4.93	0.10	99.02
216353_pl_25		53.44	0.00	27.99	0.00	0.04	0.01	0.00	0.00		11.81	4.94	0.08	98.31
216353_pl_37		52.67	0.00	27.54	0.00	0.13	0.00	0.27	0.00		11.76	4.82	0.09	97.30
216353_pl_38		53.16	0.06	27.76	0.00	0.01	0.00	0.00	0.00		11.71	4.80	0.06	97.55
216353_pl_39		55.05	0.05	26.47	0.00	0.01	0.03	0.00	0.00		10.03	5.85	0.08	97.58
216353_pl_4		52.80	0.08	28.58	0.00	0.04	0.00	0.01	0.01		12.55	4.47	0.17	98.70
216353_pl_5		54.89	0.00	28.07	0.00	0.03	0.00	0.00	0.01		11.23	5.13	0.16	99.53
216353_pl_54		53.53	0.02	28.69	0.00	0.00	0.05	0.00	0.00		12.39	4.71	0.11	99.50
216353_pl_55		52.48	0.07	29.18	0.00	0.04	0.04	0.00	0.01		12.95	4.19	0.09	99.04
216353_pl_56		53.41	0.06	28.68	0.01	0.04	0.04	0.00	0.02		12.29	4.55	0.09	99.18
216353_pl_57		52.80	0.04	28.26	0.00	0.04	0.04	0.01	0.00		12.12	4.57	0.12	97.99
216353_pl_7		53.94	0.07	29.06	0.00	0.04	0.00	0.01	0.00		12.58	4.46	0.16	100.33
216353_pl_8		53.09	0.02	27.83	0.00	0.04	0.00	0.00	0.01		11.83	5.00	0.15	97.97

Plagioclase compositions (continued)

	Depth	SiO ₂	TiO ₂	Al ₂ O ₃	Cr ₂ O ₃	FeO	MnO	MgO	NiO	CoO	CaO	Na ₂ O	K ₂ O	TOTAL
Plato PLDT001	415.31													
216347_pl_10		55.63	0.00	26.30	0.00	0.10	0.00	0.00	0.01		10.29	5.48	0.28	98.09
216347_pl_11		55.11	0.02	26.67	0.00	0.08	0.03	0.00	0.01		10.48	5.47	0.23	98.09
216347_pl_12		53.60	0.00	27.19	0.00	0.13	0.00	0.01	0.00		11.24	5.03	0.16	97.36
216347_pl_13		52.66	0.02	27.03	0.01	0.11	0.00	0.00	0.01		11.40	5.06	0.22	96.51
216347_pl_16		54.36	0.00	26.85	0.00	0.09	0.10	0.00	0.01		10.65	5.30	0.23	97.57
216347_pl_17		53.93	0.00	26.82	0.00	0.16	0.00	0.00	0.00		10.96	5.22	0.28	97.37
216347_pl_18		54.22	0.00	27.09	0.00	0.07	0.00	0.00	0.00		11.19	5.21	0.17	97.95
216347_pl_19		54.05	0.01	27.16	0.00	0.10	0.00	0.00	0.00		11.15	4.94	0.53	97.94
216347_pl_20		53.07	0.01	27.27	0.00	0.10	0.00	0.00	0.01		11.54	5.09	0.21	97.30
216347_pl_21		52.82	0.01	27.94	0.00	0.09	0.00	0.02	0.00		12.13	4.41	0.16	97.59
216347_pl_22		53.92	0.08	27.83	0.01	0.10	0.00	0.00	0.01		11.51	4.78	0.23	98.47
216347_pl_23		54.36	0.00	27.44	0.00	0.08	0.00	0.00	0.00		11.45	4.77	0.36	98.47
216347_pl_24		54.29	0.04	27.53	0.00	0.11	0.00	0.00	0.01		11.44	4.90	0.25	98.56

THE EVOLUTION OF MAFIC AND ULTRAMAFIC ROCKS OF THE
MESOPROTEROZOIC FRASER ZONE, ALBANY-FRASER OROGEN, AND
IMPLICATIONS FOR NI-CU SULFIDE POTENTIAL OF THE REGION

This Record is published in digital format (PDF) and is available as a free download from the DMP website at
<www.dmp.wa.gov.au/GSWApublications>.

Further details of geological products produced by the
Geological Survey of Western Australia can be obtained by contacting:

Information Centre
Department of Mines and Petroleum
100 Plain Street
EAST PERTH WESTERN AUSTRALIA 6004
Phone: +61 8 9222 3459 Fax: +61 8 9222 3444
www.dmp.wa.gov.au/GSWApublications

